FINITE ELEMENT MODELING AND FATIGUE ANALYSIS OF COMPOSITE TURBINE BLADES UNDER RANDOM OCEAN CURRENT AND TURBULENCE

by

Marco M. Canino

A Thesis Submitted to the Faculty of

The College of Engineering and Computer Science

In Partial Fulfillment of the Requirements for the Degree of

Master of Science

Florida Atlantic University

Boca Raton, Florida

August 2016

FINITE ELEMENT MODELING AND FATIGUE ANALYSIS OF COMPOSITE TURBINE BLADES UNDER RANDOM OCEAN CURRENT AND TURBULENCE

by

Marco Canino

This thesis was prepared under the direction of the candidate's thesis advisor, Dr. Hassan Mahfuz, Department of Ocean and Mechanical Engineering, and has been approved by the members of his supervisory committee. It was submitted to the faculty of the College of Engineering and Computer Science and was accepted in partial fulfillment of the requirements for the degree of Master of Science.

SUPERVISORY COMMITTEE:

Hassan Mahfuz, Ph.D.
Thesis Advisor

Javad Hashemi, Ph.D.

James H. VanZwieten, Ph.D.

Javad Hashemi, Ph.D.
Chair, Department of Ocean and Mechanical Engineering

Mohammad Ilyas, Ph.D.
Dean, College of Engineering and Computer Science

Deborah L. Floyd, Ed.D.
Dean, Graduate College

August 12th, 2016
Date

ACKNOWLEDGEMENTS

My greatest thanks go to my thesis advisor Dr. Hassan Mahfuz. Thank you for your extensive guidance and direction. I am truly grateful for the opportunity to work on such an interesting topic and have learned so much along the way. I want you to know that I really appreciate your dedication, and how you're always available and willing to spend time helping your students.

Thank you Dr. James VanZwieten for your encouragement, ideas, and suggestions throughout this research. I also really appreciate the advice and feedback I have received over the years from Dr. Javad Hashemi.

Many thanks to Takuya Suzuki for his tremendous help and support, especially during the many long hours spent writing conference papers and reports. Thank you Gabriel Alsenas of SNMREC for your assistance and for taking the time to show me the ocean current turbine and research facilities in person. Additionally, I would also like to thank the Southeast National Marine Renewable Energy Center and the IHI Corporation of Japan. Without their support, this research would not have been possible.

Finally, this acknowledgement would not be complete without thanking my family. Thank you for always being there for me and for providing loving support, guidance, and encouragement throughout my education. I simply would not have made it this far without you.

ABSTRACT

Author: Marco M. Canino

Title: Finite Element Modeling and Fatigue Analysis of Composite Turbine Blades under Random Ocean Current and Turbulence

Institution: Florida Atlantic University

Thesis Advisor: Dr. Hassan Mahfuz

Degree: Master of Science

Year: 2016

Several modifications have been implemented to numerical simulation codes based on blade element momentum theory (BEMT), for application to the design of ocean current turbine (OCT) blades. The modifications were applied in terms of section modulus and include adjustments due to core inclusion, buoyancy, and added mass. Hydrodynamic loads and mode shapes were calculated using the modified BEMT based analysis tools. A 3D model of the blade was developed using SolidWorks. The model was integrated with ANSYS and several loading scenarios, calculated from the modified simulation tools, were applied. A complete stress and failure analysis was then performed. Additionally, the rainflow counting method was used on ocean current velocity data to determine the loading histogram for fatigue analysis. A constant life diagram and cumulative fatigue damage model were used to predict the OCT blade life. Due to a critical area of fatigue failure being found in the blade adhesive joint, a statistical analysis was performed on experimental adhesive joint data.

FINITE ELEMENT MODELING AND FATIGUE ANALYSIS OF COMPOSITE TURBINE BLADES UNDER RANDOM OCEAN CURRENT AND TURBULENCE

LIST OF FIGURES ix

LIST OF TABLES xii

1. INTRODUCTION 1

1.1 Literature Review 4

1.1.1 Blade Element Momentum Theory 5

1.1.2 Design of Composite Turbine Blades 6

1.1.3 Blade Loading 7

1.1.4 Statistical Analysis of Experimental Fatigue Data 9

1.2 Scope of Thesis 9

2. MODELING AND NUMERICAL SIMULATION OF AN OCEAN CURRENT TURBINE BLADE 11

2.1 Overall Design and Analysis Scheme 11

2.2 Blade Properties 13

2.2.1 Geometry 13

2.2.2 Materials 15
2.3 Modification to BEMT-based Tools 17
2.3.1 Blade Structural Shell Development 17
2.3.2 Inclusion of Core Material 19
2.3.3 Added mass 21
2.3.4 Blade Modal Analysis 22
2.3.5 Buoyancy 25
2.4 Discussion 27
3. BLADE LOADING DUE TO RANDOM OCEAN CURRENT AND TURBULENCE 29
3.1 ADCP Measurements 29
3.2 Current Velocity Data 31
3.3 Rainflow Counting 33
3.4 Ocean Current Turbulence 34
3.5 Hydroelastic Simulation 39
4. BLADE LOADING AND FATIGUE ANALYSIS 43
4.1 Coupling with ANSYS 43
4.2 Blade Failure Analysis 47
4.3 Calculation of Cumulative Fatigue Damage 49
4.4 Results and Discussion 52

5. STATISTICAL ANALYSIS OF BLADE JOINT FATIGUE STRENGTH 54

5.1 Application to Static Joint Strength 55

5.2 Adhesive Joint Fatigue Strength 59

5.3 Results and Discussion 62

6. SUMMARY 65

6.1 Summary 65

6.2 Future Work 66

APPENDICES 68

A. Precomp Files 68

B. BModes Files 73

C. TurbSim Files 76

D. AeroDyn Files 78

E. FAST Files 79

REFERENCES 85

LIST OF FIGURES

Figure 1: Major Ocean Surface Currents (Lumpkin, 2016) 1

Figure 2: Time Averaged Kinetic Energy Flux over 0.5 kW/m^2 at a depth of 50 meters .. 2

Figure 3a & 3b : IHI and SNRMEC's OCT Design 3

Figure 4: Aerodynamic Loading on Horizontal Axis Turbine Blade Geometry 5

Figure 5: Conventional Wind Turbine Procedure 11

Figure 6: Modified Structural Analysis Procedure for OCT Blades 12

Figure 7: Testing of SNMREC's OCT in the Gulf Stream 13

Figure 8: SolidWorks 3-D Curves 15

Figure 9: Stacking Sequence, Orientation, and Polar Properties 16

Figure 10: SolidWorks Model of OCT Blade 17

Figure 11: Blade Reference Axes for NREL Codes 19

Figure 12: Blade Flap and Edgewise Mode Shapes 23

Figure 13: ANSYS Generated Flapwise Bending Mode 2 25

Figure 14: OCT Blade Buoyancy Distribution 26

Figure 15: Effect of Added Mass and Core Inclusion 27

Figure 16: Map of SNMREC's Past ADCP Measurement Sites 30

Figure 17: Probability Mass of Current Magnitude 31

Figure 18: Analysis of ADCP Data from Site B2 32

Figure 19: Rainflow Counted Distribution of Site B2 at -50m 33

Figure 20: Distribution of 20 Turbulence Bins 36

Figure 21: Bin 10 with 5% I_u 37
Figure 22: Bin 20 with 7.5% I_u 37
Figure 23: Bin 10 Histogram at 5% I_u 38
Figure 24: Bin 10 Histogram at 7.5% I_u 38
Figure 25: RFC at 5% Turbulence Intensity 38
Figure 26: RFC at 7.5% Turbulence Intensity 38
Figure 27: Normal and Tangential Loading Relations (J M Jonkman, 2003) 40
Figure 28: Normal and Tangential Forces at Bin 10 (1.55 m/s) 41
Figure 29: Normal Force Output of AeroDyn 42
Figure 30: Tangential Force Output of AeroDyn 42
Figure 31: Ply Orientation in Shell Element 181 43
Figure 32: Shell181 Element 44
Figure 33: Solid186 Element 44
Figure 34: Finite Element Model of the OCT Blade 45
Figure 35: Blade deformation with Undeformed Edge 46
Figure 36: Comparison of Tip Deformation between FAST and ANSYS 46
Figure 37: Tsai-Wu Failure in Composite Skin 48
Figure 38: Failure Analysis based on Maximum Stress and Tsai-Wu Criteria 49
Figure 39: Equivalent Stress Conversion using the Goodman Diagram 50
Figure 40: S-N Diagram for Blade Core (Ferreira et al., 2010) 51
Figure 41: Longitudinal Stress Distribution of Blade Skin (Top Layer) at 2.75 m/s 52
Figure 42: Mises Stress Distribution on Blade Core Surface at 2.75 m/s 52
Figure 43: Specimen Test Configuration 55

Figure 44: Probability Density of von Mises Stress from Tensile Testing..... 58

Figure 45: Fatigue Reliability at 26.6°..... 60

Figure 46: Fatigue Reliability at 45°..... 60

Figure 47: Adhesive Joint S-N curve at 26.6° 64

Figure 48: Adhesive Joint S-N curve at 45° 64

LIST OF TABLES

Table 1: Blade Design Characteristics 14

Table 2: Material Properties 16

Table 3: Skin Structural Properties Computed by PreComp 18

Table 4: Added Mass of the OCT Blade 22

Table 5: Blade Mass Properties 26

Table 6: ADCP Measurement Site History 29

Table 7: Strength of Carbon/Epoxy Composites (Daniel & Ishai, 2005) 48

Table 8: Strength of Syntactic Foam (Ferreira, Salviano, Costa, & Capela, 2010) 48

Table 9: Blade Core Fatigue Life Comparison 53

Table 10: Static Adhesive Joint Experimental Data 56

Table 11: Weibull Characterization of Static Adhesive Joint Data 58

Table 12: Results of Adhesive Joint Fatigue Test 60

Table 13: Weibull Characterization of Adhesive Joint Fatigue Data 63

1. INTRODUCTION

Powerful ocean currents encompass our planet and contain an enormous amount of untapped energy. These currents flow in complex patterns and are affected by wind, temperature, ocean floor topography, the earth's rotation, and water salinity. Figure 1 displays the locations of major surface currents around the world (Lumpkin, 2016). These

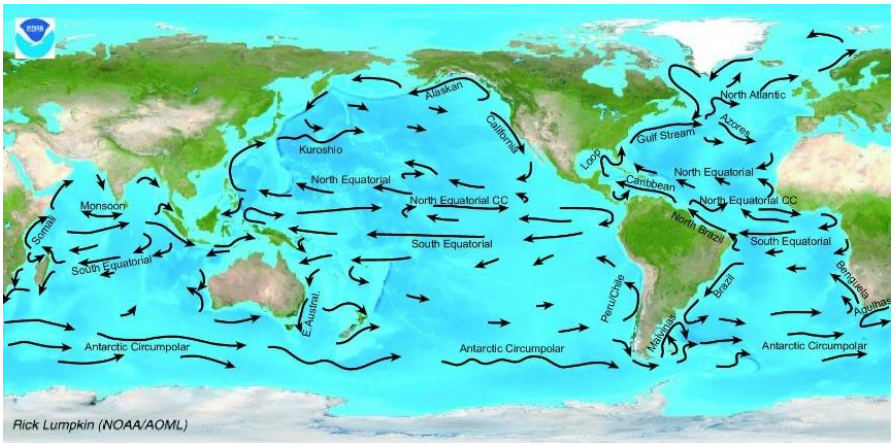

Figure 1: Major Ocean Surface Currents (Lumpkin, 2016)

currents vary in strength, consistency, and accessibility. One of the strongest, most easily accessible, and consistent ocean currents is the Gulf Stream along Southeast Florida (VanZwieten, 2003). The Gulf Stream carries approximately 1 billion cubic feet of seawater per second through the Florida Strait, where it is tightly focused between Florida and Cuba (Cenedese & Gordon, 2011). This results in a mass transport greater than 30 times the total freshwater flow of all the rivers in the world (Lemanski, 2006).

The sister current to the Gulf Stream in the North Pacific is the Kuroshio, meaning "Black Current" in Japanese ("Kuroshio," 2016). Both move warm water into the Arctic Ocean with a similar transport and array of eddies. In order to visualize the power of these two currents, Figure 2 displays the time averaged kinetic energy flux from 2009 to 2011 in excess of 500 W/m^2 and at a depth of 50 meters below the surface (VanZwieten, Alsenas, Smentek-Duerr, & Hanson, 2013). More recent studies have shown the average energy density at 50 meters below sea level to be 3 kW/m^2 in the Florida Gulf Stream core (Carolina, Machado, Vanzwieten, & Pinos, 2016). Compared to even the best wind turbine locations, these currents have over double the kinetic energy density (Lemanski, 2006).

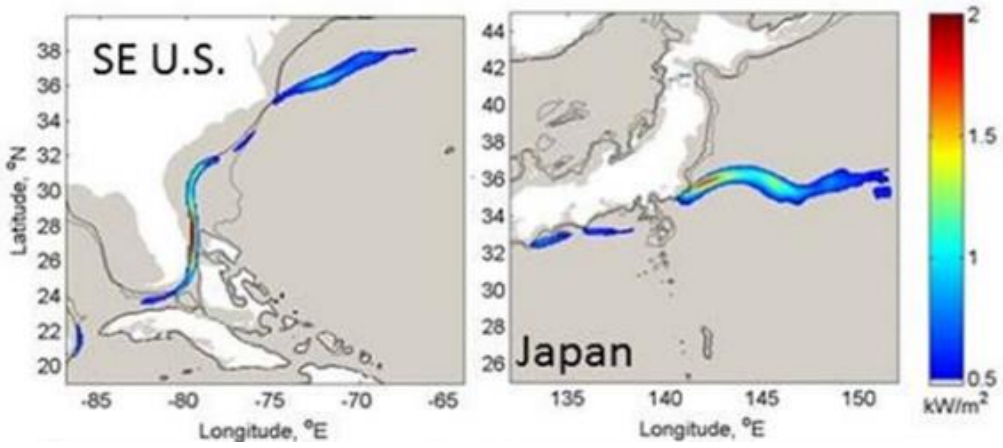

Figure 2: Time Averaged Kinetic Energy Flux over 0.5 kW/m^2 at a depth of 50 meters

The Kuroshio and Gulf Stream currents have been identified as potential candidates for harnessing ocean current energy (VanZwieten et al., 2013). Technologies are currently being developed and tested to convert kinetic energy from ocean currents into usable power. The most common design is the horizontal axis turbine, which has its rotor axis parallel to the current flow. Two examples of horizontal axis in-stream hydrokinetic turbines are shown in Figure 3.

Since 2011, Japan's New Energy and Industrial Technology Development Organization (NEDO) has promoted the Research and Development (R&D) of ocean energy power generation "with the goal of developing world-leading technology and contributing to lower CO2 emissions." As a result, IHI and Toshiba, together with the University of Tokyo and Mitsui Global Strategic Studies Institute have conducted R&D financed by NEDO in order to prove the viability of ocean energy power generation, create the framework for an industry, and contribute to improved energy security for Japan (Toshiba, 2014). The underwater ocean current turbine system, shown in Figure 3a, is anchored to the sea floor and floats like a kite, with two counter-rotating turbines being driven by the ocean current. IHI is taking the lead on the project, responsible for manufacturing the turbine and floating body, and Toshiba is supplying the electronic devices, including the generator and transformer (Toshiba, 2014).

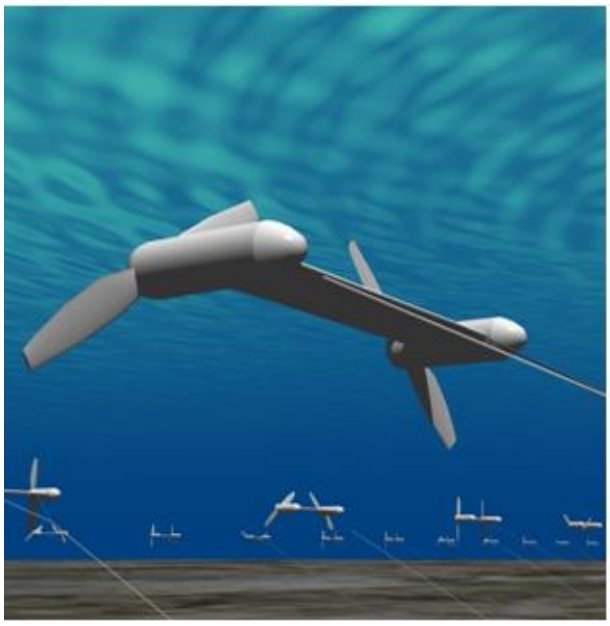

(a) **(b)**

Figure 3a: IHI and Toshiba's OCT Design (Toshiba, 2014),

Figure 3b: SNMREC's Experimental OCT (Harbor Branch, 2015)

The Southeast National Marine Renewable Energy Center (SNMREC) is one of three U.S. Department of Energy centers designated to marine renewables. SNMREC is the only center serving the Eastern U.S. and is currently a part of Florida Atlantic University's Division of Research. SNMREC's focus is on harnessing open-ocean currents like the Gulf Stream for utility scale power generation (SNMREC, 2015). For over six years, the center has collected a large amount of Gulf Stream resource data essential to OCT design, regulation, and site selection. Figure 3b shows the horizontal axis in-stream hydrokinetic research turbine designed and tested by SNRMEC.

For both of these OCT systems, before energy can be extracted efficiently, a multistep design process must be followed. Research has already been performed in order to optimize blade geometry and materials for the oceanic environment, but a procedure still needs to be developed for converting ocean current velocity data for application to blade design and the prediction of fatigue life. Having an accurate fatigue life estimation is necessary in order to determine the economic viability of ocean current turbine systems.

1.1 Literature Review

Various devices, such as horizontal axis cross-flow turbines, open center turbine fans, oscillating hydrofoils, propeller blade turbines, vortex-induced vibration hydrokinetic turbines, and underflow water wheel turbines, are currently being studied to extract energy from wave motion and steady flowing ocean current. Although, different in operational methods, all of these devices utilize environmentally induced hydrodynamic forces to extract kinetic energy (J M Jonkman & Buhl, 2004). A brief description of the theoretical concepts of blade design and the importance of fatigue analysis is discussed in this section.

1.1.1 Blade Element Momentum Theory

BEM theory is a combination of momentum theory and blade element theory, which was originally developed for the design of wind turbine blades. In momentum theory, the rate of change of momentum due to a pressure difference across the rotor plane is considered, and the induced velocities in the axial and tangential directions are calculated (Suzuki, Mahfuz, & Canino, 2015). The expressions for the differential contribution to the thrust and torque are described by Eqs. 1 and 2 (Manwell, McGowan, & Rogers, 2009)

$$dT = \rho U^2 4a(1-a)\pi r dr \qquad \text{Eq. 1}$$

$$dQ = 4a'(1-a)\rho U \pi r^3 \Omega dr \qquad \text{Eq. 2}$$

Where, ρ is the density of the fluid, U is the far-field velocity, a is the axial induction factor, a' is the angular induction factor, Ω is the angular velocity, r is the radius of the blade element, and dr is its length.

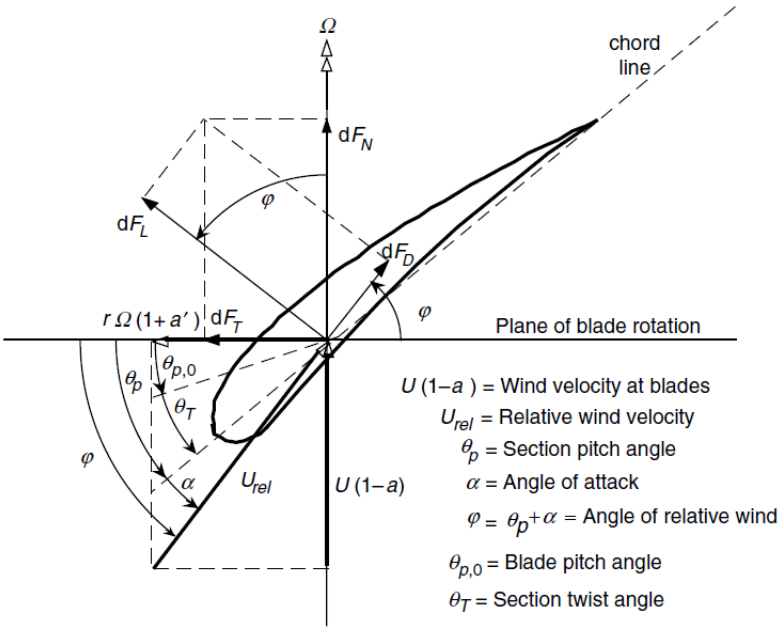

Figure 4: Aerodynamic Loading on Horizontal Axis Turbine Blade Geometry

In blade element theory, a blade is divided into small blade elements, each of which act independently as two-dimensional airfoils in order to calculate the aerodynamic loads. The aerodynamic loads of each blade element are given by Eqs. 3 and 4 (Manwell et al., 2009);

$$dF_N = \frac{1}{2}\rho U_{rel}^2 (C_l \cos\phi + C_d \sin\phi) c dr \qquad \text{Eq. 3}$$

$$dF_T = \frac{1}{2}\rho U_{rel}^2 (C_l \sin\phi - C_d \cos\phi) c dr \qquad \text{Eq. 4}$$

where, F_N is the normal force to the rotational plane, that is equal to dT, F_T is the tangential force, U_{rel} is the relative flow velocity into the airfoil, C_l and C_d are the lift and drag coefficients of the airfoil, ϕ is the sum of section pitch angle and angle of attack, and c is the chord length. The relation of these loads with respect to airfoil geometry is shown in Figure 4. By combining Eqs. 1 to 4 and iterating for the axial and angular induction factors, the aerodynamic loads can be calculated at each airfoil (Suzuki et al., 2015).

1.1.2 Design of Composite Turbine Blades

Developing a framework for the design of composite OCT blades is an important step in advancing technological readiness. Previous studies have determined that designing OCT blades using a composite skin material and solid foam core results in increased performance and blade life (Asseff, 2009). OCT blades are designed with a composite skin to better resist the corrosive marine environment. Core materials chosen should have high buckling resistance, water impermeability and result in a neutral buoyancy in water. Neutrally buoyant blades experience reduced stress near the blade joint and improve power

production by canceling the inertial forces resisting blade rotation. Other important features include dimensional stability, low water absorption and chemical resistance (Akram, 2010).

1.1.3 Blade Loading

Initially, wind turbine design was governed by static and quasi-static analyses. Unfortunately, this oversimplification resulted in over-engineered blades and blades that experienced premature failures. The latter is exemplified by the high failure rate observed in early Californian wind farms. It was soon realized that wind turbines are fatigue critical machines (Sutherland, 1999). Current methods for determining equivalent damage loading for Horizontal Axis Wind Turbines (HAWT) have proven to be reliable models of blade fatigue life (Freebury & Musial, 2000). This research serves as a basis for estimating the fatigue life of a composite OCT blade with core inclusion under measured Gulf Stream velocity conditions.

Loading spectrum is one of the most important parameters for fatigue analysis. A loading spectrum may contain mean and amplitude loading, sequences of loading, frequencies and loading cycle repetition. Laboratory tests are done mostly at a constant amplitude and frequency for fatigue analysis, but service loads will not always be constant in amplitude and frequency. Therefore, a loading spectrum should defined for fatigue analysis of any component in operation. OCT blades are subject to several fatigue loads in operation. These can originate from the randomness of ocean current due to tide, turbulence, waves, and velocity shear. The resulting loads contribute to alternating flapwise

bending of the blades, which is responsible for more than 90% of the damage in both wind and OCT blades (Kong, Kim, Han, & Sugiyama, 2006).

Verdant Power, a New York, NY based marine and hydrokinetic energy company established in 2000, has been testing kinetic hydropower systems in the NY East River since 2002. Early installations experienced stronger than expected currents, resulting in the failure of six turbines over the course of three weeks at the connection point between the blade root and hub (LaMonica, 2011; NRC, 2013). Based on this information, a reliable design procedure that considers the effect of flapwise bending fatigue is necessary.

Ocean currents are inherently random in nature. They vary due to the lunar effect of tides, seasonal rainfall, and wind velocity. Due to this, ocean currents can vary hourly, monthly, or annually. This variation is further intensified if turbulence is taken into consideration. Since blade loading is related to ocean current velocity, a varying ocean current will always cause a fluctuating load on the turbine. The variable loads on the OCT will create alternating bending as well as shear stresses (Akram, 2010). In order to account for these loading variations, previous studies have used a simulated time history (Cooper & Mcgillem, 1988).

Since the Gulf Stream current approximately follows a normal Gaussian distribution (Raye, 2002), a preliminary estimate of blade fatigue life can be obtained from this method. Most recently, the National Renewable Energy Laboratory (NREL) codes have been utilized to design and load OCT blades (Fang Zhou, 2013). Previous methods however, have not taken into account the inclusion of a core material for the blade.

1.1.4 Statistical Analysis of Experimental Fatigue Data

In this study a fatigue analysis has been performed using a numerical simulation. However, to validate any numerical simulation, experiments are necessary. In an attempt to generate fatigue data, the IHI Corporation of Japan has conducted extensive fatigue tests on joints that are used in OCT blade construction. These joints are most vulnerable during fatigue and will likely be the first to fail. To characterize the experimental fatigue data, a 2P Weibull analysis has been employed to generate the stress-load cycle (S-N) diagram. Further procedures for generating S-N diagrams from fatigue data with a known reliability, are also described.

1.2 Scope of Thesis

The objective of this thesis is to develop and evaluate a method for estimating the fatigue life of an OCT blade using measured current speed data. In order to successfully complete this objective, the following has been completed.

1. Gulf Stream current velocity data from SNMREC was gathered and reduced using the rainflow counting method at the target turbine placement depth.

2. A composite ocean current turbine blade was designed with a sandwich structure having an orthotropic skin and isotropic core.

3. The NREL Software Suite was modified in order to account for oceanic conditions as well as the inclusion of a blade core.

4. A stress and failure analysis was performed under the various turbulence intensities by means of the finite element software ANSYS.

5. Fatigue life of the OCT blade was estimated using a constant life diagram in conjunction with a cumulative damage method.

6. Statistical analysis was performed on experimental OCT blade joint fatigue data with a known level of reliability.

Although studies have been performed on composite OCT blades (Akram, 2010; Asseff, 2009), such research was based on statistically generated data. Using such data is fine for horizontal axis wind turbines, due to accurate models being already developed and verified over many years. Since ocean current turbines are at an early stage of development, an acceptable method of design is necessary for OCT blades by employing measured ocean current velocity data and satisfying other hydrodynamic requirements such as neutral buoyancy and added mass.

2. MODELING AND NUMERICAL SIMULATION OF AN OCEAN CURRENT TURBINE BLADE

2.1 Overall Design and Analysis Scheme

The conventional procedure for studying blade response to aerodynamic loading is shown in Figure 5 (Fang Zhou, 2013). The NREL codes consisting of PreComp, BModes, TurbSim, and FAST, are used in conjunction with gathered wind data in order to calculate blade loading and tip deflection. Over the years, these tools have motivated design and

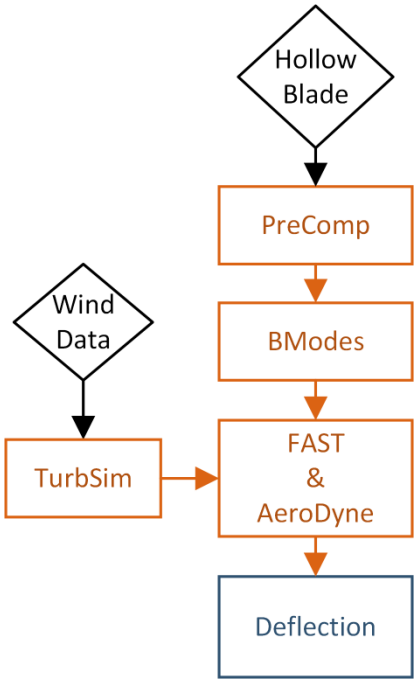

Figure 5: Conventional Wind Turbine Procedure

performance improvements in wind turbines. Although this method has proved to be applicable for HAWTs, several modifications are necessary for application to solid OCT

blades subject to oceanic conditions. Figure 6 depicts the modified structural analysis procedure for OCT blades (Fang Zhou, 2013).

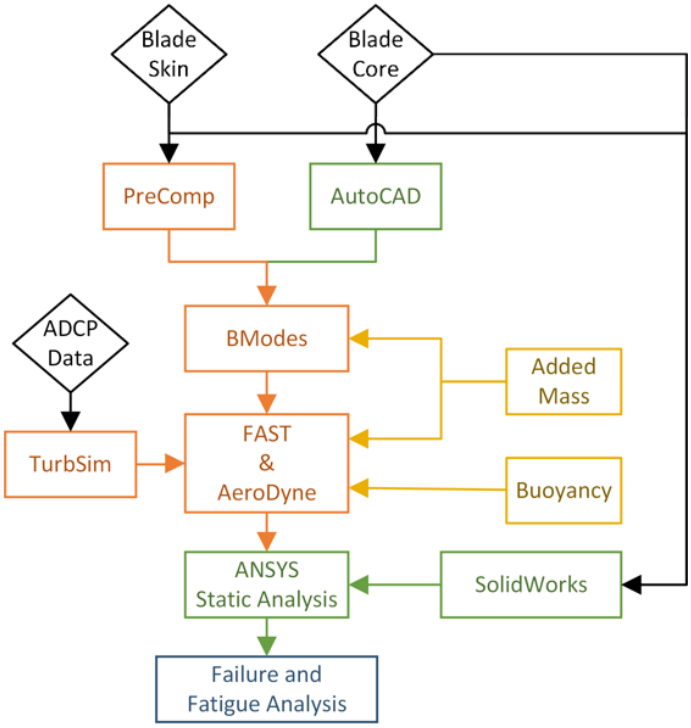

Figure 6: Modified Structural Analysis Procedure for OCT Blades

The following portions of the modified OCT procedure will be discussed in this chapter. Blade geometry and material properties for the orthotropic blade skin were loaded into PreComp in order to compute the structural properties along the blade span. AutoCAD has been used to determine the structural properties of the isotropic core material at each cross section. The skin and core properties were combined, along with added mass, for input into BModes. Three mode shapes from BModes were selected for use in the dynamic blade simulation of FAST.

2.2 Blade Properties

2.2.1 Geometry

In order to perform a blade analysis, a realistic blade model must first be developed. SNMREC's composite turbine blade was used as a guide (Borghi et al., 2013). Table 1 displays the blade parameters provided by SNMREC. Twenty five cross sectional areas were modeled using twenty-three unique Wortmann FX77-series hydrofoils, with the last hydrofoil repeated two additional times. The turbine has a diameter of 3 m, a blade length of 1.22 m, and was designed to rotate at 50 rpm under normal conditions. Figure 7 depicts the prototype SNMREC blade during a test deployment in the Gulf Stream.

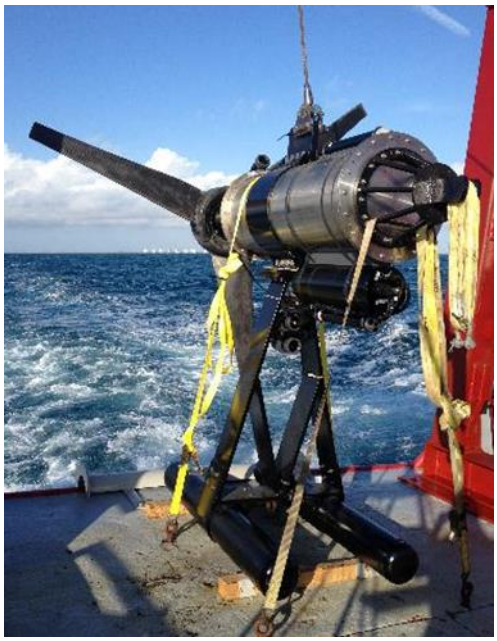

Figure 7: Testing of SNMREC's OCT in the Gulf Stream

Table 1: Blade Design Characteristics

Station Number	Radius (m)	Blade Fraction	Chord (m)	Twist (deg)	Hydrofoil
1	0.277	0.000	0.311	26.34	fx77_02349
2	0.287	0.008	0.309	25.52	fx77_02336
3	0.306	0.024	0.305	24.07	fx77_02301
4	0.334	0.047	0.299	22.23	fx77_02273
5	0.371	0.077	0.290	20.22	fx77_02223
6	0.416	0.114	0.279	18.17	fx77_02162
7	0.469	0.157	0.267	16.13	fx77_02092
8	0.528	0.206	0.253	14.24	fx77_02012
9	0.593	0.259	0.239	12.47	fx77_01925
10	0.662	0.316	0.224	10.90	fx77_01832
11	0.735	0.375	0.210	9.50	fx77_01734
12	0.811	0.437	0.196	8.27	fx77_01633
13	0.888	0.500	0.182	7.22	fx77_01530
14	0.964	0.563	0.170	6.30	fx77_01486
15	1.040	0.625	0.159	5.49	fx77_01442
16	1.113	0.684	0.149	4.76	fx77_01400
17	1.182	0.741	0.140	4.10	fx77_01360
18	1.247	0.794	0.133	3.50	fx77_01323
19	1.306	0.843	0.127	2.95	fx77_01289
20	1.359	0.886	0.122	2.44	fx77_01258
21	1.404	0.923	0.118	1.99	fx77_01232
22	1.441	0.953	0.115	1.61	fx77_01211
23	1.469	0.976	0.114	1.30	fx77_01210
24	1.488	0.992	0.112	1.10	fx77_01210
25	1.498	1.000	0.112	0.99	fx77_01210

In order to have an accurate model, each hydrofoil was scaled to the appropriate chord length, rotated about its aerodynamic center to match the twist angle, and then positioned at the respective radial distance from the rotor hub. A MATLAB code was written to perform all of these actions and output 25 comma separated values (CSV) text files. These files were then loaded into SolidWorks as 3-D curves, shown in Figure 8. The

cross-sectional areas were lofted together to form a solid body and then shelled, in order to create a 4.015 mm skin. The hollow interior was then filled with a foam core.

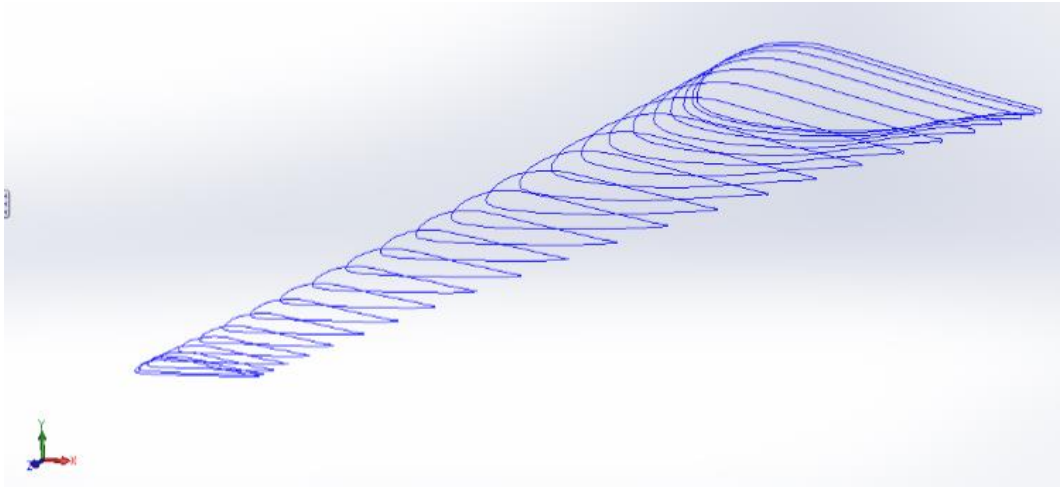

Figure 8: SolidWorks 3-D Curves

2.2.2 Materials

Each component of an OCT needs to be designed with the harsh environmental conditions of the ocean in mind. In order to survive the intense blade loading, the turbine shell is required to have a high modulus and strength, carbon/epoxy composites were chosen for this purpose. A pre-preg 24K carbon/epoxy unidirectional tape (Daniel & Ishai, 2005; Matweb, 2016a) was used to provide strength along the longitudinal axis of the blade and a 12K 2x2 twill weave carbon/epoxy pre-preg (FGDC, 2010; Matweb, 2016b) was used for multi-axial strength and stiffness. Material properties are shown in Table 2. Figure 9 displays the stacking sequence, orientation, and polar properties where the polar properties are in MPa and *t* is the ply thickness in mm.

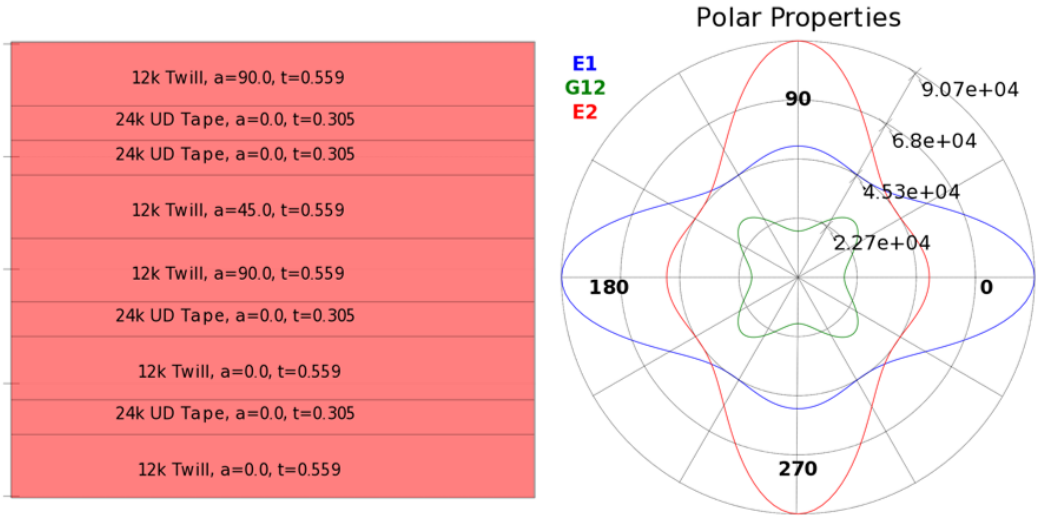

Figure 9: Stacking Sequence, Orientation, and Polar Properties

Additionally, a lightweight core material is required for OCT blades to achieve neutral buoyancy and resist hydrostatic collapse. For this purpose, an epoxy based syntactic foam with 50% glass micro-balloons was chosen (Bibin John & Reghunadhan, 2010; Daniel & Ishai, 2005). The material properties are displayed in Table 2. Figure 10, depicts the completed OCT blade model.

Table 2: Material Properties

Material	Density	E_1	E_2	E_3	G_{12}	G_{23}	G_{13}	ν_{12}	ν_{12}	ν_{12}
	[kg/m^3]	[GPa]	[GPa]	[GPa]	[GPa]	[GPa]	[GPa]	[-]	[-]	[-]
UD Carbon/Epoxy	1556	143	10.3	10.3	7.0	3.7	7.0	0.27	0.54	0.27
Twill Carbon/Epoxy	1697	71.0	71.0	6.9	19.5	2.7	2.7	0.04	0.30	0.30
Syntactic Foam	690	1.79			0.673			0.33		

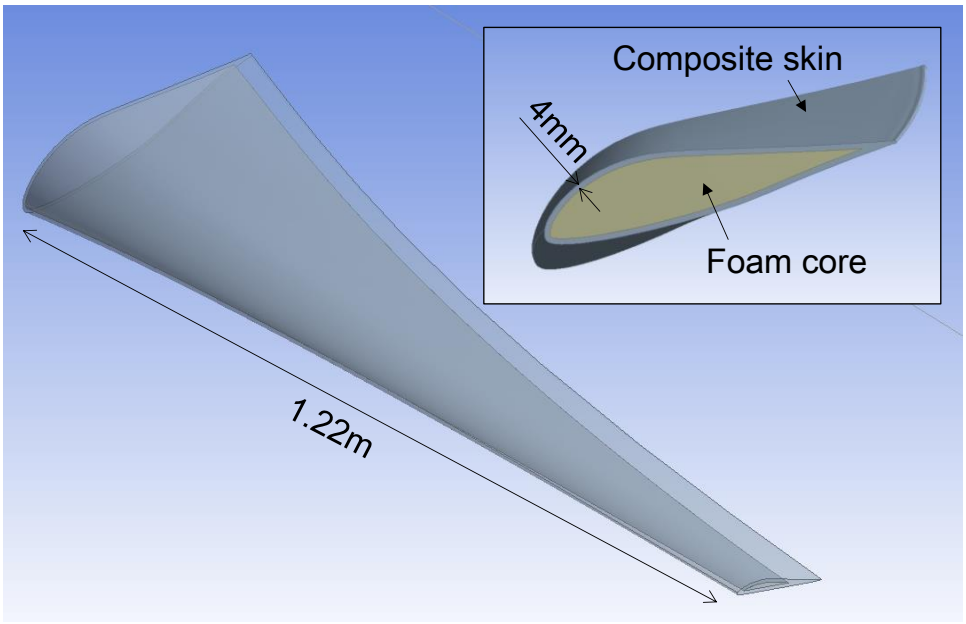

Figure 10: SolidWorks Model of OCT Blade

2.3 Modification to BEMT-based Tools

The hydrodynamic loads on the OCT blade were calculated by modifying the inputs of the following conventional BEMT-based software developed by the NREL: PreComp, BModes, TurbSim, FAST and AeroDyn. Modifications were applied in terms of section modulus and include adjustments to mass density, buoyancy, and added mass.

2.3.1 Blade Structural Shell Development

NREL's PreComp (Pre-processor for computing Composite blade structural properties) was used to determine the structural properties of the OCT blade's composite skin (G Bir, 2006). Each hydrofoil was written in unscaled format to a text file using 150 coordinate pairs. Node numbering began with the leading edge at (0,0), progressing clockwise through the trailing edge at (1,0). The material properties of the twill fabric and

unidirectional tape were defined as well as the lamina stacking sequence, ply thickness, and fiber orientation. Using the nodal plots, material properties, and blade section data from Table 1 & 2, PreComp was able to compute the blade stiffness and inertial properties. Table 3 depicts PreComp's output for the hollow OCT blade. The span location, structural twist, mass density, flap and edge inertia, flap and edge stiffness, torsional stiffness, axial stiffness, and shear center offset are displayed.

Table 3: Skin Structural Properties Computed by PreComp

span_loc	str_tw	mass_den	flp_iner	edge_iner	flp_stff	edge_stff	tor_stff	axial_stff	sc_offst
(-)	(deg)	(kg/m)	(kg-m)	(kg-m)	(Nm^2)	(Nm^2)	(Nm^2)	(N)	(m)
0	24.54	4.38	2.45E-03	3.75E-02	1.33E+05	2.04E+06	7.38E+04	2.39E+08	0.073
0.0079	23.722	4.36	2.37E-03	3.68E-02	1.29E+05	2.00E+06	7.15E+04	2.37E+08	0.073
0.0235	22.266	4.29	2.22E-03	3.53E-02	1.21E+05	1.92E+06	6.69E+04	2.34E+08	0.072
0.0467	20.42	4.20	2.00E-03	3.30E-02	1.09E+05	1.80E+06	6.03E+04	2.29E+08	0.07
0.077	18.402	4.07	1.73E-03	3.01E-02	9.42E+04	1.64E+06	5.22E+04	2.21E+08	0.068
0.114	16.328	3.91	1.44E-03	2.67E-02	7.85E+04	1.45E+06	4.36E+04	2.13E+08	0.066
0.157	14.272	3.72	1.16E-03	2.32E-02	6.31E+04	1.26E+06	3.50E+04	2.03E+08	0.063
0.2055	12.357	3.52	9.01E-04	1.97E-02	4.90E+04	1.07E+06	2.71E+04	1.92E+08	0.06
0.2586	10.563	3.32	6.76E-04	1.65E-02	3.67E+04	8.96E+05	2.03E+04	1.81E+08	0.057
0.3156	8.962	3.10	4.93E-04	1.35E-02	2.68E+04	7.37E+05	1.47E+04	1.69E+08	0.053
0.3754	7.531	2.89	3.49E-04	1.10E-02	1.90E+04	5.99E+05	1.03E+04	1.58E+08	0.05
0.4372	6.262	2.69	2.42E-04	8.86E-03	1.31E+04	4.83E+05	7.05E+03	1.47E+08	0.047
0.5	5.165	2.50	1.64E-04	7.13E-03	8.92E+03	3.89E+05	4.70E+03	1.36E+08	0.044
0.5628	4.243	2.33	1.21E-04	5.75E-03	6.57E+03	3.13E+05	3.40E+03	1.27E+08	0.041
0.6246	3.429	2.17	8.98E-05	4.66E-03	4.86E+03	2.54E+05	2.46E+03	1.18E+08	0.038
0.6844	2.704	2.03	6.71E-05	3.82E-03	3.63E+03	2.08E+05	1.79E+03	1.11E+08	0.036
0.7414	2.047	1.91	5.11E-05	3.19E-03	2.76E+03	1.74E+05	1.33E+03	1.04E+08	0.034
0.7945	1.443	1.81	3.98E-05	2.71E-03	2.15E+03	1.47E+05	1.02E+03	9.86E+07	0.032
0.843	0.89	1.73	3.19E-05	2.35E-03	1.73E+03	1.28E+05	8.10E+02	9.40E+07	0.031
0.886	0.385	1.66	2.64E-05	2.08E-03	1.42E+03	1.14E+05	6.86E+02	9.03E+07	0.03
0.923	-0.065	1.61	2.26E-05	1.90E-03	1.22E+03	1.03E+05	6.25E+02	8.75E+07	0.029
0.9533	-0.448	1.57	2.00E-05	1.76E-03	1.08E+03	9.59E+04	5.89E+02	8.54E+07	0.028
0.9765	-0.755	1.54	1.88E-05	1.67E-03	1.02E+03	9.11E+04	5.62E+02	8.39E+07	0.028
0.9921	-0.961	1.52	1.81E-05	1.62E-03	9.75E+02	8.80E+04	5.44E+02	8.30E+07	0.027
1	-1.065	1.51	1.77E-05	1.59E-03	9.54E+02	8.64E+04	5.35E+02	8.25E+07	0.027

2.3.2 Inclusion of Core Material

OCT blades usually include a core material to achieve neutral buoyancy as well as to resist hydrostatic pressure. However, PreComp was originally designed to calculate the section properties of hollow turbine blades. Therefore, the core properties were calculated separately by a commercial CAD software, and then added to the properties of the skin. The two-dimensional section properties of the core: the flap-, edge- and torsion-wise stiffness, axial stiffness and the mass density were calculated by AutoCAD. The procedure was repeated for each hydrofoil section, and the input file of BModes was overwritten by adding the core properties.

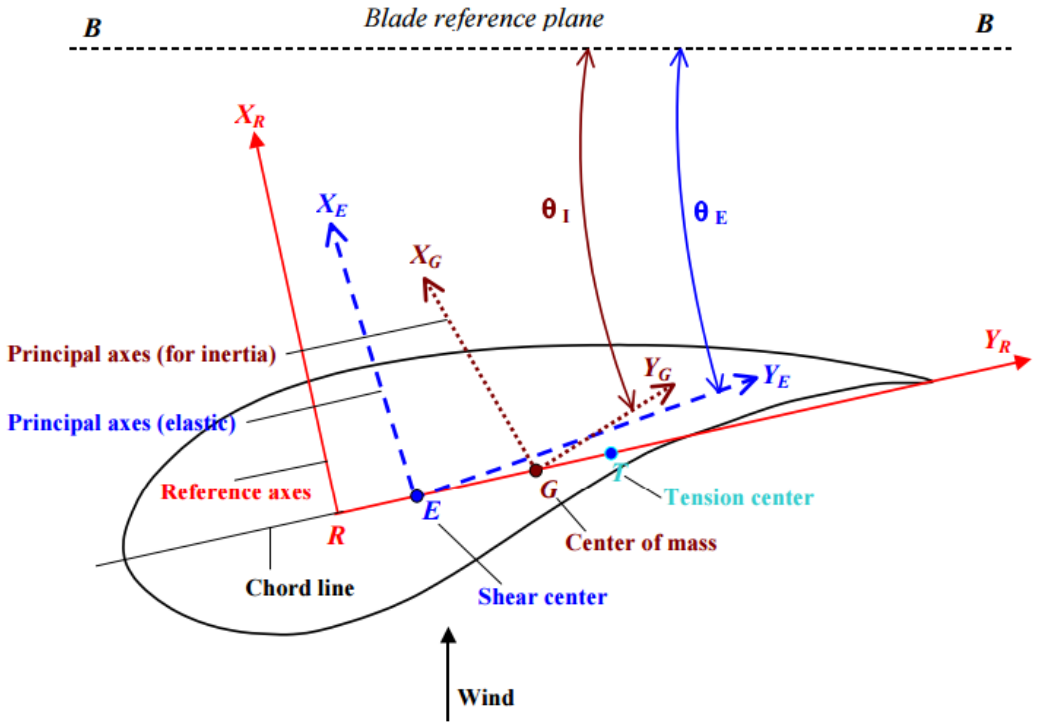

Figure 11: Blade Reference Axes for NREL Codes

Equation 5 was used to calculate the blade section mass per unit length.

$$mass\_den = \int\int \rho(x,y)\,dxdy \qquad \text{Eq. 5}$$

Where, $\rho(x,y)$ is the mass density in kg/m^3 and x and y are the flapwise and edgewise distances in meters from the blade section mass center to the differential area element respectively.

Equation 6 was used to calculate the blade section flapwise mass inertia per unit length about the Y_G inertia axis, shown in Figure 11. Equation 7 was used to calculate the blade edgewise mass inertia per unit length about the X_G inertia axis, shown in Figure 11.

$$flp\_iner = \int\int \rho(x,y)\,x^2 dxdy \qquad \text{Eq. 6}$$

$$edg\_iner = \int\int \rho(x,y)\,y^2 dxdy \qquad \text{Eq. 7}$$

Equation 8 and 9 were used to calculate the blade section flapwise bending stiffness about the Y_E elastic axis and the blade edgewise bending stiffness about the X_E elastic axis respectively, as shown in Figure 11.

$$flp\_stff = \int\int E(x,y)\,x^2 dxdy \qquad \text{Eq. 8}$$

$$edge\_stff = \int\int E(x,y)\,y^2 dxdy \qquad \text{Eq. 9}$$

Where, $E(x,y)$ is the modulus of elasticity in N/m^2 and x and y are the flapwise and edgewise distances in meters from the blade section elastic center to the differential area element respectively.

Equations 10 and 11 were used to calculate the blade section torsional and extensional stiffness respectively.

$$tor\_stff = \int\int G(x,y)\left(x^2 + y^2\right)dxdy \quad \text{Eq. 10}$$

$$axial\_stff = \int\int E(x,y)\,dxdy \quad \text{Eq. 11}$$

Where, $G(x,y)$ is the modulus of rigidity in N/m^2 and x and y are the flapwise and edgewise distances in meter from the blade section elastic center to the differential area element respectively.

2.3.3 Added mass

Added mass is the result of fluid surrounding a body being accelerated or decelerated. As blades rotate, fluid is accelerated simultaneously in the surrounding area. Added mass is not accounted for in the conventional BEM codes for wind turbine blades due to the low density of air. Added mass needs to be considered for OCT blades when formulating the blade equation of motion since sea water is approximately 830 times denser than air. This was taken into consideration using Eq. 12 (Fang Zhou, 2013):

$$m_a = \rho C_A S \quad \text{Eq. 12}$$

Where, m_a is the added mass density, ρ is the density of water, C_A is the added mass coefficient, and S is the blade section area. C_A=0.5 was used since, according to the DNV Offshore Standard, this gives a reasonable estimation for hydrofoils (DNV, 2011). Table 4

depicts the added mass and total mass calculated at each blade section. The input file of BModes was overwritten to include the calculated added mass and core properties.

Table 4: Added Mass of the OCT Blade

Blade Section	Mass of Blade & Core (kg/m)	Mass of Displaced Water (kg/m)	Added Mass (kg/m)	Total Mass (kg/m)
1	12.39	14.64	7.32	19.71
2	12.23	14.38	7.19	19.42
3	11.90	13.84	6.92	18.82
4	11.30	13.04	6.52	17.81
5	10.51	12.01	6.00	16.51
6	9.58	10.82	5.41	14.99
7	8.61	9.55	4.77	13.38
8	7.67	8.27	4.13	11.80
9	6.75	7.03	3.52	10.26
10	5.86	5.89	2.95	8.81
11	5.04	4.87	2.44	7.48
12	4.33	3.99	1.99	6.33
13	3.72	3.24	1.62	5.34
14	3.28	2.73	1.36	4.64
15	2.91	2.30	1.15	4.06
16	2.62	1.97	0.98	3.61
17	2.36	1.69	0.85	3.21
18	2.16	1.48	0.74	2.90
19	2.01	1.31	0.66	2.66
20	1.88	1.17	0.59	2.47
21	1.79	1.08	0.54	2.33
22	1.72	1.01	0.51	2.22
23	1.68	0.98	0.49	2.17
24	1.66	0.95	0.48	2.13
25	1.64	0.94	0.47	2.11

2.3.4 Blade Modal Analysis

BModes is a finite-element code that provides dynamically coupled modes for rotor blades and towers (G Bir, 2005). Although primarily developed for wind turbine

applications, by incorporating added mass and the core material, BModes can be successfully used on OCT blades. Specification of rotor speed, blade geometry, and the distribution of structural properties along the blade are required as inputs. These values were derived from PreComp and the modified output file. The program considers each blade as a flexible cantilevered beam with continuously distributed stiffness and mass in order to calculate the natural frequencies and mode shapes.

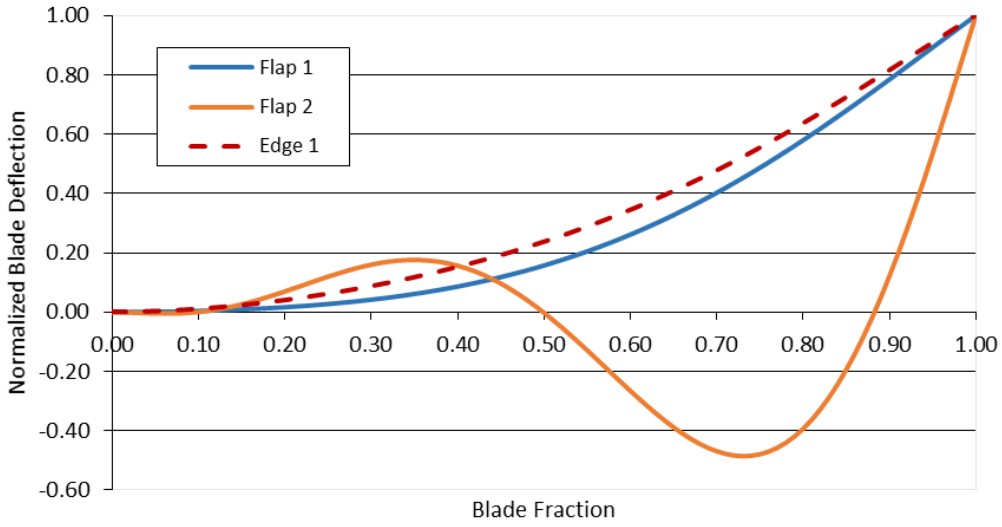

Figure 12: Blade Flap and Edgewise Mode Shapes

The output data from BModes is provided in Appendix B.2. The computed flap displacement is the modal displacement normal to the blade reference plane and the lag displacement is the modal displacement in the blade reference plane. These values must be represented as a normalized 6^{th} order polynomial for input to FAST. The NREL's ModeShape Workbook was used to calculate the normalized coefficients of each mode shape using the normalized projection method. The coefficients must sum to unity with the first two being equal to zero. Since the mode shapes are cantilevered at the root, the

deflection and slope must be zero at that point. The ModeShape Workbook results are plotted in Figure 12 and shown in Equations 13 to 15:

Flapwise mode 1:

$$y = 0.4240x^2 - 0.4472x^3 + 2.3125x^4 - 1.0963x^5 - 0.1930x^6 \quad \text{Eq. 13}$$

Flapwise mode 2:

$$y = -4.3539x^2 + 61.4626x^3 - 195.7783x^4 + 221.2758x^5 - 81.6062x^6 \quad \text{Eq. 14}$$

Edgewise mode 1:

$$y = 1.0854x^2 - 0.4865x^3 - 0.0642x^4 + 1.4427x^5 - 0.9773x^6 \quad \text{Eq. 15}$$

BModes computed the first flapwise, second flapwise, and first edgewise bending modes at 44 Hz, 140 Hz, and 224 Hz, respectively. An ANSYS modal analysis was completed in order to verify the BModes results. The block Lanczos algorithm was used with the sparse matrix solver in order to extract the blade mode shapes. The block Lanczos algorithm is a robust eigensolver that is compatible with the element types used in our model. First flapwise, second flapwise, and first edgewise bending modes were calculated at 54 Hz, 166 Hz, and 231 Hz. The small difference in frequency is likely due to exclusion of added mass from the ANSYS model. The flapwise bending mode 2 is displayed in Figure 13.

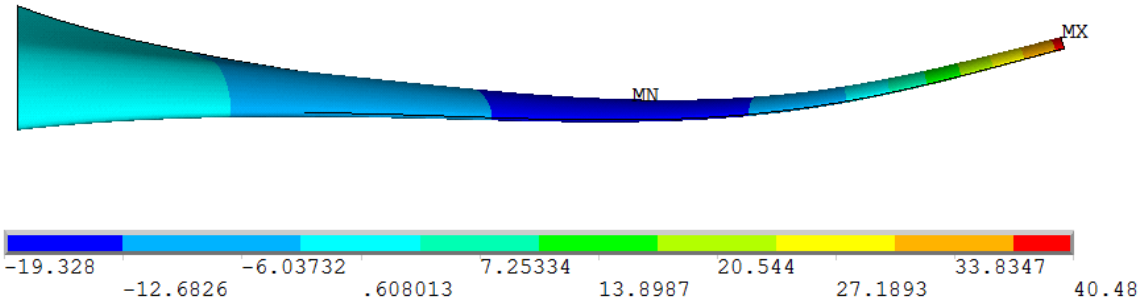

Figure 13: ANSYS Generated Flapwise Bending Mode 2

2.3.5 Buoyancy

The OCT blade is also subject to buoyancy under oceanic conditions, however, this is not considered in the simulation of FAST. Since FAST only accepts a constant gravitational acceleration, the average gravitational acceleration was calculated for the blade using Eq. 16.

$$g_A = \frac{m_B - m_W}{m_B + m_A} g \qquad \text{Eq. 16}$$

Where, g_A is the average gravitational acceleration, m_B is the mass of the turbine blade (skin and core), m_W is the mass of the displaced water, m_A is the blade added mass, and g is the gravitational acceleration. Using the blade data from Table 5 the gravitational reduction due to buoyant force was calculated to be 91% along the blade span. Therefore, the gravitational acceleration input was set to 0.865 m/s^2 (8.82% of 9.81 m/s^2) in FAST's primary input file. The data from Table 5 was calculated using blade volume.

Table 5: Blade Mass Properties

Blade Mass (Skin + Core)	6.71 kg
Mass of Displaced Water	5.86 kg
Blade Added Mass (Eq. 16)	2.93 kg

Blade buoyancy as a function of blade span is plotted in Figure 14 with a linear best fit trendline displayed. As depicted, the blade is negatively buoyant near the root, neutrally buoyant at one third of the blade radius, and becomes increasingly buoyant towards the tip. Previous studies have averaged the ratio of net blade gravity to total mass (Fang Zhou, 2013), but this results in a bias if the cross sectional areas are not distributed evenly. In addition, averaging does not properly account for the larger cross sections having more of an impact on buoyancy. As the blade fraction increases the cross sectional area decreases, this results in a negatively buoyant blade, despite the area under the trendline being positive.

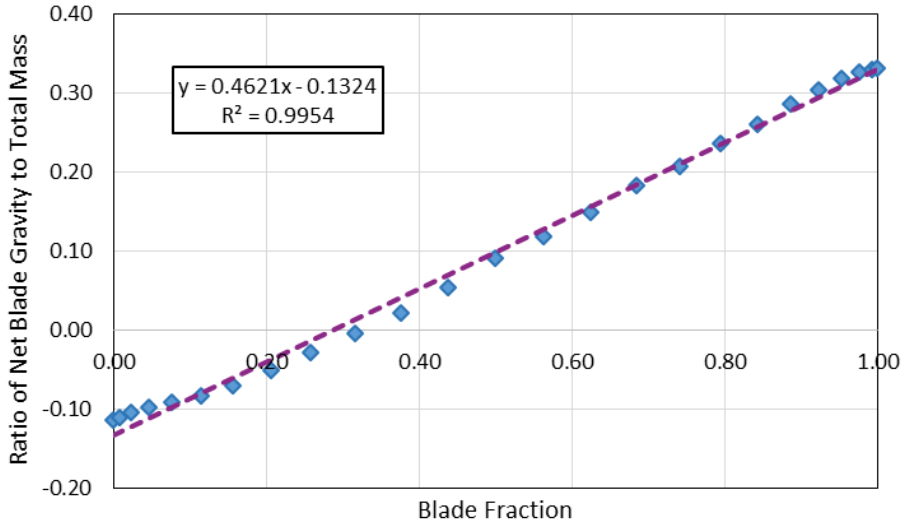

Figure 14: OCT Blade Buoyancy Distribution

2.4 Discussion

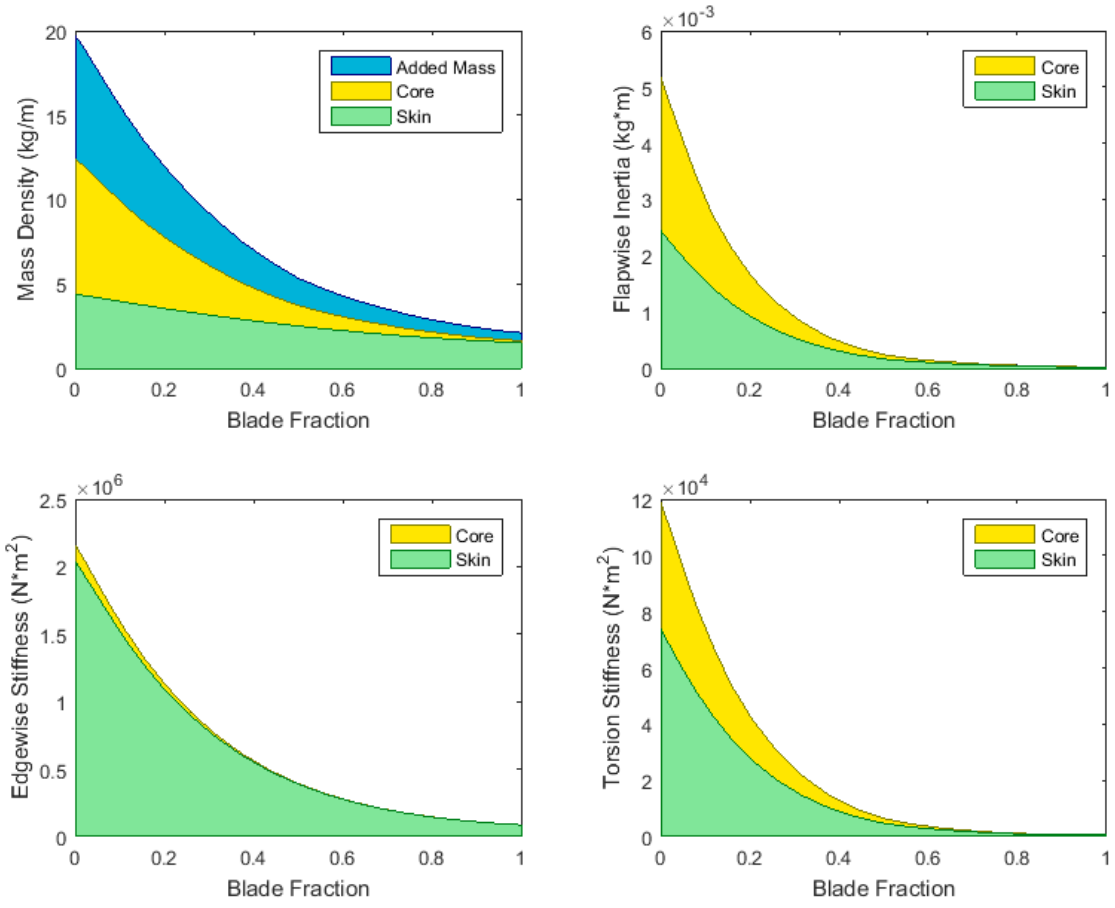

Figure 15: Effect of Added Mass and Core Inclusion

Figure 15 depicts the increase in mass density, flapwise inertia, edgewise stiffness, and torsional stiffness from the modified OCT design procedure. The hollow blade experiences an average blade mass density increase of 85% from core inclusion and a 91% increase from fluid acceleration. An average increase of 113% in flapwise inertia is contributed from the core. The blade edgewise stiffness is increased by a maximum of 5.9% at the blade root and on average the blade torsion stiffness increases by 67% after core inclusion. As illustrated by all four graphs in Figure 15, the core material has its

greatest impact near the root of the blade, due to the cross sectional area being highest at this position.

3. BLADE LOADING DUE TO RANDOM OCEAN CURRENT AND TURBULENCE

3.1 ADCP Measurements

In order to better understand the variability of the Florida Current, SNMREC has undertaken an observational program using long-term deployments of Acoustic Doppler Current Profilers (ADCPs) (Carolina et al., 2016). These systems transmit "pings" of sound at distinct and known frequencies into the water. As the sound waves travel, a small number ricochet off suspended particles and reflect back to the instrument. By calculating the Doppler shift, the instrument can determine how fast these particles and surrounding waters are moving (Gordon, 1996). By positioning upward-looking acoustic current profilers near the seafloor, it is possible to obtain the velocity distribution through the water column. The current profiles are measured and time averaged over a specified time interval in order to reduce noise. By using several of these profilers, variations over time and space can be inferred, analyzed, and assessed for OCT applications ("AVAILABLE DATA," 2014).

Table 6: ADCP Measurement Site History

Site	Location	Depth	Measurement Period
B1	26° 04' N, 79° 45' W	496m	February 2009 – March 2010
B2	26° 04' N, 79° 51' W	315m	May 2013 – April 2014
B3	26° 04' N, 79° 55' W	251m	November 2011 – April 2012
B5	26° 01' N, 79° 53' W	273m	May 2013 – April 2014
B6	26° 08' N, 79° 53' W	270m	May 2013 – April 2014

A map of the ADCP deployment locations is shown in Figure 16. Table 6 depicts the ADCP deployment history since 2009. The placement depths, latitude and longitude coordinates, and measurement periods are shown. These sites were selected to collect data from the western edge of the Gulf Stream to its core. On each site, the Teledyne RDI 75kHz Long Ranger Workhorse ADCPs were moored to the sea floor and mounted inside a 54" Flotation Technologies syntactic foam buoy. Each measurement bin had a spatial resolution of 5 meters and temporal resolution between 10 to 30 minutes depending on the measurement period. The bins near the transducer and sea surface were eliminated from the following analysis due to increased Doppler noise. This is caused by sidelobe interference and is identified by elevated standard deviation values (Nystrom, Rehmann, & Oberg, 2007).

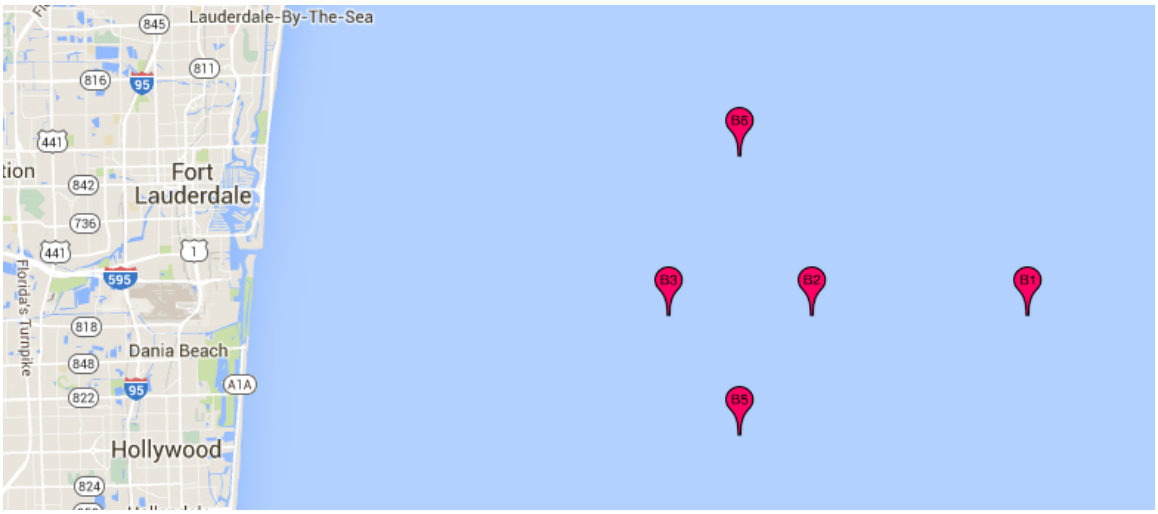

Figure 16: Map of SNMREC's Past ADCP Measurement Sites

3.2 Current Velocity Data

The most recently published ADCP datasets from SNMREC are B2, B5, and B6. In order to determine which location to use for OCT fatigue analysis, a probability mass histogram of ocean current magnitude has been developed. Figure 18 displays current magnitude distribution at the OCT placement depth of 50 meters below sea level. From this data it is clear that the ocean current velocity can be modeled by a Gaussian distribution at depths far from the surface and seafloor. This is because the wind effect is significant near the sea surface, and viscous effects are significant near the sea floor.

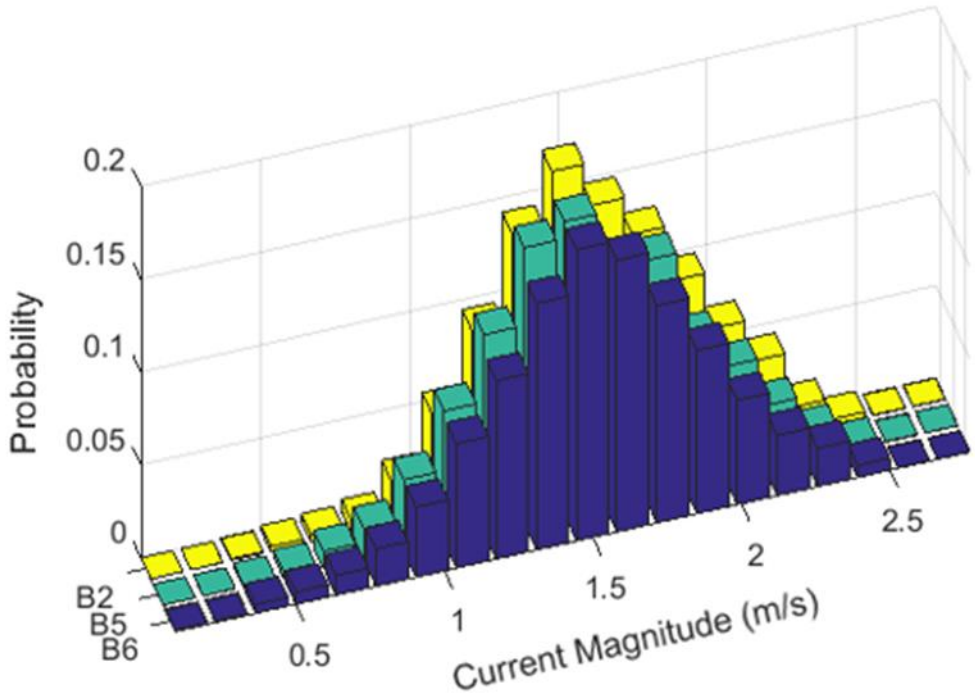

Figure 17: Probability Mass of Current Magnitude

B2, B5, and B6 have a mean current speed of 1.58, 1.53, and 1.54 m/s respectively. Out of the three locations, site B2 is the deepest and the closest to the Florida Gulf Stream core. Figure 17 shows that the bins with the highest current magnitude, Bins 11-20, have

the greatest probability of occurrence for site B2. Since higher current magnitudes will increase blade stress, the measurement data from site B2 was used as an aggressive location for our blade fatigue analysis. This will result in a more conservative blade life.

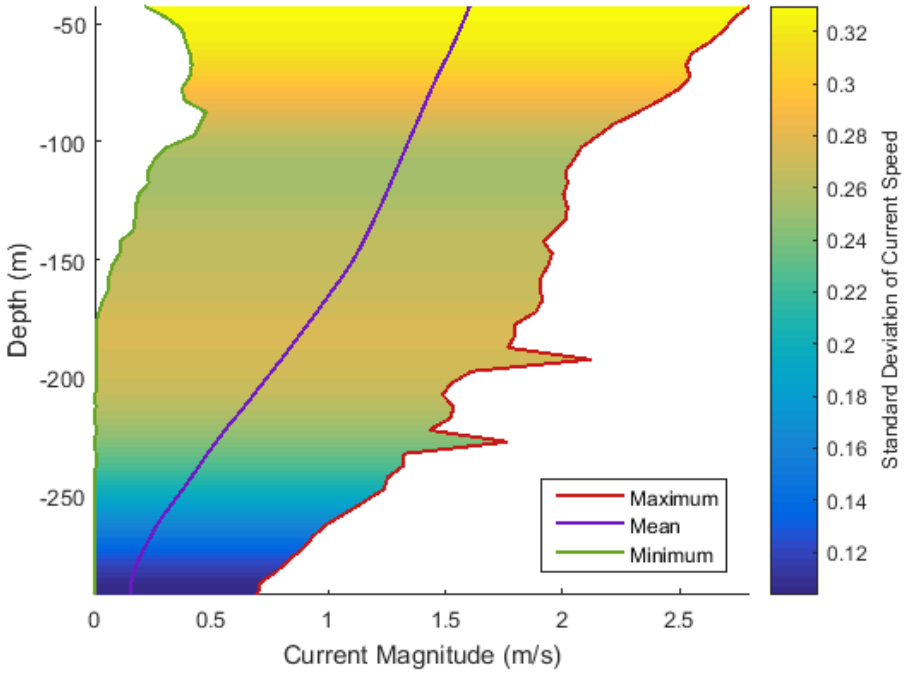

Figure 18: Analysis of ADCP Data from Site B2

The current magnitude distribution for site B2 is shown in Figure 18 as a function of depth. This figure gives insight into the velocity shear along the water column. We notice that the current speed range and standard deviation are highest near the sea surface. As depth increases the mean velocity decreases and the variability of current magnitude is reduced.

3.3 Rainflow Counting

The most widely used counting method for fatigue is the rainflow counting (RFC) algorithm. It was first introduced by Endo (Endo, Mitsunaga, & Nakagawa, 1967) and its complex sequential structure decomposes arbitrary sequences of loads into cycles. Typically, to compute a life estimate from a given structural stress input, the RFC method is applied by counting cycles and extrema, followed by Palmgren-Miner's rule, to calculate the expected damage.

The purpose of the RFC algorithm is to identify the closed hysteresis loops in the stress signals. By associating the values to individual cycles or hysteresis loops, one assumes that the underlying process is rate independent, implying that the hysteresis loops themselves are important, not the speed with which they are traversed. Therefore, in the case of damage, it does not matter how fast the stress occurs, but rather its magnitude. The

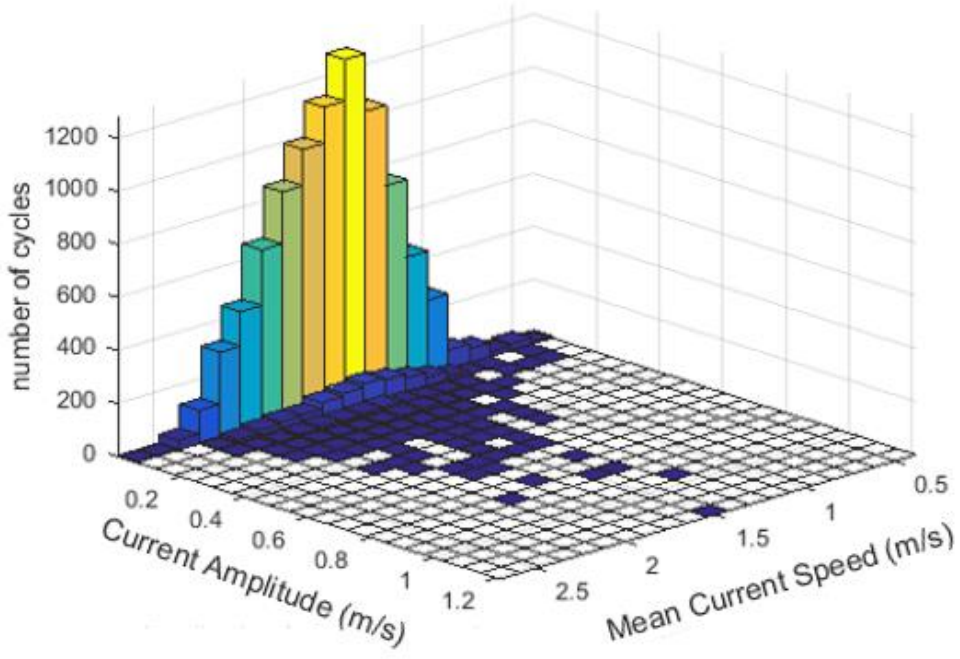

Figure 19: Rainflow Counted Distribution of Site B2 at -50m

velocity time history at site B2 was analyzed using the RFC method, as specified in ASTM Standard E1049-85 (ASTM, 2011). Although originally applied to metals, its use for composite materials has been observed (Manwell et al., 2009).

The 3D histogram of rainflow counted data at site B2 50 meters below sealevel, is depicted in Figure 19. The number of cycles at each mean current speed follows a normal distribution, but the cycle count rapidly decays as amplitude increases. Although there are very few large amplitude current intensities, these will likely cause significant damage to the blade.

3.4 Ocean Current Turbulence

A complete characterization of Gulf Stream turbulence would require observations in time and space spanning orders of magnitude that are unrealistic with current technology. In order to properly sample, a large array of instruments would need to be sampling with high temporal frequency over a long period of time. Without such instrumentation, a method is needed to add turbulence to ADCP data.

In this study, NREL's TurbSim (B. J. Jonkman & Kilcher, 2012a) was used to simulate turbulence data in the Gulf Stream. TurbSim contains a tidal spectral model that is tailored to marine and hydrokinetic (MHK) energy. The tidal channel turbulence model chosen uses a logarithmic velocity profile for MHK models. The logarithmic mean current velocity profile calculates the average flow speed at height z using Eq. 17

$$\bar{u}(z) = \frac{U_*}{\kappa} \ln\left(\frac{z}{z_{\text{Ref}}}\right) + U_{\text{Ref}} \qquad \text{Eq. 17}$$

Where, $\kappa = 0.41$ is the von Karmon constant, *z* is the depth, U_{Ref} is the reference velocity at z_{Ref}, and $U_* = 0.05U_{\text{Ref}}$ is the friction or shear velocity averaged over the rotor disk.

The mean Reynolds stresses at the rotor hub shown in Eq. 18:

$$PC_{UW} = -U_*^2\left(1-\frac{H_H}{H_{\text{Ref}}}\right) \qquad \text{Eq. 18}$$

Where, H_H is the hub height and H_{Ref} is the reference height at which U_{Ref} is measured.

The spectral model used defines velocity spectra using the local height and current speed. The spectral amplitude is scaled directly with the turbulent kinetic energy (TKE) and shear of the flow as shown in Eq. 19 (B. J. Jonkman & Kilcher, 2012b)

$$S_u(f) = \frac{\sigma_u^2 s_{1,u}\left(\frac{\partial u}{\partial z}\right)^{-1}}{1+s_{2,u}\left(\frac{f}{\partial u/\partial z}\right)^{5/3}} \qquad \text{Eq. 19}$$

Where, the empirically determined coefficients are $s_{1,u} = 1.21$ and $s_{2,u} = 4.30$ for frequency, *f*, and the shear, $\partial u/\partial z$, is in hertz. The shear is calculated internally from the logarithmic velocity profile and is proportional to *u/z*. The TKE level is determined based on the following exponential profile shown in Eq. 20.

$$\sigma_u^2 = 4.5U_*^2 \exp\left(\frac{-2z}{H_{\text{Ref}}}\right) \qquad \text{Eq. 20}$$

The International Electrotechnical Commission's (IEC) standard metric for quantifying the level of turbulence at wind energy sites is the turbulence intensity (T.I.) (IEC, 2005). Turbulence intensity I_u, is the ratio of the standard deviation of the velocity to the mean, with a noise-corrected term subtracted for acoustic Doppler measurements. It is defined as shown in Eq. 21.

$$I_u = \frac{\sigma_u}{\bar{u}} = \frac{\sqrt{\bar{u}'^2 - n^2}}{\bar{u}} \qquad \text{Eq. 21}$$

Where, the overline indicates a 15 minutes average (McCaffrey, Fox-Kemper, Hamlington, & Thomson, 2015). The turbulence intensity was adjusted by altering H_{Ref} and U_{Ref}.

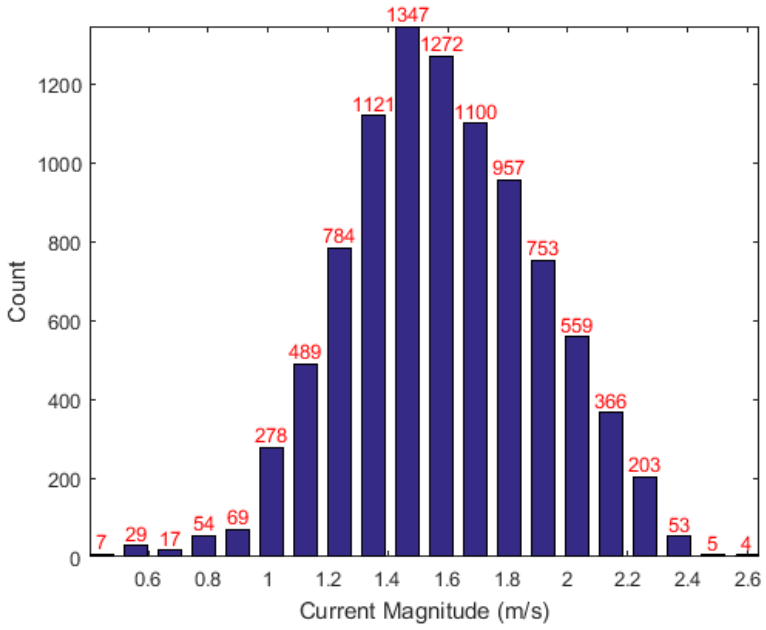

Figure 20: Distribution of 20 Turbulence Bins

The rainflow counted ADCP data was converted into 20 turbulence bins shown in Figure 20. TurbSim was then run at each of the 20 mean velocities. Since a turbulence characterization has not yet been completed by SNMREC, preliminary estimates of 5%

and 7.5% turbulence intensity were used. Figures 21 and 22 display plots of the current velocity at bin 10 and bin 20 with a turbulence intensity of 5% and 7.5% respectively.

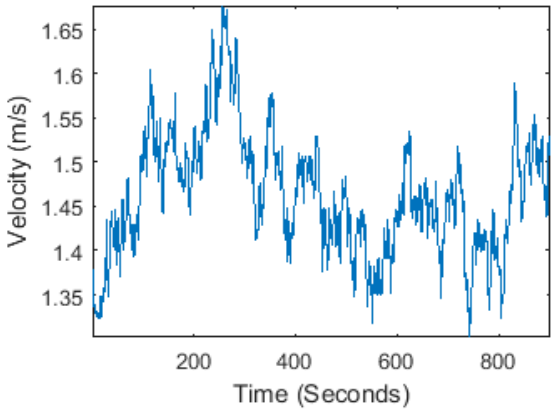

Figure 21: Bin 10 with 5% I_u

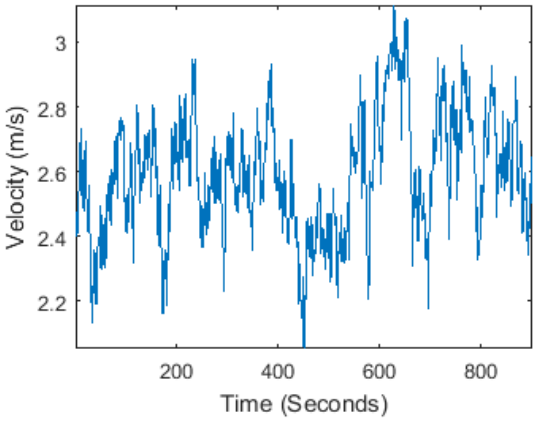

Figure 22: Bin 20 with 7.5% I_u

Lüscher's level 3 "Luxury Pseudorandom Numbers" (RanLux) (Lüscher, 1994) were used to generate the turbulent time histories in this fatigue analysis. The RanLux pseudorandom number generator (pRNG) is based on a subtract-and-borrow algorithm with a period in the order of 10171 and is modified by throwing numbers away to destroy correlations (James, 1994). A random seed between -2147483648 and 2147483647 was used for each of the 20 turbulence bins. Figures 23 and 24 show an example of how the distributions differ between seeds.

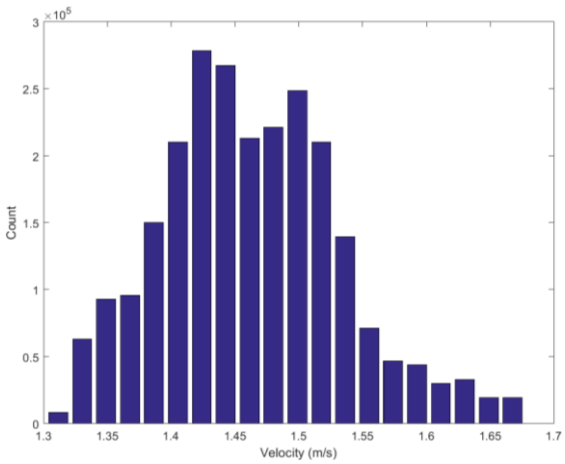

Figure 23: Bin 10 Histogram at 5% I_u

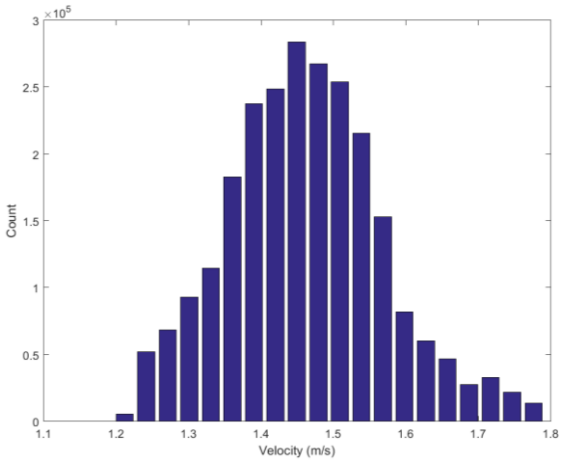

Figure 24: Bin 10 Histogram at 7.5% I_u

Next, rainflow counting was carried out on the turbulence data at each bin and intensity level. The results were then added to the initial rainflow counted ADCP data as shown in Figure 25 and 26. It is evident that the current amplitude increases with higher turbulence intensity.

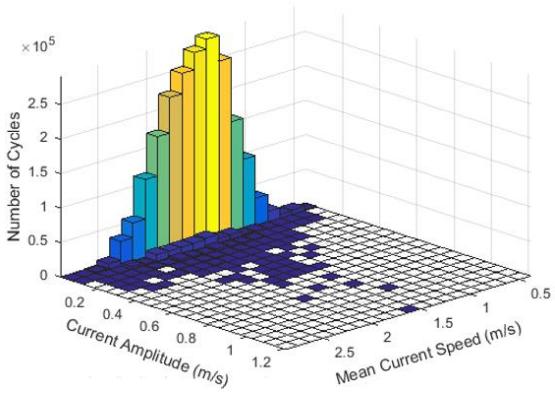

Figure 25: RFC at 5% Turbulence Intensity

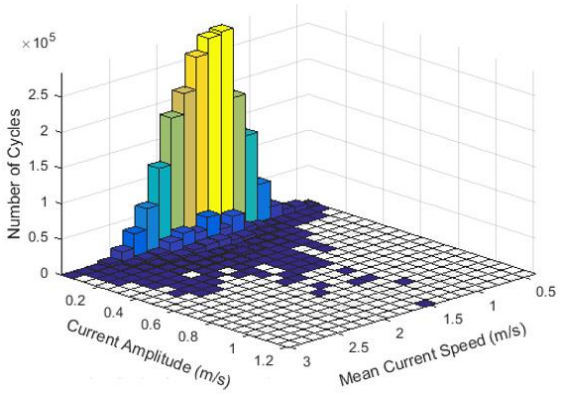

Figure 26: RFC at 7.5% Turbulence Intensity

3.5 Hydroelastic Simulation

NREL's FAST (Fatigue, Aerodynamics, Structures, and Turbulence) code is an aeroelastic simulator capable of predicting both extreme and fatigue loads in horizontal axis wind turbine blades. FAST uses an assumed-modes approach that takes into consideration the blade modes and structural properties in order to compute modal integrals for its equations of motion (Jason M Jonkman & Buhl, 2005). The results generated from PreComp provide the blade structural properties and the output from BModes is used to extract the three blade mode shapes. FAST uses uncoupled modes for flapwise and edgewise degrees of freedom. The BModes-computed flap, lag, and torsion coupled modes implicitly account for the torsional DOFs, shear center, tension center, and center of mass (Gunjit Bir, 2010). The structural model of FAST considers the blades to be flexible cantilevered beams with continuously distributed mass and stiffness.

AeroDyn gathers information about the turbine geometry, operating conditions, blade velocity, and element locations from the input files (David & Hansen, 2002). This information is used to calculate the distributed forces and corresponding deflection of the turbine blades. Sea water conditions such as fluid viscosity, fluid density, blade buoyancy, and blade added mass were also taken into consideration by AeroDyn and FAST. The integration time step is specified in FAST by the user. AeroDyn is called by FAST at each time step in order to calculate the changing hydrodynamic forces on each blade element. (Moriarty & Hansen, 2005). The equations of motion, including the inertial and structural properties are then used to calculate the response to these loads.

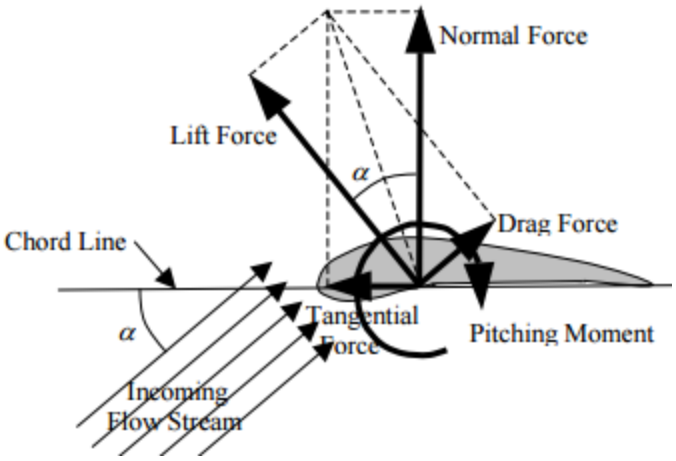

Figure 27: Normal and Tangential Loading Relations (J M Jonkman, 2003)

The normal and tangential forces are also calculated and passed back to the dynamic routine. The normal force is the component of the net force acting normal to the plane of rotation and the tangential force is the component of the net force acting tangential to the plane of rotation. These characteristics are shown in Figure 27 (J M Jonkman & Buhl, 2004).

Output files are generated by FAST and AeroDyn with data being printed at an interval specified by the user. The primary FAST output file includes the time series, ocean current velocity, blade tip deflections, rotor power, and flap and edgewise shear force and moment at the blade root. The AeroDyn output file is a tab-delimited time series containing, but not limited to the dynamic pressure, coefficient of lift and drag, pitch angle, Reynolds number, and normal and tangential force for each blade element selected (Fang Zhou, 2013).

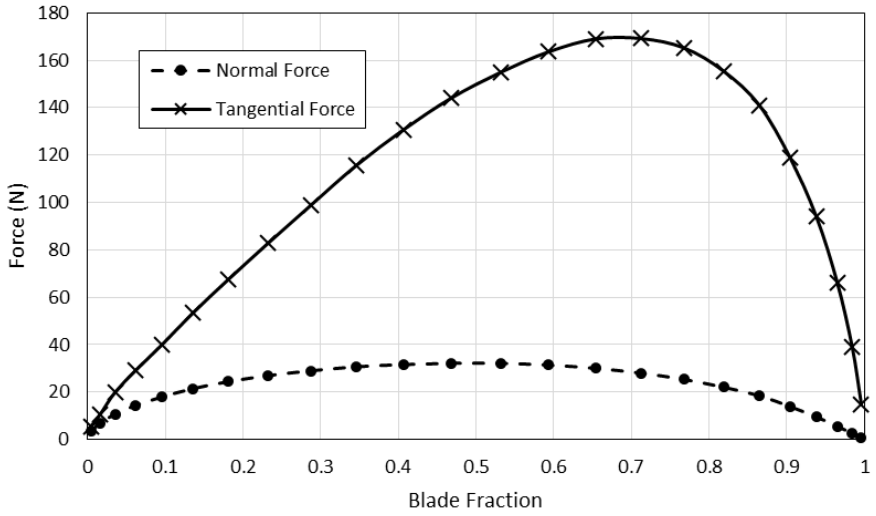

Figure 28: Normal and Tangential Forces at Bin 10 (1.55 m/s)

Each simulation subjected the OCT blade to a steady ocean current speed, without velocity shear. In the FAST primary input file, the time-marching simulation was selected for OCT analysis without any pitch control and with a fixed rotation speed of 50 rpm. The blade DOFs were enabled and all other DOFs, such as tower, yaw, and generator DOFs, were disabled. The normal and tangential loading at load step 10 with a current magnitude of 1.55 m/s is illustrated in Figure 28. The normal and tangential loads over the entire current magnitude range of site B2 are shown in Figure 29 and 30 respectively. The normal force is greater than the tangential along the blade span. This indicates that flapwise bending is the primary cause of fatigue damage.

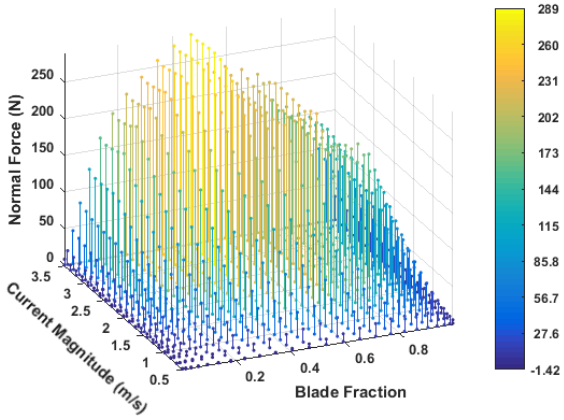

Figure 29: Normal Force Output of AeroDyn

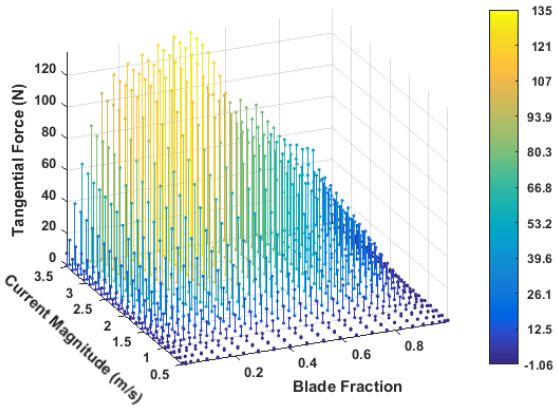

Figure 30: Tangential Force Output of AeroDyn

4. BLADE LOADING AND FATIGUE ANALYSIS

4.1 Coupling with ANSYS

The SolidWorks model of the blade skin and core was imported into ANSYS in order to perform a static structural analysis. The blade skin was meshed using 2-D shell elements (SHELL181) with 4-nodes, shown in Figure 32. Simulations with shell elements are more efficient because they provide a more accurate stiffness than a solid representation of a thin section and do not require multiple elements through the thickness. This results in less nodes and faster runtimes. Figure 31 illustrates the stacking sequence and orientation used within the shell. Material 2 is the unidirectional carbon/epoxy and material 3 is the

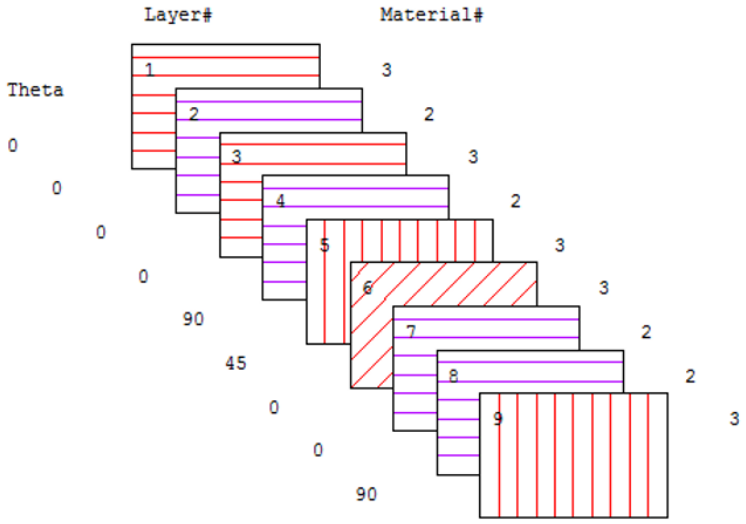

Figure 31: Ply Orientation in Shell Element 181

woven twill carbon/epoxy defined in Table 2. Mapped area meshing was used on the blade surface with hex-dominant conditions in order to generate uniform shell elements. The

blade core was defined using 3-D structural solid elements (SOLID186) with 20-nodes, shown in Figure 33. The blade core was filled with solid elements that were swept along the blade span.

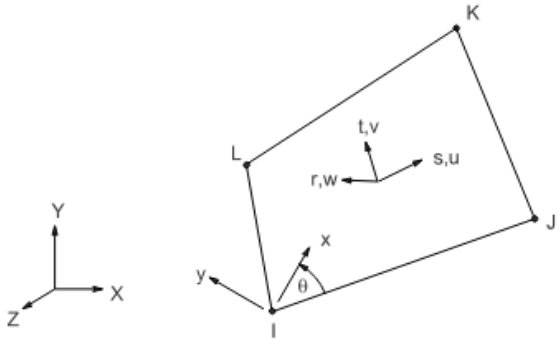

Figure 32: Shell181 Element

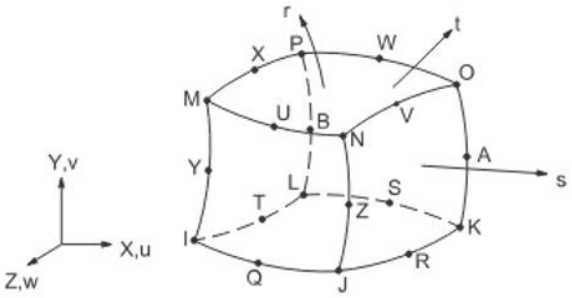

Figure 33: Solid186 Element

The number of elements in the model was 22,407, and the number of nodes was 64,031. The hydrodynamic loads calculated by the modified OCT codes at each hydrofoil cross section, were applied to nearest node of the quarter chord as shown in Figure 34. The hydrodynamic loads have two components: F_N is the force normal to the rotational plane, and F_T is the force tangential to the direction of rotation. At the blade root section, all the degrees of freedom were constrained.

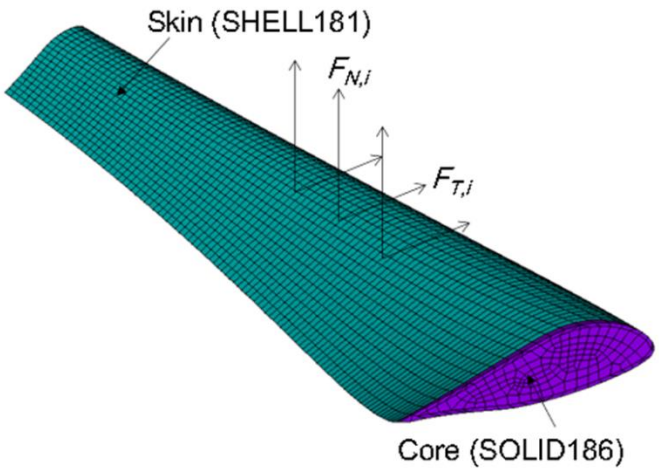

Figure 34: Finite Element Model of the OCT Blade

Figure 35 shows the deformation of the OCT blade under an ocean current speed of 1.55 m/s, and Figure 36 displays a comparison of the blade tip deflection calculated by FAST and ANSYS. The tip deflections from the two methods were found to be almost identical over the range of 0.35 m/s to 1.70 m/s. A maximum difference of 4.1% is observed at velocities greater than 1.70 m/s. Therefore, it was demonstrated that the properties of the core were successfully implemented into the BEM theory. At 2.0 m/s a decrease in the hydrodynamic load is due to stall, which makes the velocity-stress relationship nonlinear.

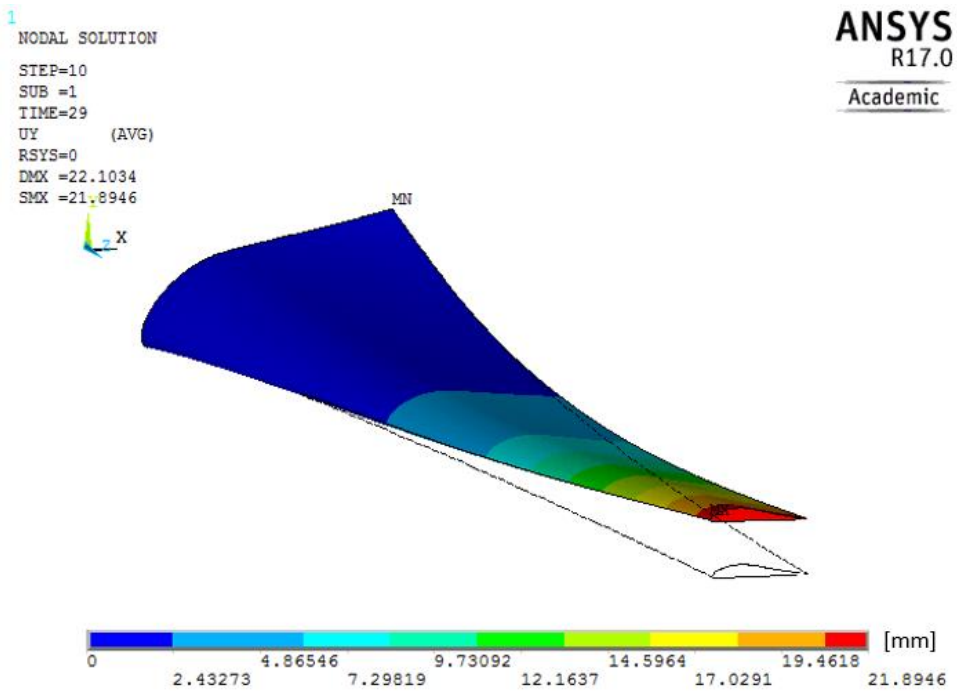

Figure 35: Blade deformation with Undeformed Edge

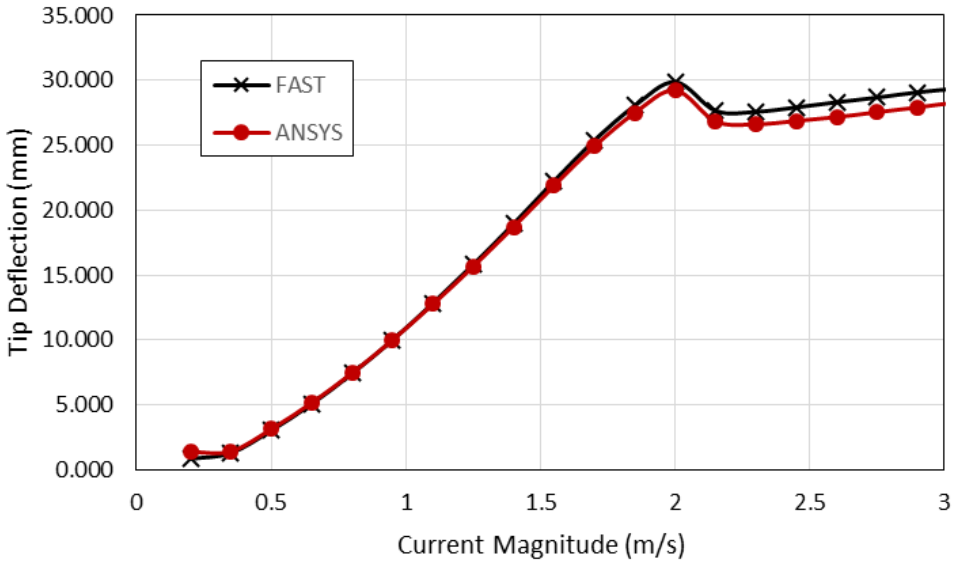

Figure 36: Comparison of Tip Deformation between FAST and ANSYS

4.2 Blade Failure Analysis

The Tsai-Wu failure criterion was selected in order to calculate OCT skin failure. Tsai-Wu has been widely used in calculating composite material failure and is based on a simplification of general failure theory for anisotropic materials first proposed by Gol'denblat and Kapnov (S. W. Tsai & Wu, 1971). It is capable of predicting strength under 18 general states of stress even if there is no experimental data available. The concept of strength tensors is used in order to transform from one coordinate system to another (Rahman, 2013).

$$F_1\sigma_1+F_2\sigma_2+F_3\sigma_3+F_4\sigma_4+F_5\sigma_5+F_6\sigma_6+F_{11}\sigma_1^2+F_{22}\sigma_2^2+F_{33}\sigma_3^2+F_{44}\sigma_4^2+F_{55}\sigma_5^2+F_{66}\sigma_6^2 + 2F_{12}\sigma_1\sigma_2+2F_{13}\sigma_1\sigma_3+2F_{23}\sigma_2\sigma_3 \le 1 \quad \text{Eq. 22}$$

$$F_1=\frac{1}{\sigma_{1t}}-\frac{1}{\sigma_{1c}};\quad F_2=\frac{1}{\sigma_{2t}}-\frac{1}{\sigma_{2c}};\quad F_3=\frac{1}{\sigma_{3t}}-\frac{1}{\sigma_{3c}};\quad F_4=F_5=F_6=0$$
$$F_{11}=\frac{1}{\sigma_{1c}\sigma_{1t}};\quad F_{22}=\frac{1}{\sigma_{2c}\sigma_{2t}};\quad F_{33}=\frac{1}{\sigma_{3c}\sigma_{3t}};\quad F_{44}=\frac{1}{\tau_{23}^2};\quad F_{55}=\frac{1}{\tau_{31}^2};\quad F_{66}=\frac{1}{\tau_{12}^2} \quad \text{Eq. 23}$$

Where, $\sigma_{1t},\sigma_{1c},\sigma_{2t},\sigma_{2c},\sigma_{3t},\sigma_{3c}$ are the failure strengths in uni-axial tension and compression in the three directions of anisotropy. $\tau_{12},\tau_{23},\tau_{13}$ are the shear strengths in the three planes of symmetry. $\sigma_1,\sigma_2,\sigma_3$ are the normal stresses and $\sigma_4,\sigma_5,\sigma_6$ are the shear stresses in the three directions. Failure will occur if the failure index $I_F \ge 1.0$. Figure 30 displays the Tsai-Wu failure plot generated by ANSYS using the materials strengths from Table 7.

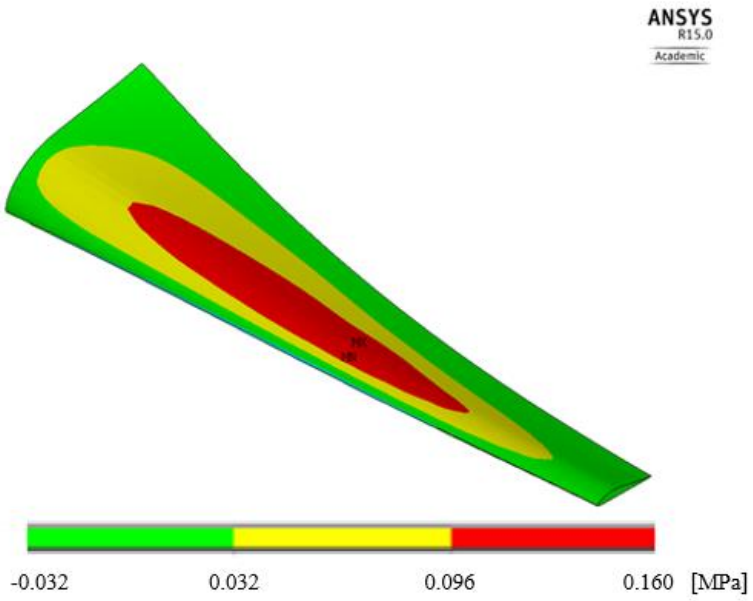

Figure 37: Tsai-Wu Failure in Composite Skin

The max stress criteria uses the max ratio of stress and strength in the failure calculation. As shown in Figure 38, the failure index reaches unity in the core material first, therefore fatigue life will be based on the blade core properties.

Table 7: Strength of Carbon/Epoxy Composites (Daniel & Ishai, 2005)

Properties (MPa)	σ_{1t}	σ_{2t}	σ_{3t}	σ_{1c}	σ_{2c}	σ_{3c}	τ_{12}
Carbon/Epoxy	2280	57	57	1725	228	228	76

Table 8: Strength of Syntactic Foam (Ferreira, Salviano, Costa, & Capela, 2010)

Material	Ultimate Shear Strength (MPa)[1]	Ultimate Flexure Strength (MPa)[2]
Syntactic Foam	6.07	41.3

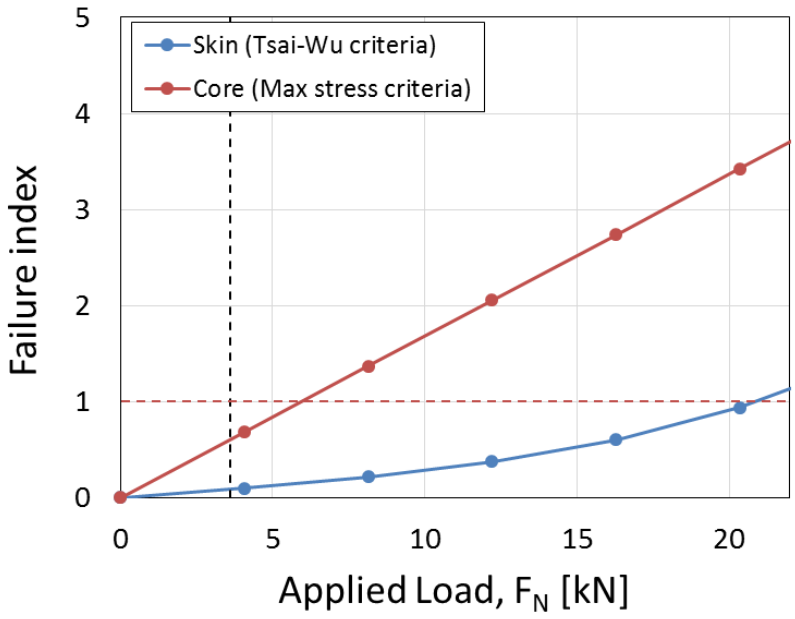

Figure 38: Failure Analysis based on Maximum Stress and Tsai-Wu Criteria

4.3 Calculation of Cumulative Fatigue Damage

Using the core stress values at each velocity load step, the rainflow counted current speed data can be converted to mean and alternate stresses. These stresses were then converted to their equivalent stress values at a particular stress ratio using the Goodman diagram described by Eq. 24 and Figure 39 (Suzuki et al., 2015).

$$\sigma_a = \sigma_w \left(1 - \frac{\sigma_m}{\sigma_t}\right) \qquad \text{Eq. 24}$$

Where, σ_m and σ_a are the mean and alternate stresses, σ_t is the tensile strength, and σ_w is the fatigue strength at R=-1.0. A pair of σ_m and σ_a on the Goodman diagram has a constant fatigue life, therefore, it is called as constant life diagram (CLD). Several CLD models have been proposed (Vassilopoulos, Manshadi, & Keller, 2010), however, the Goodman diagram was used in the present study for its simplicity.

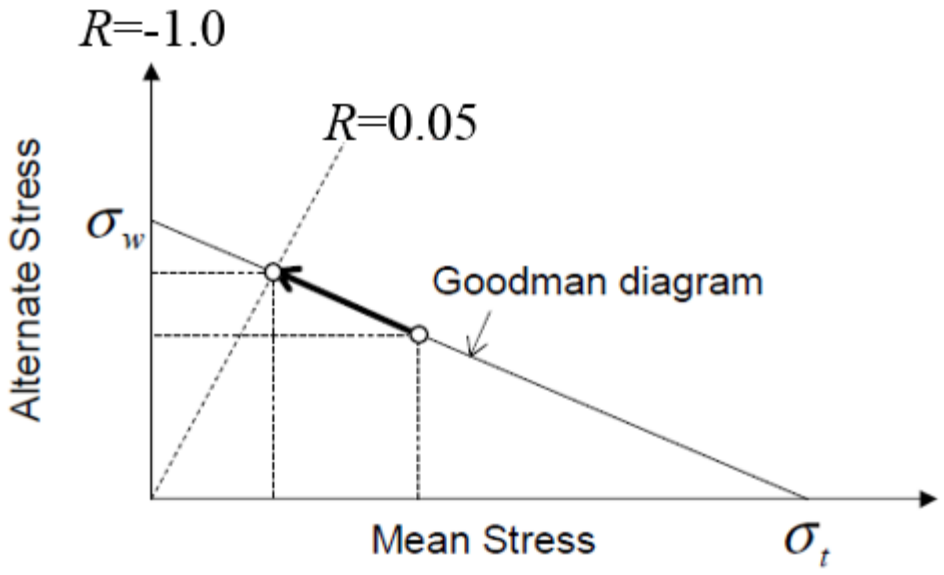

Figure 39: Equivalent Stress Conversion using the Goodman Diagram

Equivalent stress conversion was carried out at *R*=0.05 since the following S-N diagram was obtained at this stress ratio. The effective mean and alternating stress values were converted to a stress ratio of 0.05 using Eq. 25 to 27 (Campbell, 2008).

$$\sigma_a' = \sigma_m' \left(\frac{1-R}{1+R} \right) \quad \text{Eq. 25}$$

$$\sigma_m' = \frac{\sigma_w}{\left(\frac{1-R}{1+R} \right) + \frac{\sigma_w}{\sigma_t}} \quad \text{Eq. 26}$$

$$\sigma_{\max}' = \sigma_m' + \sigma_a' \quad \text{Eq. 27}$$

Where, σ_m' is the effective mean stress, σ_a' is the effective mean alternate stress, and σ_{max}' is the maximum effective stress.

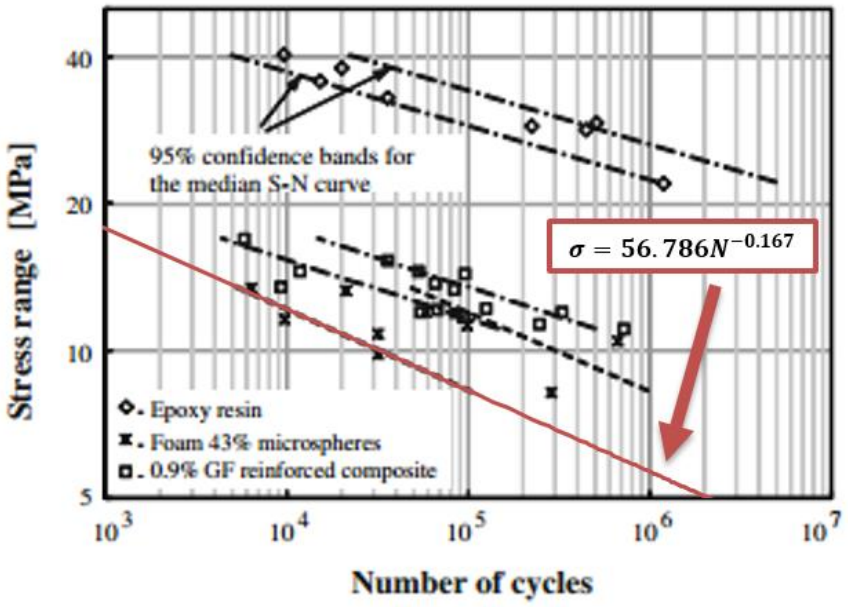

Figure 40: S-N Diagram for Blade Core (Ferreira et al., 2010)

Figure 40 shows the S-N diagram used for fatigue life estimation at site B2 at a depth of 50 meters (Ferreira et al., 2010). Finally, the cumulative fatigue damage over the measurement period was calculated using the S-N curve of the material and Palmgren-Miner's rule described by Eq. 28 (Miner, 1945);

$$D = \sum_{i=1}^{k} D_i = \sum_{i=1}^{k} \frac{n_i}{N_i} \qquad \text{Eq. 28}$$

Where, D is the cumulative fatigue damage, D_i is the damage at a particular stress range, n_i is the number of cycles, and N_i is the fatigue life. The fatigue failure is expected to occur when D reaches unity.

4.4 Results and Discussion

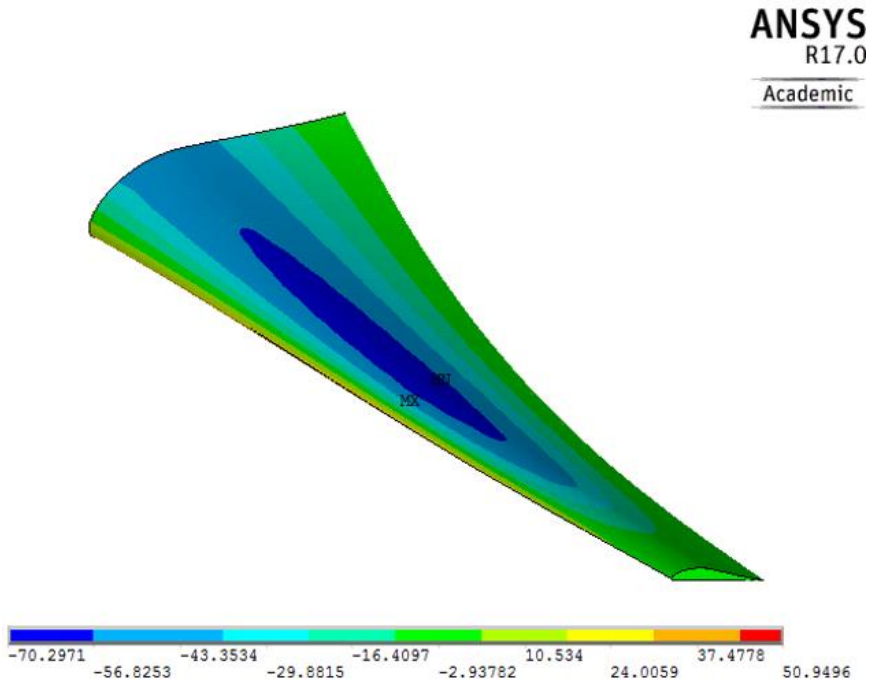

Figure 41: Longitudinal Stress Distribution of Blade Skin (Top Layer) at 2.75 m/s

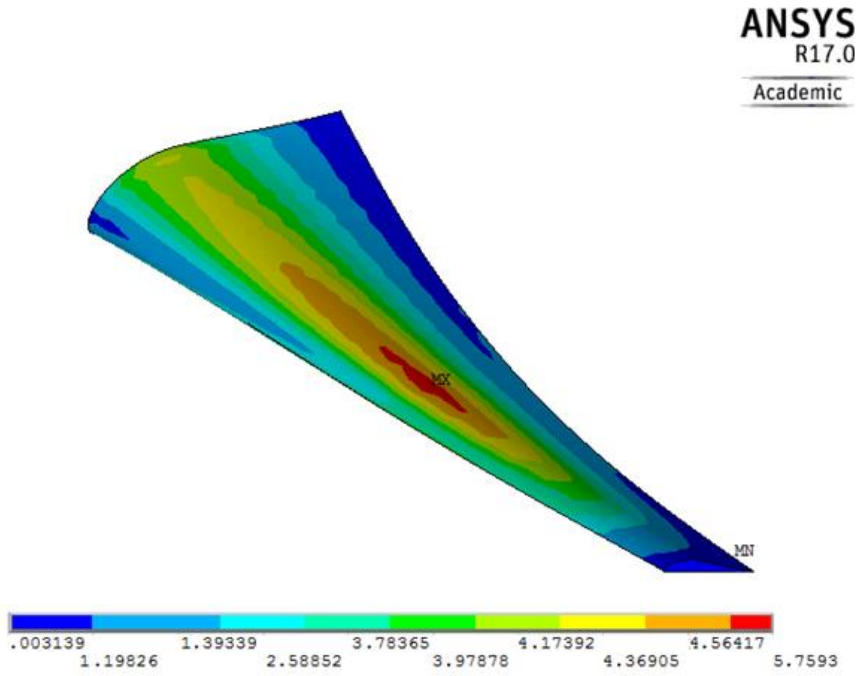

Figure 42: Mises Stress Distribution on Blade Core Surface at 2.75 m/s

Figure 41 and 42 show the stress distributions of the skin and core under a current magnitude of 2.75 m/s. Flapwise bending is seen to be dominant under these conditions. High compressive stress is seen at the skin root and near the blade mid-span. The maximum stresses of the core was used to calculate the cumulative fatigue damage.

Table 9: Blade Core Fatigue Life Comparison

Velocity Model	Fatigue Life: Foam Core
ADCP	18.74 years
ADCP + 5% T.I.	18.51 years
ADCP + 7.5% T.I.	14.06 years

The S-N diagram for syntactic foam and the maximum core stress distribution, were used in conjunction with the Goodman diagram and Miner's rule to calculate fatigue damage. Table 9 shows the fatigue life of the core considering 0%, 5%, and 7.5% turbulence. As the turbulence intensity increases, we notice an exponential decay in blade core life. From this investigation, we see that a turbulence intensity of 5% or less does not damage the blade core significantly. On the other hand, at turbulence intensity levels of 7.5% or greater, the core experiences a large increase in damage. This result indicates the need for a turbulence characterization at the blade placement depth.

5. STATISTICAL ANALYSIS OF BLADE JOINT FATIGUE STRENGTH

In this section, a statistical method is described to evaluate blade joint reliability and fatigue strength. All specimen manufacturing and testing was carried out by Japan's IHI Corp. The intended use for this adhesive, is to connect the skin and shear web of IHI's OCT blade. A reliability assessment is especially important when dealing with a limited number of specimens. In order to assess the reliability of small data sets, a Weibull analysis has traditionally been used since Professor Weibull's publication of "A Statistical Distribution Function of Wide Applicability" in 1951 (Waloddi Weibull, 1951). The Weibull parameters provide information for classifying failure modes and offer insight in regards to increasing reliability. The two parameter Weibull is therefore, used in this study to carry out the statistical analysis. A reliability analysis has also been performed in order to estimate S-N relations for any desired level of reliability.

5.1 Application to Static Joint Strength

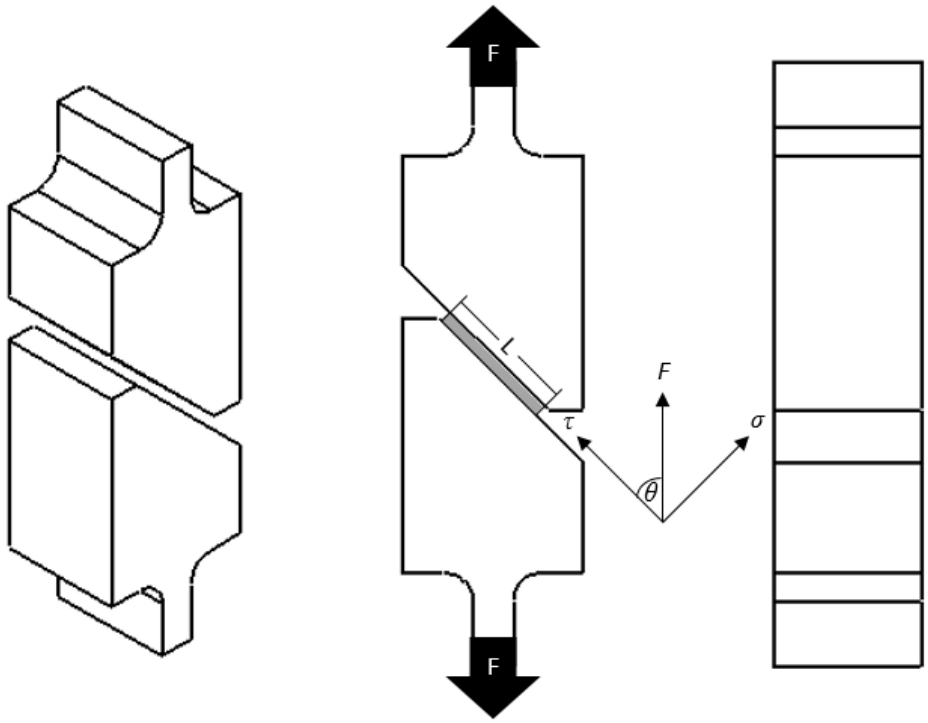

Figure 43: Specimen Test Configuration

Edge-loaded specimens, as shown in Figure 43, were used for all monotonic tensile and fatigue experiments. Due to export controls and technical data restrictions, all specimen dimensions have been removed. Tensile tests were conducted at three angles, 0°, 26.6° and 45°, with 5 specimens loaded at each angle. The adhesive was applied to area L^2 with a thickness of 1 mm. The force applied to each specimen has been normalized with respect to the maximum load at each angle and the resulting stresses have been normalized with respect to the maximum von Mises Stress at each angle.

Table 10: Static Adhesive Joint Experimental Data

Specimen ID	Angle	Maximum Normalized			
		Force	Shear Stress	Normal Stress	Von Mises Stress
S1-1	0.0°	0.9670	0.5553	0.0000	0.9619
S1-2	0.0°	0.9756	0.5623	0.0000	0.9739
S1-3	0.0°	0.9928	0.5736	0.0000	0.9934
S1-4	0.0°	0.9928	0.5720	0.0000	0.9907
S1-5	0.0°	1.0000	0.5774	0.0000	1.0000
S2-1	26.6°	0.8546	0.4724	0.2366	0.8517
S2-2	26.6°	0.9312	0.5207	0.2608	0.9389
S2-3	26.6°	0.9701	0.5380	0.2694	0.9699
S2-4	26.6°	0.9844	0.5474	0.2741	0.9870
S2-5	26.6°	1.0000	0.5546	0.2777	1.0000
S3-1	45.0°	0.9546	0.4810	0.4810	0.9620
S3-2	45.0°	0.9697	0.4873	0.4873	0.9747
S3-3	45.0°	0.9794	0.4937	0.4937	0.9873
S3-4	45.0°	0.9945	0.4966	0.4966	0.9932
S3-5	45.0°	1.0000	0.5000	0.5000	1.0000

In order to describe the probability of survival, the two parameter Weibull reliability function shown in Eq. 29 was used with the location parameter being zero. (Nelson, 2004).

$$R(N) = \exp\left[-\left(\frac{N}{\beta}\right)^{\alpha}\right] \qquad \text{Eq. 29}$$

Where, N is the strength for static tests, and life cycle number for fatigue tests, α is the shape parameter of the distribution, and β is the scale parameter. α, β, and N are always

positive. The Cumulative Distribution Function (CFD) *F(N)* in Eq. 30, describes the fraction of the population that will fail by the given stress or cycle number *(N)*.

$$F(N) = 1 - R(N) \qquad \text{Eq. 30}$$

Although the Weibull analysis is extremely flexible in fitting data, estimation of its parameters is not easy. Various techniques, including, Probability plotting, Hazard plotting, Maximum likelihood, and Linear estimation, are usually employed to estimate α and β (Mahfuz, Maniruzzaman, Vaidya, Brown, & Jeelani, 1997). Traditionally, the Maximum Likelihood method has been used for fatigue analysis, since it allows for runout specimen and the confidence intervals of α and β can be easily computed (Goglio & Rossetto, 2004).

The Maximum Likelihood equation in absence of the location parameter can be written as:

$$\frac{\sum_{i=1}^{n} N_i^{\alpha} \ln N_i}{\sum_{i=1}^{n} N_i^{\alpha}} - \frac{1}{\alpha} - \frac{\sum_{i=1}^{n} N_i}{n} = 0 \qquad \text{Eq. 31}$$

and

$$\beta = \left[\frac{1}{n} \sum_{i=1}^{n} N_i^{\alpha} \right]^{1/\alpha} \qquad \text{Eq. 32}$$

Where N_i is the stress or fatigue life cycles for order *i*, and *n* is the number of failures.

Table 11: Weibull Characterization of Static Adhesive Joint Data

Angle	Max Mises Stress	Shape Parameter α	Scale Parameter β	Arithmetic Average	R(N)
0°	0.962	91.25	0.99	0.98	0.934
	0.974				0.808
	0.993				0.270
	0.991				0.360
	1.000				0.092
26.6°	0.852	26.50	0.97	0.95	0.970
	0.939				0.671
	0.970				0.389
	0.987				0.223
	1.000				0.120
45°	0.962	90.54	0.99	0.98	0.927
	0.975				0.780
	0.987				0.450
	0.993				0.257
	1.000				0.080

The reliability, $R(N)$, for each test is shown in Table 11 using Eq. 29. The variation of $R(N)$ is another way of assessing the probability of survival. It is observed for all test conditions that the rate is slow initially and then increases sharply after the lowest N value is reached in each category.

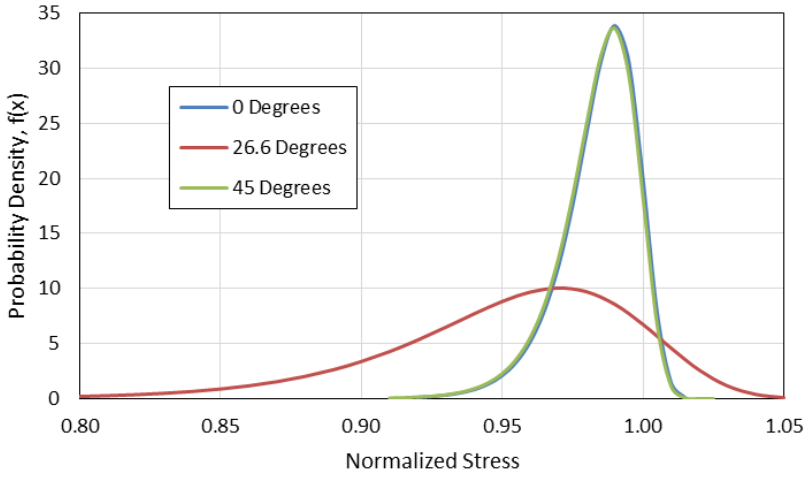

Figure 44: Probability Density of von Mises Stress from Tensile Testing

Figure 44, plotted using Eq. 33, depicts the low variability in the data, characterized by a large shape parameter in the data. As the shape parameter approaches infinity ($\beta \to \infty$), the Weibull distribution asymptotically converges to a Dirac delta function centered at α and the system behavior becomes increasingly more typical of a brittle response (Krajcinovic, 1996).

$$f(N) = \left(\frac{\alpha}{\beta^{\alpha}}\right) N^{\alpha-1} \exp\left[-\left(\frac{N}{\beta}\right)^{\alpha}\right] \qquad \text{Eq. 33}$$

5.2 Adhesive Joint Fatigue Strength

The experimental fatigue results of adhesive specimens manufactured at three different angles are shown in Table 12. Testing was performed by IHI, using a stress ratio of 0.1 and a frequency of 5 Hz. Since fatigue testing is very time intensive, only 2-4 samples were tested at each of the respective stresses and angles. Weibull parameters were calculated using Eq. 31 and 32 for each angle and stress level. Figs. 45 and 46 illustrate the Weibull characterization for the specimens at 26.6° and 45°. Three different stress levels are depicted for each angle. The slope of each curve indicates the variability between specimens, with a high slope signifying low variability. The shape factor at 26.6° with 67% maximum von Mises stress exhibits a shape factor close to unity, meaning that the failure is more of a random nature.

Table 12: Results of Adhesive Joint Fatigue Test

Specimen ID	Angle	Maximum Normalized			Cycles to Failure
		Shear Stress	Normal Stress	Von Mises Stress	
F1-1	0.0°	0.428	0.000	0.741	247186
F1-2					655000
F1-3					994000
F2-1	26.6°	0.320	0.160	0.577	6500000
F2-2					7986470
F2-3		0.374	0.187	0.674	54324
F2-4					659171
F2-5					918197
F2-6					1053378
F2-7		0.427	0.214	0.770	90016
F2-8					96774
F2-9					141273
F2-10					96309
F3-1	45.0°	0.329	0.329	0.658	261290
F3-2					558386
F3-3					658645
F3-4		0.384	0.384	0.767	19537
F3-5					91082
F3-6					125046
F3-7		0.438	0.438	0.877	3769
F3-8					3797
F3-9					3974

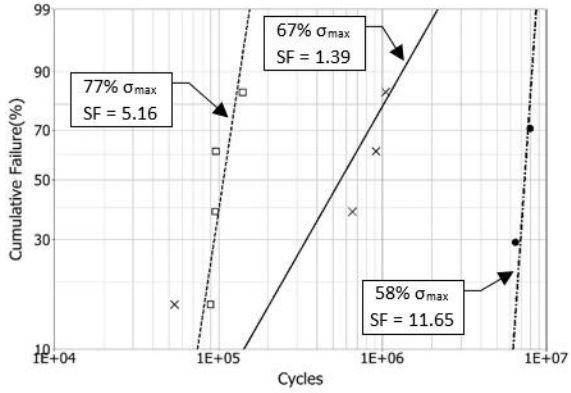

Figure 45: Fatigue Reliability at 26.6°

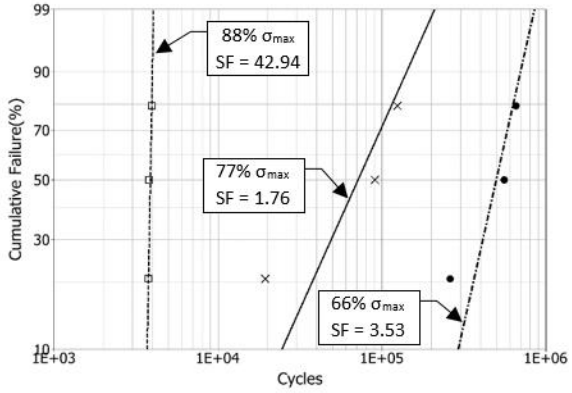

Figure 46: Fatigue Reliability at 45°

Equations 34 and Eq. 35 were used for the fatigue tests with the realization that *n* specimens were tested at *m* stress levels. The shape and scale factors are obtained from the experimental data such as $N_{i1}, N_{i2}, \dots, N_{in}$ under the *ith* level of stress with $i = 1,2,3, \dots, m$.

In the following method, it is assumed that the shape parameter (α) will remain equal for each stress level, by normalizing the cycle numbers with respect to the scale parameter (β). The scale factor is normalized by letting $\bar{N}_{ij} = N_{ij}/\beta_i$, for $j = 1,2,3,\dots,n$. The maximum likelihood equation for the normalized data can therefore be written as (Stephen W. Tsai, 1988):

$$\frac{\sum_{i=1}^{m}\sum_{j=1}^{n}\bar{N}_{ij}^{\tilde{\alpha}}\ln\left(\bar{N}_{ij}\right)}{\sum_{i=1}^{m}\sum_{j=1}^{n}\bar{N}_{ij}^{\tilde{\alpha}}} - \frac{1}{\tilde{\alpha}} - \frac{\sum_{i=1}^{m}\sum_{j=1}^{n}\left(\bar{N}_{ij}\right)}{mn} = 0 \qquad \text{Eq. 34}$$

and

$$\tilde{\beta}_i = \left[\frac{1}{n}\sum_{j=1}^{n}N_{ij}^{\tilde{\alpha}}\right]^{1/\tilde{\alpha}} \quad i = 1,2,3,\dots,m \qquad \text{Eq. 35}$$

Where, $\tilde{\alpha}$ is the common shape parameter and $\tilde{\beta}_i$ are the corresponding scale parameters. The common shape parameter $\tilde{\alpha}$ can now be determined by treating Eq. 34 as $f(\tilde{\alpha}) = 0$. Once $\tilde{\alpha}$ is computed, $\tilde{\beta}_i$ can be determined from Eq. 35.

Assuming that the fatigue data follow the classical power law as well as the two parameter Weibull distribution, the S-N curve representation takes the form:

$$CNS^b = 1 \qquad \text{Eq. 36}$$

Where, N = cycle number and S = stress level. The two parameters C and b of Eq. 36 are related with the straight line representation of the S-N curve, and are determined using the least square linear regression. It is also important during fatigue characterization that the desired level of reliability is known. Eq. 29 is used to determine the probability of survival.

Equation 37 can be derived by combining Eqs. 29 and 36, and solving for S (Mahfuz et al., 1997).

$$S = K\left\{\left[-\ln R(N)\right]^{-(1/\tilde{\alpha}b)}\right\}\beta^{-(1/b)} \qquad \text{Eq. 37}$$

Where, $K = C^{-(1/b)}$.

By setting N = β and substituting $-\ln R(\beta) = 1$ into Eq. 37, we see that,

$$\ln(S_i) = -\frac{1}{b}\ln(\beta_i) + \ln(K),\ i = 1,2,\ldots m \qquad \text{Eq. 38}$$

Where, *i* is the stress level. Eq. 38 represents a straight line in the $\ln(S_i)$ and $\ln(\beta_i)$ plane with $\left(-\frac{1}{b}\right)$ and $\ln(K)$ being the slope and y-intercept respectively. Eq. 38 has been used in this investigation to draw the Weibull characteristic line shown in Figures 47 and 48. If a particular level of reliability is required, Eq. 38 can be reformulated as (Whitney, 1981):

$$S = K\left\{\left[-\ln R(N)\right]^{-(1/\tilde{\alpha}b)}\right\}N^{-(1/b)} \qquad \text{Eq. 39}$$

5.3 Results and Discussion

The common characteristic values calculated in Table 13 indicate that 63.2% of the population will fail at the given cycle number. If we substitute $N=\beta$ into Eq. 29, $F(N) = 1 - \exp\left[-(\beta/\beta)^{\alpha}\right] = 0.632$ suggests that 0.632 fraction of the population will fail

at the characteristic level regardless of the value of α. The common alpha is significantly decreased for both angles, in order to provide a more conservative estimate of reliability.

Table 13: Weibull Characterization of Adhesive Joint Fatigue Data

Angle	Max Mises Stress	Cycles to Failure	Average Cycles	Alpha	Beta	Common Alpha	Common Beta (Characteristic)	95% Survivability
0.0°	74%	247186	6.32E+05	2.24	7.16E+05	-	-	-
		655000						
		994000						
26.6°	58%	6500000	7.24E+06	11.65	7.58E+06	2.94	7.32E+06	2.66E+06
		7986470						
	67%	54324	6.71E+05	1.39	7.21E+05		8.21E+05	2.99E+05
		659171						
		918197						
		1053378						
	77%	90016	1.06E+05	5.16	1.15E+05		1.10E+05	4.01E+04
		96774						
		141273						
		96309						
45.0°	66%	261290	4.93E+05	3.53	5.51E+05	3.11	5.44E+05	2.09E+05
		558386						
		658645						
	77%	19537	7.86E+04	1.76	8.78E+04		9.73E+04	3.75E+04
		91082						
		125046						
	88%	3769	3.85E+03	42.94	3.89E+03		3.85E+03	1.48E+03
		3797						
		3974						

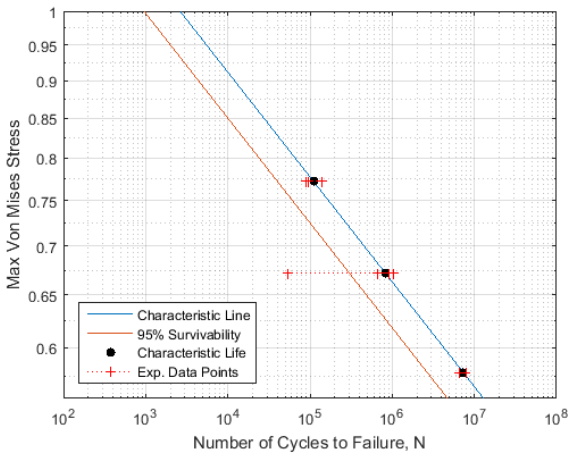

Figure 47: Adhesive Joint S-N curve at 26.6°

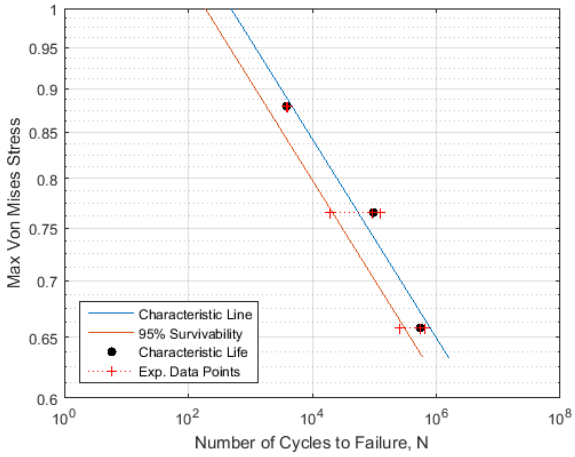

Figure 48: Adhesive Joint S-N curve at 45°

The above characterization of joint fatigue data was carried out in order to plot an S-N curve with a known degree of reliability such that a level of confidence can be associated. The S-N curves for 26.6° and 45° are shown in Figs. 47 and 48. In both figures, two S-N curves are drawn; one is the characteristic line and the other is the 95% survivability line. According to the Weibull analysis, low variation is observed at the upper and lower stress levels. The middle stress levels of 67% at 26.6° and 77% at 45°, both contain a sample that failed early. This may be a result of voids forming in the adhesive layer. The common shape parameter for both angled specimen is close to 3.0, indicating that adhesive joint behaves in a predictable manner. It is also observed in Figs. 47 and 48 that as the confidence level increases to 95%, the number of cycles to failure at a particular stress level reduces significantly. This suggests that the 95% survivability line can be used as a conservative fatigue design curve.

6. SUMMARY

6.1 Summary

- Several modifications have been implemented to numerical simulation tools based on blade element momentum theory for application to ocean current turbine blade design. These modifications were in terms of adding a core material for the blade, computing section moduli for both the blade shell and core, taking into account buoyancy, and considering the effect of added mass due to fluid acceleration.

- A blade was designed and analyzed considering the above parameters. A static analysis on the blade was performed through ANSYS by employing hydrodynamic loads computed via the modified NREL codes.

- Failure analysis of the blade was conducted using Tsai-Wu failure criteria for the composite skin and Maximum Stress theory for the core material. The analysis revealed that core failure occurs first at 6 kN of normal force.

- The Rainflow counting algorithm was used on ocean current speed data according to ASTM Standard E1049-85 in order to generate a loading histogram for cumulative fatigue analysis. The results were combined with turbulence characteristics determined at 5% and 7.5% intensities and fatigue life of OCT blade was predicted.

- The numerical fatigue analysis showed that blade fatigue life would be around 18.7 years without any turbulence intensity. If turbulence is included, predicted life reduces to 18.5 years with 5% intensity - meaning that at lower intensity turbulence has minimal effect. However, when turbulence intensity increases to 7.5%, predicted life reduces by approximately 25% to 14.06 years.

- The statistical analysis of experimental fatigue data indicated low variability in fatigue failure data suggesting good consistency among different batches used for joint manufacturing. S-N diagrams were generated from the experimental data using a statistical Weibull analysis with both characteristic and 95% confidence levels. A conservative design curve for fatigue life is recommended at the 95% survivability line.

6.2 Future Work

- In the present study, blade loading was accomplished by applying concentrated normal and tangential forces at each hydrofoil cross section. A comparison between this method and a CFD generated pressure distribution should be made. CFD analysis is very time and resource intensive. Therefore, efficiency and cost-effectiveness must also be weighed against solution accuracy.
- The added mass coefficient used in this research was based on the DNV offshore standard. The accuracy of the added mass calculation, can be improved by determining the specific added mass coefficient of each hydrofoil shape used in the blade design.

- Finally, a turbulence characterization of the Florida Gulf Stream has not currently been calculated. By measuring the turbulence intensity at the intended blade placement location and depth, blade fatigue life could be calculated with greater confidence.

APPENDICES

A. Precomp Files

A.1. Main Input File

********** main input file for PreComp **********
Composite Blade Section Properties

General information ----------
1.22 Bl_length : blade length (m)
25 N_sections : no of blade sections (-)
2 N_materials : no of materials listed in the materials table (material.inp)
3 Out_format : output file (1: general format, 2: BModes-format, 3: both)
f TabDelim (true: tab-delimited table; false: space-delimited table)

Blade-sections-specific data ----------
Sec span l.e. chord aerodynamic af_shape int str layup
location position length twist file file
Span_loc Le_loc Chord Tw_aero Af_shape_file Int_str_file
(-) (-) (m) (degrees) (-) (-)

0.00000000000000000	0.25	0.311394621266602	26.339390214820200	'fx77_1.inp'	'int01.inp'
0.00788529868552215	0.25	0.309464482544235	25.519352879194500	'fx77_2.inp'	'int01.inp'
0.02353154018584670	0.25	0.305355955924390	24.069281972569400	'fx77_3.inp'	'int01.inp'
0.04669197392590190	0.25	0.298882097225342	22.230941356584300	'fx77_4.inp'	'int01.inp'
0.07700134603023450	0.25	0.290114157095989	20.223728032535100	'fx77_5.inp'	'int01.inp'
0.11398165959481800	0.25	0.279351627480788	18.165916862893000	'fx77_6.inp'	'int01.inp'
0.15704971298377000	0.25	0.266960623130768	16.128018200809300	'fx77_7.inp'	'int01.inp'
0.20552629726754000	0.25	0.253416996262952	14.236234742245100	'fx77_8.inp'	'int01.inp'
0.25864690775346400	0.25	0.239078545790451	12.468952381205200	'fx77_9.inp'	'int01.inp'
0.31557380068146400	0.25	0.224468405811598	10.899339100867200	'fx77_10.inp'	'int01.inp'
0.37540920494358900	0.25	0.209911797279662	9.504249389275310	'fx77_11.inp'	'int01.inp'
0.43720948047068700	0.25	0.195733628609357	8.273887966543490	'fx77_12.inp'	'int01.inp'
0.50000000000000000	0.25	0.182402596885931	7.222987555346210	'fx77_13.inp'	'int01.inp'
0.56279051952931300	0.25	0.170012493899392	6.300249712956810	'fx77_14.inp'	'int01.inp'
0.62459079505641100	0.25	0.158761856525380	5.486416914558650	'fx77_15.inp'	'int01.inp'
0.68442619931853600	0.25	0.148788000726653	4.760780592835610	'fx77_16.inp'	'int01.inp'
0.74135309224653700	0.25	0.140161461683999	4.104120389424850	'fx77_17.inp'	'int01.inp'
0.79447370273246000	0.25	0.132881712634192	3.501774891196840	'fx77_18.inp'	'int01.inp'
0.84295028701623000	0.25	0.126874209227510	2.946778671911910	'fx77_19.inp'	'int01.inp'
0.88601834040518200	0.25	0.121988787948812	2.442996515121750	'fx77_20.inp'	'int01.inp'
0.92299865396976600	0.25	0.118261857851171	1.992480576539810	'fx77_21.inp'	'int01.inp'
0.95330802607409800	0.25	0.115455633231132	1.608370157340090	'fx77_22.inp'	'int01.inp'
0.97646845981415300	0.25	0.113511833678055	1.302858538740080	'fx77_23.inp'	'int01.inp'
0.99211470131447800	0.25	0.112198682224285	1.096467388236550	'fx77_23.inp'	'int01.inp'
1.00000000000000000	0.25	0.111536888052689	0.992451617565034	'fx77_23.inp'	'int01.inp'

Webs (spars) data ----------

0 Nweb : number of webs (-) ! enter 0 if the blade has no webs
0 Ib_sp_stn : blade station number where inner-most end of webs is located (-)
0 Ob_sp_stn : blade station number where outer-most end of webs is located (-)

A.2. Hydrofoil Nodes

150 N_af_nodes :no of airfoil nodes, counted clockwise starting with leading edge (see users' manual, fig xx)

Xnode	Ynode	!! chord-normalized coordinated of the airfoil nodes
0.00E+00	0.00E+00	!! the first node, a leading-edge node, must be (0,0)
0.001248	0.011302	
0.003768	0.020987	
0.00692	0.02813	
0.010156	0.034537	
0.013568	0.040037	
0.017358	0.045003	
0.021315	0.049853	
0.0252	0.05465	
0.029107	0.05922	
0.033239	0.063503	
0.037672	0.067638	
0.042318	0.071805	
0.047021	0.076064	
0.051769	0.08028	
0.056667	0.084335	
0.06187	0.088224	
0.067425	0.09209	
0.073264	0.096064	
0.079235	0.100136	
0.085309	0.10414	
0.091593	0.107966	
0.098269	0.11165	
0.105413	0.115358	
0.112912	0.119195	
0.120546	0.123041	
0.128293	0.126698	
0.136373	0.130101	
0.145045	0.133403	
0.154319	0.136767	
0.163821	0.140142	
0.173307	0.143276	
0.182975	0.146066	
0.193184	0.148641	
0.203959	0.151161	
0.214817	0.153578	
0.225468	0.15567	
0.236171	0.157343	
0.247332	0.158705	
0.25896	0.159898	
0.270556	0.160908	
0.281872	0.161567	
0.293222	0.161764	
0.30509	0.161555	
0.317581	0.161067	
0.330224	0.160357	
0.342725	0.159301	
0.355406	0.157747	
0.368844	0.155656	

0.383296	0.153074
0.398513	0.150054
0.414431	0.146535
0.431498	0.142478
0.449773	0.13812
0.468458	0.133619
0.48728	0.12881
0.506514	0.123853
0.525951	0.118992
0.545254	0.113992
0.564535	0.108863
0.603928	0.098897
0.624201	0.093552
0.64505	0.088197
0.66648	0.082754
0.688419	0.076999
0.711013	0.071231
0.757131	0.059515
0.780325	0.053841
0.803145	0.048237
0.84687	0.037933
0.886781	0.028922
0.922536	0.021093
0.953481	0.014548
0.966963	0.0118
0.979182	0.009301
0.990534	0.007036
0.99893	0.005145
1.000000	0.000000
0.99893	-0.00476
0.98801	-0.004641
0.971283	-0.005027
0.95368	-0.005874
0.935036	-0.007075
0.915447	-0.008672
0.895106	-0.010508
0.873884	-0.012823
0.851971	-0.01539
0.829292	-0.018437
0.805995	-0.021707
0.782242	-0.025434
0.75791	-0.029434
0.734083	-0.033687
0.710001	-0.038205
0.687106	-0.042674
0.665241	-0.047199
0.643956	-0.051517
0.623921	-0.055628
0.605696	-0.059355
0.588107	-0.062428
0.569404	-0.065118
0.549952	-0.067705
0.531188	-0.069851
0.511927	-0.071487
0.491191	-0.072998

0.47053	-0.074345
0.449808	-0.075254
0.428068	-0.075969
0.40676	-0.076542
0.385822	-0.076687
0.364406	-0.076618
0.343828	-0.076448
0.324108	-0.075931
0.304702	-0.075264
0.286509	-0.074596
0.269569	-0.073676
0.253327	-0.0726
0.23808	-0.071626
0.224094	-0.070602
0.211026	-0.069367
0.198629	-0.068103
0.187029	-0.066992
0.176315	-0.065905
0.166334	-0.064669
0.156884	-0.063329
0.147905	-0.062056
0.139445	-0.060937
0.131527	-0.059849
0.124086	-0.058662
0.117017	-0.057346
0.103747	-0.05477
0.097552	-0.053652
0.091674	-0.052555
0.086093	-0.051382
0.08076	-0.05008
0.070624	-0.047397
0.061107	-0.045051
0.056625	-0.043885
0.05233	-0.042592
0.048186	-0.041137
0.040123	-0.038116
0.032264	-0.035381
0.028515	-0.033896
0.024905	-0.03214
0.021345	-0.030152
0.014104	-0.026007
0.01069	-0.023659
0.007652	-0.020616
0.004714	-0.016788
0.001708	-0.012363
0.000002	-0.005961

A.3. Materials

Mat_Id (-)	E1 (Pa)	E2 (Pa)	G12 (Pa)	Nu12 (-)	Density (Kg/m^3)	Mat_Name (-)
1	71.0e+9	71.0e+9	19.5e+9	0.04	1697.37	(Twill Fabric)
2	143e+9	10.3e+9	7.0e+9	0.27	1555.55	(UD Tape)

A.4. Composite Layup File

Composite laminae lay-up inside the blade section

********** TOP SURFACE **********
1 N_scts(1): no of sectors on top surface

normalized chord location of nodes defining airfoil sectors boundaries (xsec_node)
0.0 1.00
.....
Sect_num no of laminae (N_laminas)
1 8

lamina number lam_num	num of plies N_plies	thickness of ply (m) Tply	fibers_direction (deg) Tht_lam	composite_material ID (-) Mat_id
1	1	0.000559	0	1 (Twill Fabric)
2	1	0.000305	0	2 (UD Tape)
3	1	0.000559	0	1 (Twill Fabric)
4	1	0.000305	0	2 (UD Tape)
5	1	0.000559	90	1 (Twill Fabric)
6	1	0.000559	45	1 (Twill Fabric)
7	2	0.000305	0	2 (UD Tape)
8	1	0.000559	90	1 (Twill Fabric)

********** BOTTOM SURFACE **********
1 N_scts(2): no of sectors on bottom surfaces

normalized chord location of surface nodes defining sector boundaries (xsec_node)
0.0 1.00
.....
Sect_num no of laminae
1 8

lamina number lam_num	num of plies N_plies	thickness of ply (m) Tply	fibers_direction (deg) Tht_lam	composite_material ID (-) Mat_id
1	1	0.000559	0	1 (Twill Fabric)
2	1	0.000305	0	2 (UD Tape)
3	1	0.000559	0	1 (Twill Fabric)
4	1	0.000305	0	2 (UD Tape)
5	1	0.000559	90	1 (Twill Fabric)
6	1	0.000559	45	1 (Twill Fabric)
7	2	0.000305	0	2 (UD Tape)
8	1	0.000559	90	1 (Twill Fabric)

A.5. Output File

```
================================================================================
Results generated by PreComp (v1.00.03, 11-Jun-2012, compiled using double precision) on 19-Jun-2016 at 20:01:27.
Composite Blade Section Properties
================================================================================

 blade length (meters) =   1.22
```

span (-)	loc str_tw (deg)	tw_iner (deg)	mass_den (kg/m)	flp_iner (kg-m)	edge_iner (kg-m)	flp_stff (Nm^2)	edge_stff (Nm^2)	tor_stff (Nm^2)	axial_stff (N)	cg_offst (m)	sc_offst (m)	tc_offst (m)
0.0000	24.540	24.540	0.4384E+01	0.2449E-02	0.3752E-01	0.1332E+06	0.2044E+07	0.7377E+05	0.2388E+09	0.073	0.073	0.073
0.0079	23.722	23.722	0.4355E+01	0.2372E-02	0.3679E-01	0.1290E+06	0.2004E+07	0.7146E+05	0.2372E+09	0.073	0.073	0.073
0.0235	22.266	22.266	0.4292E+01	0.2219E-02	0.3527E-01	0.1207E+06	0.1921E+07	0.6688E+05	0.2338E+09	0.072	0.072	0.072
0.0467	20.420	20.420	0.4195E+01	0.1999E-02	0.3298E-01	0.1087E+06	0.1796E+07	0.6027E+05	0.2285E+09	0.070	0.070	0.070
0.0770	18.402	18.402	0.4065E+01	0.1732E-02	0.3005E-01	0.9418E+05	0.1637E+07	0.5223E+05	0.2214E+09	0.068	0.068	0.068
0.1140	16.328	16.328	0.3905E+01	0.1444E-02	0.2670E-01	0.7853E+05	0.1454E+07	0.4355E+05	0.2127E+09	0.066	0.066	0.066
0.1570	14.272	14.272	0.3722E+01	0.1161E-02	0.2318E-01	0.6310E+05	0.1262E+07	0.3496E+05	0.2027E+09	0.063	0.063	0.063
0.2055	12.357	12.357	0.3524E+01	0.9010E-03	0.1972E-01	0.4897E+05	0.1074E+07	0.2709E+05	0.1919E+09	0.060	0.060	0.060
0.2586	10.563	10.563	0.3315E+01	0.6762E-03	0.1645E-01	0.3674E+05	0.8961E+06	0.2026E+05	0.1805E+09	0.057	0.057	0.057
0.3156	8.962	8.962	0.3103E+01	0.4927E-03	0.1353E-01	0.2676E+05	0.7370E+06	0.1468E+05	0.1690E+09	0.053	0.053	0.053
0.3754	7.531	7.531	0.2893E+01	0.3492E-03	0.1100E-01	0.1896E+05	0.5990E+06	0.1031E+05	0.1576E+09	0.050	0.050	0.050
0.4372	6.262	6.262	0.2690E+01	0.2416E-03	0.8864E-02	0.1311E+05	0.4827E+06	0.7046E+04	0.1465E+09	0.047	0.047	0.047
0.5000	5.165	5.166	0.2500E+01	0.1644E-03	0.7133E-02	0.8915E+04	0.3885E+06	0.4704E+04	0.1362E+09	0.044	0.044	0.044
0.5628	4.243	4.243	0.2327E+01	0.1213E-03	0.5751E-02	0.6573E+04	0.3132E+06	0.3401E+04	0.1267E+09	0.041	0.041	0.041
0.6246	3.429	3.429	0.2170E+01	0.8975E-04	0.4664E-02	0.4862E+04	0.2540E+06	0.2459E+04	0.1182E+09	0.038	0.038	0.038
0.6844	2.704	2.704	0.2031E+01	0.6711E-04	0.3824E-02	0.3633E+04	0.2083E+06	0.1794E+04	0.1106E+09	0.036	0.036	0.036
0.7414	2.047	2.047	0.1911E+01	0.5107E-04	0.3186E-02	0.2763E+04	0.1735E+06	0.1333E+04	0.1041E+09	0.034	0.034	0.034
0.7945	1.443	1.443	0.1809E+01	0.3980E-04	0.2707E-02	0.2152E+04	0.1474E+06	0.1018E+04	0.9855E+08	0.032	0.032	0.032
0.8430	0.890	0.890	0.1726E+01	0.3192E-04	0.2350E-02	0.1725E+04	0.1280E+06	0.8102E+03	0.9400E+08	0.031	0.031	0.031
0.8860	0.385	0.385	0.1658E+01	0.2637E-04	0.2084E-02	0.1424E+04	0.1135E+06	0.6861E+03	0.9031E+08	0.030	0.030	0.030
0.9230	-0.065	-0.065	0.1606E+01	0.2259E-04	0.1895E-02	0.1220E+04	0.1032E+06	0.6247E+03	0.8749E+08	0.029	0.029	0.029
0.9533	-0.448	-0.448	0.1567E+01	0.1999E-04	0.1761E-02	0.1079E+04	0.9592E+05	0.5890E+03	0.8537E+08	0.028	0.028	0.028
0.9765	-0.755	-0.755	0.1541E+01	0.1881E-04	0.1673E-02	0.1015E+04	0.9111E+05	0.5620E+03	0.8393E+08	0.028	0.028	0.028
0.9921	-0.961	-0.961	0.1523E+01	0.1806E-04	0.1615E-02	0.9745E+03	0.8797E+05	0.5440E+03	0.8296E+08	0.027	0.027	0.027
1.0000	-1.065	-1.065	0.1514E+01	0.1769E-04	0.1587E-02	0.9544E+03	0.8642E+05	0.5351E+03	0.8247E+08	0.027	0.027	0.027

B. BModes Files

B.1. Main Input File

```
======================   BModes v1.03 Main Input File   ==================
Composite OCT Blade (output is space-delimited)

--------- General parameters -----------------------------------------------------------------
False     Echo        Echo input file contents to *.echo file if true.
1         beam_type   1: blade, 2: tower (-)
50.0      romg:       rotor speed, automatically set to zero for tower modal analysis (rpm)
1.0       romg_mult:  rotor speed muliplicative factor (-)
1.4975    radius:     rotor tip radius measured along coned blade axis OR tower height (m)
0.2775    hub_rad:    hub radius measured along coned blade axis OR tower rigid-base height (m)
0.        precone:    built-in precone angle, automatically set to zero for a tower (deg)
0.        bl_thp:     blade pitch setting, automatically set to zero for a tower (deg)
1         hub_conn:   hub-to-blade connection [1: cantilevered; other options not yet available] (-)
10        modepr:     number of modes to be printed (-)
t         TabDelim    (true: tab-delimited output tables; false: space-delimited tables)
f         mid_node_tw  (true: output twist at mid-node of elements; false: no mid-node outputs)

--------- Blade-tip or tower-top mass properties ---------------------------------------------
0.        tip_mass    blade-tip or tower-top mass (kg)
```

0. cm_loc tip-mass c.m. offset from the blade axis measured along the tip section y reference axis (m)
0. ixx_tip blade lag mass moment of inertia about the tip-section x ref axis (kg-m^2)
0. iyy_tip blade flap mass moment of inertia about the tip-section y ref axis (kg-m^2)
0. izz_tip torsion mass moment of inertia about the tip-section z ref axis (kg-m^2)
0. ixy_tip cross product of inertia about x and y reference axes(kg-m^2)
0. izx_tip cross product of inertia about z and x reference axes(kg-m^2)
0. iyz_tip cross product of inertia about y and z reference axes(kg-m^2)

--------- Distributed-property identifiers ----------
1 id_mat: material_type [1: isotropic; non-isotropic composites option not yet available]
'SkinPlusFoamPlusAM.dat' sec_props_file name of beam section properties file (-)

Property scaling factors.....
1.0 sec_mass_mult: mass density multiplier (-)
1.0 flp_iner_mult: blade flap or tower f-a inertia multiplier (-)
1.0 lag_iner_mult: blade lag or tower s-s inertia multiplier (-)
1.0 flp_stff_mult: blade flap or tower f-a bending stiffness multiplier (-)
1.0 edge_stff_mult: blade lag or tower s-s bending stiffness multiplier (-)
1.0 tor_stff_mult: torsion stiffness multiplier (-)
1.0 axial_stff_mult: axial stiffness multiplier (-)
1.0 cg_offst_mult: cg offset multiplier (-)
1.0 sc_offst_mult: shear center multiplier (-)
1.0 tc_offst_mult: tension center multiplier (-)

--------- Finite element discretization ----------
12 nselt: no of blade or tower elements (-)
Distance of element boundary nodes from blade or flexible-tower root (normalized wrt blade or tower length), el_loc()
0. 0.08 0.16 0.24 0.32 0.40 0.48 0.56 0.64 0.72 0.80 0.90 1.0

B.2. BModes Output File

Results generated by BModes (v1.03.01, 25-Sept-2007, compiled using double precision) on 20-Jun-2016 at 13:17:14.
Composite OCT Blade (output is space-delimited)
==========

rotating blade frequencies & mode shapes
--- only first 10 modes printed

-------- Mode No. 1 (freq = 0.40250E+02 Hz)

span_loc	flap disp	flap slope	lag disp	lag slope	twist
0.0000	0.000000	0.000000	0.000000	0.000000	0.000000
0.0800	-0.000368	-0.011184	-0.000144	-0.004162	0.001193
0.1600	-0.001600	-0.026360	-0.000563	-0.008449	0.002964

0.2400	-0.003996	-0.046681	-0.001270	-0.012950	0.005643
0.3200	-0.007935	-0.073439	-0.002277	-0.017653	0.009674
0.4000	-0.013903	-0.108521	-0.003599	-0.022566	0.015888
0.4800	-0.022527	-0.154257	-0.005249	-0.027643	0.025701
0.5600	-0.034482	-0.209899	-0.007223	-0.032499	0.040524
0.6400	-0.050213	-0.269224	-0.009485	-0.036518	0.060873
0.7200	-0.069816	-0.327779	-0.011974	-0.039476	0.087597
0.8000	-0.092984	-0.377925	-0.014614	-0.041208	0.120050
0.9000	-0.125726	-0.417594	-0.018010	-0.041912	0.161890
1.0000	-0.160303	-0.426737	-0.021425	-0.041911	0.181791

-------- Mode No. 5 (freq = 0.16310E+03 Hz)

span_loc	flap disp	flap slope	lag disp	lag slope	twist
0.0000	0.000000	0.000000	0.000000	0.000000	0.000000
0.0800	0.000138	0.003883	0.000062	0.001681	-0.025670
0.1600	0.000494	0.006543	0.000210	0.002674	-0.059338
0.2400	0.000942	0.006672	0.000397	0.002955	-0.098620
0.3200	0.001270	0.002910	0.000579	0.002553	-0.135216
0.4000	0.001188	-0.005524	0.000715	0.001631	-0.153758
0.4800	0.000411	-0.017649	0.000781	0.000528	-0.127045
0.5600	-0.001137	-0.028069	0.000787	-0.000179	-0.023848
0.6400	-0.003025	-0.027304	0.000777	0.000013	0.149160
0.7200	-0.004234	-0.007597	0.000811	0.001074	0.315567
0.8000	-0.003492	0.030079	0.000927	0.002374	0.307353
0.9000	0.001199	0.078163	0.001165	0.003183	-0.120411
1.0000	0.008449	0.092809	0.001424	0.003170	-0.500256

-------- Mode No. 7 (freq = 0.22207E+03 Hz)

span_loc	flap disp	flap slope	lag disp	lag slope	twist
0.0000	0.000000	0.000000	0.000000	0.000000	0.000000
0.0800	0.000091	0.001836	0.000229	0.006457	0.031714
0.1600	0.000146	-0.000668	0.000839	0.011963	0.068450
0.2400	-0.000094	-0.006881	0.001802	0.017401	0.098598
0.3200	-0.000860	-0.016485	0.003128	0.023107	0.101102
0.4000	-0.002366	-0.029265	0.004838	0.029207	0.049977
0.4800	-0.004799	-0.044271	0.006960	0.035736	-0.071082
0.5600	-0.008129	-0.055522	0.009526	0.042803	-0.215010
0.6400	-0.011655	-0.048524	0.012580	0.050702	-0.235716
0.7200	-0.013513	-0.003581	0.016175	0.059220	-0.006221
0.8000	-0.010777	0.088585	0.020309	0.066900	0.322922
0.9000	0.002526	0.221811	0.026027	0.072122	0.121465
1.0000	0.023286	0.266720	0.031937	0.072654	-0.460686

C. TurbSim Files

C.1. Primary Input File

TurbSim Input File. Valid for TurbSim v1.06.00, 21-Sep-2012

---------Runtime Options----------
1996681054 RandSeed1 - First random seed (-2147483648 to 2147483647)
RANLUX RandSeed2 - Second random seed (-2147483648 to 2147483647) for intrinsic pRNG, or an alternative pRNG: "RanLux" or "RNSNLW"
False WrBHHTP - Output hub-height turbulence parameters in binary form? (Generates RootName.bin)
True WrFHHTP - Output hub-height turbulence parameters in formatted form? (Generates RootName.dat)
False WrADHH - Output hub-height time-series data in AeroDyn form? (Generates RootName.hh)
False WrADFF - Output full-field time-series data in TurbSim/AeroDyn form? (Generates Rootname.bts)
True WrBLFF - Output full-field time-series data in BLADED/AeroDyn form? (Generates RootName.wnd)
False WrADTWR - Output tower time-series data? (Generates RootName.twr)
False WrFMTFF - Output full-field time-series data in formatted (readable) form? (Generates RootName.u, RootName.v, RootName.w)
False WrACT - Output coherent turbulence time steps in AeroDyn form? (Generates RootName.cts, should not be used for Hydro spectral models, ie 'TIDAL')
False Clockwise - Clockwise rotation looking downwind? (used only for full-field binary files - not necessary for AeroDyn)
1 ScaleIEC - Scale IEC turbulence models to exact target standard deviation? [0=no additional scaling; 1=use hub scale uniformly; 2=use individual scales]

--------Turbine/Model Specifications----------
2 NumGrid_Z - Vertical grid-point matrix dimension
2 NumGrid_Y - Horizontal grid-point matrix dimension
1 TimeStep - Time step [seconds]
1000 AnalysisTime - Length of analysis time series [seconds] (program will add time if necessary: AnalysisTime = MAX(AnalysisTime, UsableTime+GridWidth/MeanHHWS))
900 UsableTime - Usable length of output time series [seconds] (program will add GridWidth/MeanHHWS seconds)
39 HubHt - Hub height [m] (should be > 0.5*GridHeight)
0.01 GridHeight - Grid height [m]
0.01 GridWidth - Grid width [m] (should be >= 2*(RotorRadius+ShaftLength))
0 VFlowAng - Vertical mean flow (uptilt) angle [degrees]
0 HFlowAng - Horizontal mean flow (skew) angle [degrees]

--------Meteorological Boundary Conditions----------
"TIDAL" TurbModel - Turbulence model ("IECKAI"=Kaimal, "IECVKM"=von Karman, "GP_LLJ", "NWTCUP", "SMOOTH", "WF_UPW", "WF_07D", "WF_14D", "TIDAL", or "NONE")
"1-ED3" IECstandard - Number of IEC 61400-x standard (x=1,2, or 3 with optional 61400-1 edition number (i.e. "1-Ed2"))
"A" IECturbc - IEC turbulence characteristic ("A", "B", "C" or the turbulence intensity in percent) ("KHTEST" option with NWTCUP model, not used for other models)
"NTM" IEC_WindType - IEC turbulence type ("NTM"=normal, "xETM"=extreme turbulence, "xEWM1"=extreme 1-year wind, "xEWM50"=extreme 50-year wind, where x=wind turbine class 1, 2, or 3)

default ETMc - IEC Extreme Turbulence Model "c" parameter [m/s]
"H2L" WindProfileType - Wind profile type ("JET";"LOG"=logarithmic;"PL"=power law;"H2L"=Log law for TIDAL spectral model;"IEC"=PL on rotor disk, LOG elsewhere; or "default")
50 RefHt - Height of the reference velocity (URef) [m]
1.510164484 URef - Mean (total) velocity at the reference height [m/s] (or "default" for JET wind profile)
default ZJetMax - Jet height [m] (used only for JET wind profile, valid 70-490 m)
default PLExp - Power law exponent [-] (or "default")
default Z0 - Surface roughness length [m] (or "default")

--------Non-IEC Meteorological Boundary Conditions------------
default Latitude - Site latitude [degrees] (or "default")
0.05 RICH_NO - Gradient Richardson number
default UStar - Friction or shear velocity [m/s] (or "default")
default ZI - Mixing layer depth [m] (or "default")
default PC_UW - Hub mean u'w' Reynolds stress (or "default")
default PC_UV - Hub mean u'v' Reynolds stress (or "default")
default PC_VW - Hub mean v'w' Reynolds stress (or "default")
default IncDec1 - u-component coherence parameters
default IncDec2 - v-component coherence parameters
default IncDec3 - w-component coherence parameters
default CohExp - Coherence exponent (or "default")

--------Coherent Turbulence Scaling Parameters----------
"/Test/EventData/" CTEventPath - Name of the path where event data files are located
"Random" CTEventFile - Type of event files ("LES", "DNS", or "RANDOM")
true Randomize - Randomize the disturbance scale and locations? (true/false)
1.0 DistScl - Disturbance scale (ratio of wave height to rotor disk).
0.5 CTLy - Fractional location of tower centerline from right (looking downwind) to left side of the dataset. (Ignored when Randomize = true.)
0.5 CTLz - Fractional location of hub height from the bottom of the dataset.
30.0 CTStartTime - Minimum start time for coherent structures in RootName.cts [seconds]

C.2. Primary Output File

This hub-height turbulence-parameter file was generated by TurbSim (v1.06.00, 21-Sep-2012) on 02-Mar-2016 at 18:20:55.

Time	U	Uh	Ut	V	W	u'	v'	w'	u'w'	u'v'	v'w'	TKE	CTKE
0.00	1.379	1.379	1.380	0.030	0.032	-0.085	0.030	0.032	-0.003	-0.003	0.001	0.005	0.002
1.00	1.359	1.359	1.361	0.038	0.064	-0.106	0.038	0.064	-0.007	-0.004	0.002	0.008	0.004
2.00	1.349	1.350	1.352	0.055	0.070	-0.116	0.055	0.070	-0.008	-0.006	0.004	0.011	0.006
3.00	1.339	1.341	1.342	0.062	0.065	-0.125	0.062	0.065	-0.008	-0.008	0.004	0.012	0.006
4.00	1.328	1.330	1.333	0.077	0.078	-0.136	0.077	0.078	-0.011	-0.010	0.006	0.015	0.008
5.00	1.339	1.343	1.344	0.098	0.061	-0.125	0.098	0.061	-0.008	-0.012	0.006	0.015	0.008
6.00	1.340	1.341	1.342	0.047	0.061	-0.124	0.047	0.061	-0.008	-0.006	0.003	0.011	0.005
7.00	1.327	1.327	1.329	0.036	0.066	-0.138	0.036	0.066	-0.009	-0.005	0.002	0.012	0.005
8.00	1.327	1.329	1.330	0.062	0.053	-0.137	0.062	0.053	-0.007	-0.009	0.003	0.013	0.006
9.00	1.325	1.326	1.327	0.039	0.059	-0.139	0.039	0.059	-0.008	-0.005	0.002	0.012	0.005
10.00	1.331	1.331	1.332	0.046	0.050	-0.134	0.046	0.050	-0.007	-0.006	0.002	0.011	0.005
11.00	1.328	1.328	1.330	0.019	0.063	-0.136	0.019	0.063	-0.009	-0.003	0.001	0.011	0.005
12.00	1.328	1.328	1.329	0.016	0.062	-0.137	0.016	0.062	-0.008	-0.002	0.001	0.011	0.004
13.00	1.322	1.322	1.323	0.006	0.057	-0.142	0.006	0.057	-0.008	-0.001	0.000	0.012	0.004
14.00	1.333	1.333	1.334	0.012	0.047	-0.132	0.012	0.047	-0.006	-0.002	0.001	0.010	0.003
15.00	1.339	1.340	1.340	0.030	0.041	-0.125	0.030	0.041	-0.005	-0.004	0.001	0.009	0.003
16.00	1.349	1.350	1.350	0.054	0.030	-0.116	0.054	0.030	-0.003	-0.006	0.002	0.009	0.004
17.00	1.348	1.348	1.349	0.037	0.035	-0.117	0.037	0.035	-0.004	-0.004	0.001	0.008	0.003

18.00	1.325	1.325	1.326	0.001	0.063	-0.139	0.001	0.063	-0.009	0.000	0.000	0.012	0.004
19.00	1.335	1.335	1.337	-0.028	0.062	-0.129	-0.028	0.062	-0.008	0.004	-0.002	0.011	0.004
20.00	1.345	1.347	1.348	-0.061	0.051	-0.119	-0.061	0.051	-0.006	0.007	-0.003	0.010	0.005
21.00	1.348	1.348	1.349	-0.033	0.052	-0.117	-0.033	0.052	-0.006	0.004	-0.002	0.009	0.004
22.00	1.358	1.359	1.360	-0.056	0.048	-0.107	-0.056	0.048	-0.005	0.006	-0.003	0.008	0.004
23.00	1.352	1.353	1.353	-0.054	0.011	-0.113	-0.054	0.011	-0.001	0.006	-0.001	0.008	0.003
24.00	1.361	1.362	1.362	-0.043	0.011	-0.103	-0.043	0.011	-0.001	0.004	0.000	0.006	0.002
25.00	1.360	1.360	1.360	-0.028	0.012	-0.105	-0.028	0.012	-0.001	0.003	0.000	0.006	0.002

D. AeroDyn Files

D.1. Primary Input File

Composite OCT Blade Hydrodynamic parameters for FAST.
SI SysUnits - System of units for used for input and output [must be SI for FAST] (unquoted string)
STEADY StallMod - Dynamic stall included [BEDDOES or STEADY] (unquoted string)
USE_CM UseCm - Use aerodynamic pitching moment model? [USE_CM or NO_CM] (unquoted string)
EQUIL InfModel - Inflow model [DYNIN or EQUIL] (unquoted string)
SWIRL IndModel - Induction-factor model [NONE or WAKE or SWIRL] (unquoted string)
0.005 AToler - Induction-factor tolerance (convergence criteria) (-)
PRANDtl TLModel - Tip-loss model (EQUIL only) [PRANDtl, GTECH, or NONE] (unquoted string)
NONE HLModel - Hub-loss model (EQUIL only) [PRANdtl or NONE] (unquoted string)
"AeroData/Bin17.wnd" WindFile - Name of file containing wind data (quoted string)
10.0 HH - Wind reference (hub) height [TowerHt+Twr2Shft+OverHang*SIN(ShftTilt)] (m)
0.0 TwrShad - Tower-shadow velocity deficit (-)
0.1 ShadHWid - Tower-shadow half width (m)
0.0 T_Shad_Refpt - Tower-shadow reference point (m)
1025 AirDens - Air density (kg/m^3)
1.05e-6 KinVisc - Kinematic air viscosity (m^2/sec)
0.0001 DTAero - Time interval for aerodynamic calculations (sec)
23 NumFoil - Number of airfoil files (-)
"AeroData/1.DAT" FoilNm - Names of the airfoil files [NumFoil lines] (quoted strings)
"AeroData/2.DAT"
"AeroData/3.DAT"
"AeroData/4.DAT"
"AeroData/5.DAT"
"AeroData/6.DAT"
"AeroData/7.DAT"
"AeroData/8.DAT"
"AeroData/9.DAT"
"AeroData/10.DAT"
"AeroData/11.DAT"
"AeroData/12.DAT"
"AeroData/13.DAT"
"AeroData/14.DAT"
"AeroData/15.DAT"
"AeroData/16.DAT"
"AeroData/17.DAT"
"AeroData/18.DAT"
"AeroData/19.DAT"
"AeroData/20.DAT"
"AeroData/21.DAT"
"AeroData/22.DAT"
"AeroData/23.DAT"
24 BldNodes - Number of blade nodes used for analysis (-)

RNodes	AeroTwst	DRNodes	Chord	NFoil	PrnElm
0.282225576174620	25.92937154700730	0.00962140690435670	0.310429551905419	1	PRINT
0.296581818863939	24.79431742588200	0.01909107847428190	0.307410219234313	2	PRINT
0.320257194267185	23.15011166457690	0.02825967233221010	0.302119026574866	3	PRINT
0.352878327571264	21.22733469455970	0.03698259427594940	0.294498127160665	4	PRINT
0.393930764017052	19.19482244771400	0.04512227861562600	0.284732892288389	5	PRINT
0.442767082158261	17.14696753185110	0.05255035766679140	0.273156125305778	6	PRINT
0.498617104084401	15.18212647152720	0.05914968618548950	0.260188809696860	7	PRINT
0.560600041586513	13.35259356172520	0.06481618881873290	0.246247771026701	8	PRINT
0.627738386713374	11.68414574103620	0.06946050143498990	0.231773475801025	9	PRINT
0.698973327655832	10.20179424507130	0.07300938044992530	0.217190101545630	10	PRINT

0.773181446841532	8.88906867790940	0.07540685792147550	0.202822712944509	11	PRINT
0.849192437901135	7.74843776094485	0.07661512419773040	0.189068112747644	12	PRINT
0.925807562098865	6.76161863415151	0.07661512419773040	0.176207545392661	13	PRINT
1.001818553158470	5.89333331375773	0.07540685792147530	0.164387175212386	14	PRINT
1.076026672344170	5.12359875369713	0.07300938044992540	0.153774928626016	15	PRINT
1.147261613286630	4.43245049113023	0.06946050143499030	0.144474731205326	16	PRINT
1.214399958413490	3.80294764031085	0.06481618881873260	0.136521587159096	17	PRINT
1.276382895915600	3.22427678155438	0.05914968618548940	0.129877960930851	18	PRINT
1.332232917841740	2.69488759351683	0.05255035766679140	0.124431498588161	19	PRINT
1.381069235982950	2.21773854583078	0.04512227861562600	0.120125322899992	20	PRINT
1.422121672428740	1.80042536693995	0.03698259427594920	0.116858745541152	21	PRINT
1.454742805732820	1.45561434804008	0.02825967233220990	0.114483733454593	22	PRINT
1.478418181136060	1.19966296348831	0.01909107847428190	0.112855257951170	23	PRINT
1.492774423825380	1.04445950290079	0.00962140690435676	0.111867785138487	23	PRINT

D.2. Ocean Current Speed Input

! Current Speed file.

! Time		Current Speed	Current Dir	Vert. Speed	Horiz. Shear		Vert. Shear	LinV Shear	Gust Speed
!									
0.0		0.00	0.0	0.0	0.0		0.0	0.0	0.0
0.1		2.6	0.0	0.0	0.0		0.0	0.0	0.0
999.9	2.6	0.0	0.0	0.0		0.0	0.0	0.0	

E. FAST Files

E.1. Main Input File

```
---------------------------------------------------------------------------
------- FAST INPUT FILE -------------------------------------------------------
FAST Composite OCT Blade.
Compatible with FAST v7.02.00.
---------------------- SIMULATION CONTROL --------------------------------------
False       Echo        - Echo input data to "echo.out" (flag)
  1         ADAMSPrep   - ADAMS preprocessor mode {1: Run FAST, 2: use FAST as a preprocessor to create an
ADAMS model, 3: do both} (switch)
  1         AnalMode    - Analysis mode {1: Run a time-marching simulation, 2: create a periodic linearized model}
  3         NumBl       - Number of blades (-)
  3         TMax        - Total run time (s)
  0.0001    DT          - Integration time step (s)
---------------------- TURBINE CONTROL -----------------------------------------
  0         YCMode      - Yaw control mode {0: none, 1: user-defined from routine UserYawCont, 2: user-defined from
Simulink/Labview} (switch)
9999.9      TYCOn       - Time to enable active yaw control (s) [unused when YCMode=0]
  0         PCMode      - Pitch control mode {0: none, 1: user-defined from routine PitchCntrl, 2: user-defined from
Simulink/Labview} (switch)
9999.9      TPCOn       - Time to enable active pitch control (s) [unused when PCMode=0]
  0         VSContrl    - Variable-speed control mode {0: none, 1: simple VS, 2: user-defined from routine UserVSCont,
3: user-defined from Simulink/Labview} (switch)
9999.9      VS_RtGnSp   - Rated generator speed for simple variable-speed generator control (HSS side) (rpm) [used
only when VSContrl=1]
9999.9      VS_RtTq     - Rated generator torque/constant generator torque in Region 3 for simple variable-speed
generator control (HSS side) (N-m) [used only when VSContrl=1]
9999.9      VS_Rgn2K    - Generator torque constant in Region 2 for simple variable-speed generator control (HSS side)
(N-m/rpm^2) [used only when VSContrl=1]
9999.9      VS_SlPc     -Rated generator slip percentage in Region 2 1/2 for simple variable-speed generator control (%)
```

```
   2       GenModel    - Generator model {1: simple, 2: Thevenin, 3: user-defined from routine UserGen} (switch) [used
only when VSContrl=0]
True       GenTiStr    - Method to start the generator {T: timed using TimGenOn, F: generator speed using SpdGenOn}
True       GenTiStp    - Method to stop the generator {T: timed using TimGenOf, F: when generator power = 0} (flag)
9999.9     SpdGenOn    - Generator speed to turn on the generator for a startup (HSS speed) (rpm)
  0.0      TimGenOn    - Time to turn on the generator for a startup (s) [used only when GenTiStr=True]
9999.9     TimGenOf    - Time to turn off the generator (s) [used only when GenTiStp=True]
   1       HSSBrMode   - HSS brake model {1: simple, 2: user-defined from routine UserHSSBr, 3: user-defined from
Labview} (switch)
9999.9     THSSBrDp    - Time to initiate deployment of the HSS brake (s)
9999.9     TiDynBrk    - Time to initiate deployment of the dynamic generator brake [CURRENTLY IGNORED] (s)
9999.9     TTpBrDp(1)  - Time to initiate deployment of tip brake 1 (s)
9999.9     TTpBrDp(2)  - Time to initiate deployment of tip brake 2 (s)
9999.9     TTpBrDp(3)  - Time to initiate deployment of tip brake 3 (s) [unused for 2 blades]
9999.9     TBDepISp(1) - Deployment-initiation speed for the tip brake on blade 1 (rpm)
9999.9     TBDepISp(2) - Deployment-initiation speed for the tip brake on blade 2 (rpm)
9999.9     TBDepISp(3) - Deployment-initiation speed for the tip brake on blade 3 (rpm) [unused for 2 blades]
9999.9     TYawManS    - Time to start override yaw maneuver and end standard yaw control (s)
9999.9     TYawManE    - Time at which override yaw maneuver reaches final yaw angle (s)
  0.0      NacYawF     - Final yaw angle for yaw maneuvers (degrees)
9999.9     TPitManS(1) - Time to start override pitch maneuver for blade 1 and end standard pitch control (s)
9999.9     TPitManS(2) - Time to start override pitch maneuver for blade 2 and end standard pitch control (s)
9999.9     TPitManS(3) - Time to start override pitch maneuver for blade 3 and end standard pitch control (s) [unused
for 2 blades]
9999.9     TPitManE(1) - Time at which override pitch maneuver for blade 1 reaches final pitch (s)
9999.9     TPitManE(2) - Time at which override pitch maneuver for blade 2 reaches final pitch (s)
9999.9     TPitManE(3) - Time at which override pitch maneuver for blade 3 reaches final pitch (s)
  0.00     BlPitch(1)  - Blade 1 initial pitch (degrees)
  0.00     BlPitch(2)  - Blade 2 initial pitch (degrees)
  0.00     BlPitch(3)  - Blade 3 initial pitch (degrees) [unused for 2 blades]
  0.00     BlPitchF(1) - Blade 1 final pitch for pitch maneuvers (degrees)
  0.00     BlPitchF(2) - Blade 2 final pitch for pitch maneuvers (degrees)
  0.00     BlPitchF(3) - Blade 3 final pitch for pitch maneuvers (degrees) [unused for 2 blades]
---------------------- ENVIRONMENTAL CONDITIONS --------------------------------
  0.865    Gravity     - Gravitational acceleration (m/s^2)
---------------------- FEATURE FLAGS -------------------------------------------
True       FlapDOF1    - First flapwise blade mode DOF (flag)
True       FlapDOF2    - Second flapwise blade mode DOF (flag)
True       EdgeDOF     - First edgewise blade mode DOF (flag)
False      TeetDOF     - Rotor-teeter DOF (flag) [unused for 3 blades]
False      DrTrDOF     - Drivetrain rotational-flexibility DOF (flag)
False      GenDOF      - Generator DOF (flag)
False      YawDOF      - Yaw DOF (flag)
False      TwFADOF1    - First fore-aft tower bending-mode DOF (flag)
False      TwFADOF2    - Second fore-aft tower bending-mode DOF (flag)
False      TwSSDOF1    - First side-to-side tower bending-mode DOF (flag)
False      TwSSDOF2    - Second side-to-side tower bending-mode DOF (flag)
True       CompAero    - Compute aerodynamic forces (flag)
False      CompNoise   - Compute aerodynamic noise (flag)
---------------------- INITIAL CONDITIONS --------------------------------------
  0.0      OoPDefl     - Initial out-of-plane blade-tip displacement (meters)
  0.0      IPDefl      - Initial in-plane blade-tip deflection (meters)
  0.0      TeetDefl    - Initial or fixed teeter angle (degrees) [unused for 3 blades]
  0.0      Azimuth     - Initial azimuth angle for blade 1 (degrees)
 50.00     RotSpeed    - Initial or fixed rotor speed (rpm)
  0.0      NacYaw      - Initial or fixed nacelle-yaw angle (degrees)
  0.0      TTDspFA     - Initial fore-aft tower-top displacement (meters)
  0.0      TTDspSS     - Initial side-to-side tower-top displacement (meters)
---------------------- TURBINE CONFIGURATION -----------------------------------
  1.49758512727756    TipRad      - The distance from the rotor apex to the blade tip (meters)
  0.277414872722441   HubRad      - The distance from the rotor apex to the blade root (meters)
```

```
   1        PSpnElN     - Number of the innermost blade element which is still part of the pitchable portion of the blade for
partial-span pitch control [1 to BldNodes] [CURRENTLY IGNORED] (-)
   0.0      UndSling    - Undersling length [distance from teeter pin to the rotor apex] (meters) [unused for 3 blades]
   0.0      HubCM       - Distance from rotor apex to hub mass [positive downwind] (meters)
  -0.5     OverHang    - Distance from yaw axis to rotor apex [3 blades] or teeter pin [2 blades] (meters)
   0.0      NacCMxn     - Downwind distance from the tower-top to the nacelle CM (meters)
   0.0      NacCMyn     - Lateral  distance from the tower-top to the nacelle CM (meters)
   0.6      NacCMzn     - Vertical distance from the tower-top to the nacelle CM (meters)
   9.4      TowerHt     - Height of tower above ground level [onshore] or MSL [offshore] (meters)
   0.6      Twr2Shft    - Vertical distance from the tower-top to the rotor shaft (meters)
   0.0      TwrRBHt     - Tower rigid base height (meters)
   0.0      ShftTilt    - Rotor shaft tilt angle (degrees)
   0.0      Delta3      - Delta-3 angle for teetering rotors (degrees) [unused for 3 blades]
   0.0      PreCone(1)  - Blade 1 cone angle (degrees)
   0.0      PreCone(2)  - Blade 2 cone angle (degrees)
   0.0      PreCone(3)  - Blade 3 cone angle (degrees) [unused for 2 blades]
   0.0      AzimB1Up    - Azimuth value to use for I/O when blade 1 points up (degrees)
---------------------- MASS AND INERTIA ----------------------------------------
   0.0      YawBrMass   - Yaw bearing mass (kg)
1747.0      NacMass     - Nacelle mass (kg)
 247.3      HubMass     - Hub mass (kg)
   0.0      TipMass(1)  - Tip-brake mass, blade 1 (kg)
   0.0      TipMass(2)  - Tip-brake mass, blade 2 (kg)
   0.0      TipMass(3)  - Tip-brake mass, blade 3 (kg) [unused for 2 blades]
 976.3      NacYIner    - Nacelle inertia about yaw axis (kg m^2)
  10.0      GenIner     - Generator inertia about HSS (kg m^2)
   9.0      HubIner     - Hub inertia about rotor axis [3 blades] or teeter axis [2 blades] (kg m^2)
---------------------- DRIVETRAIN ----------------------------------------------
 100.0      GBoxEff     - Gearbox efficiency (%)
  89.4      GenEff      - Generator efficiency [ignored by the Thevenin and user-defined generator models] (%)
  28.25     GBRatio     - Gearbox ratio (-)
False       GBRevers    - Gearbox reversal {T: if rotor and generator rotate in opposite directions} (flag)
9999.9      HSSBrTqF    - Fully deployed HSS-brake torque (N-m)
9999.9      HSSBrDt     - Time for HSS-brake to reach full deployment once initiated (sec) [used only when
HSSBrMode=1]
""          DynBrkFi    - File containing a mech-gen-torque vs HSS-speed curve for a dynamic brake
   6.0E5    DTTorSpr    - Drivetrain torsional spring (N-m/rad)
   1.0E5    DTTorDmp    - Drivetrain torsional damper (N-m/(rad/s))
---------------------- SIMPLE INDUCTION GENERATOR ------------  Crude approximation of torque/speed curve.
   2.222    SIG_SlPc    - Rated generator slip percentage (%) [used only when VSContrl=0 and GenModel=1]
1800.0      SIG_SySp    - Synchronous (zero-torque) generator speed (rpm)
 314.3      SIG_RtTq    - Rated torque (N-m) [used only when VSContrl=0 and GenModel=1]
   1.75     SIG_PORt    - Pull-out ratio (Tpullout/Trated) (-) [used only when VSContrl=0 and GenModel=1]
---------------------- THEVENIN-EQUIVALENT INDUCTION GENERATOR -----------------
  60.0      TEC_Freq    - Line frequency [50 or 60] (Hz) [used only when VSContrl=0 and GenModel=2]
   4        TEC_NPol    - Number of poles [even integer > 0] (-) [used only when VSContrl=0 and GenModel=2]
   4.92E-02 TEC_SRes    - Stator resistance (ohms) [used only when VSContrl=0 and GenModel=2]
   5.34E-04 TEC_RRes    - Rotor resistance (ohms) [used only when VSContrl=0 and GenModel=2]
 480.0      TEC_VLL     - Line-to-line RMS voltage (volts) [used only when VSContrl=0 and GenModel=2]
   1.00E-04 TEC_SLR     - Stator leakage reactance (ohms) [used only when VSContrl=0 and GenModel=2]
   1.00E-04 TEC_RLR     - Rotor leakage reactance (ohms) [used only when VSContrl=0 and GenModel=2]
   4.49E-03 TEC_MR      - Magnetizing reactance (ohms) [used only when VSContrl=0 and GenModel=2]
---------------------- PLATFORM ------------------------------------------------
   0        PtfmModel   - Platform model {0: none, 1: onshore, 2: fixed bottom offshore, 3: floating offshore} (switch)
"unused"    PtfmFile    - Name of file containing platform properties (quoted string) [unused when PtfmModel=0]
---------------------- TOWER ---------------------------------------------------
  11        TwrNodes    - Number of tower nodes used for analysis (-)
"AOC_Tower.dat" TwrFile - Name of file containing tower properties (quoted string)
---------------------- NACELLE-YAW ---------------------------------------------
   0.0      YawSpr      - Nacelle-yaw spring constant (N-m/rad)
   0.0      YawDamp     - Nacelle-yaw damping constant (N-m/(rad/s))
```

```
  0.0     YawNeut     - Neutral yaw position--yaw spring force is zero at this yaw (degrees)
---------------------- FURLING -----------------------------------------------
False       Furling     - Read in additional model properties for furling turbine (flag)
"unused"    FurlFile    - Name of file containing furling properties (quoted string) [unused when Furling=False]
---------------------- ROTOR-TEETER ------------------------------------------
  0       TeetMod     - Rotor-teeter spring/damper model {0: none, 1: standard, 2: user-defined from routine UserTeet}
(switch) [unused for 3 blades]
  0.0     TeetDmpP    - Rotor-teeter damper position (degrees) [used only for 2 blades and when TeetMod=1]
  0.0     TeetDmp     - Rotor-teeter damping constant (N-m/(rad/s)) [used only for 2 blades and when TeetMod=1]
  0.0     TeetCDmp    - Rotor-teeter rate-independent Coulomb-damping moment (N-m) [used only for 2 blades and
when TeetMod=1]
  0.0     TeetSStP    - Rotor-teeter soft-stop position (degrees) [used only for 2 blades and when TeetMod=1]
  0.0     TeetHStP    - Rotor-teeter hard-stop position (degrees) [used only for 2 blades and when TeetMod=1]
  0.0     TeetSSSp    - Rotor-teeter soft-stop linear-spring constant (N-m/rad) [used only for 2 blades and when
TeetMod=1]
  0.0     TeetHSSp    - Rotor-teeter hard-stop linear-spring constant (N-m/rad)
---------------------- TIP-BRAKE ---------------------------------------------
  0.0     TBDrConN    - Tip-brake drag constant during normal operation, Cd*Area (m^2)
  0.0     TBDrConD    - Tip-brake drag constant during fully-deployed operation, Cd*Area (m^2)
  0.0     TpBrDT      - Time for tip-brake to reach full deployment once released (sec)
---------------------- BLADE -------------------------------------------------
"SkinPlusFoamPlusAM.dat"        BldFile(1) - Name of file containing properties for blade 1 (quoted string)
"SkinPlusFoamPlusAM.dat"        BldFile(2) - Name of file containing properties for blade 2 (quoted string)
"SkinPlusFoamPlusAM.dat"        BldFile(3) - Name of file containing properties for blade 3
---------------------- AERODYN -----------------------------------------------
"OCT_AD.ipt"        ADFile     - Name of file containing AeroDyn input parameters (quoted string)
---------------------- NOISE -------------------------------------------------
"unused"    NoiseFile   - Name of file containing aerodynamic noise input parameters (quoted string) [used only when
CompNoise=True]
---------------------- ADAMS -------------------------------------------------
"AOC_ADAMS.dat"         ADAMSFile  - Name of file containing ADAMS-specific input parameters (quoted string)
[unused when ADAMSPrep=1]
---------------------- LINEARIZATION CONTROL ---------------------------------
"AOC_Linear.dat"        LinFile    - Name of file containing FAST linearization parameters (quoted string) [unused
when AnalMode=1]
---------------------- OUTPUT ------------------------------------------------
True        SumPrint    - Print summary data to "<RootName>.fsm" (flag)
1           OutFileFmt  - Format for tabular (time-marching) output file(s) (1: text file [<RootName>.out], 2: binary file
[<RootName>.outb], 3: both)
True        TabDelim    - Use tab delimiters in text tabular output file? (flag)
"ES10.3E2"  OutFmt      - Format used for text tabular output (except time).  Resulting field should be 10 characters.
  1.0     TStart      - Time to begin tabular output (s)
  100       DecFact     - Decimation factor for tabular output {1: output every time step} (-)
  1.0     SttsTime    - Amount of time between screen status messages (sec)
  0.0     NcIMUxn     - Downwind distance from the tower-top to the nacelle IMU (meters)
  0.0     NcIMUyn     - Lateral  distance from the tower-top to the nacelle IMU (meters)
  0.0     NcIMUzn     - Vertical distance from the tower-top to the nacelle IMU (meters)
  0.5     ShftGagL    - Distance from rotor apex [3 blades] or teeter pin [2 blades] to shaft strain gages [positive for
upwind rotors] (meters)
  0       NTwGages    - Number of tower nodes that have strain gages for output [0 to 9] (-)
  0       TwrGagNd    - List of tower nodes that have strain gages [1 to TwrNodes] (-) [unused if NTwGages=0]
  0       NBlGages    - Number of blade nodes that have strain gages for output [0 to 9] (-)
 1,3,5,7,9,11,14,17,20       BldGagNd    - List of blade nodes that have strain gages [1 to BldNodes] (-)
          OutList     - The next line(s) contains a list of output parameters.  See OutList.xlsx for a listing of available
output channels, (-)
"WindVxi"
"TipDxb1"
"TipDyb1"
"RootFxb1,RootFyb1"
"RotPwr"
END of FAST input file (the word "END" must appear in the first 3 columns of this last line).
```

E.2. Blade Input File

---------- FAST INDIVIDUAL BLADE FILE ----------
Properties generated on 03-July-2016
---------- BLADE PARAMETERS ----------
25 NBlInpSt - Number of blade input stations (-)
F CalcBMode - Calculate blade mode shapes internally {T: ignore mode shapes from below, F: use mode shapes from below}
1.5 BldFlDmp(1) - Blade flap mode #1 structural damping in percent of critical (%%)
1.5 BldFlDmp(2) - Blade flap mode #2 structural damping in percent of critical (%%)
1.5 BldEdDmp(1) - Blade edge mode #1 structural damping in percent of critical (%%)
---------- BLADE ADJUSTMENT FACTORS ----------
1 FlStTunr(1) - Blade flapwise modal stiffness tuner, 1st mode (-)
1 FlStTunr(2) - Blade flapwise modal stiffness tuner, 2nd mode (-)
1 AdjBlMs - Factor to adjust blade mass density (-)
1 AdjFlSt - Factor to adjust blade flap stiffness (-)
1 AdjEdSt - Factor to adjust blade edge stiffness (-)
---------- DISTRIBUTED BLADE PROPERTIES ----------

BlFract	AeroCent	StrcTwst	BMassDen	FlpStff	EdgStff	GJStff	EAStff	Alpha	FlpIner	EdgIner
(-)	(-)	(deg)	(kg/m)	(Nm^2)	(Nm^2)	(Nm^2)	(N)	(-)	(kg m)	(kg m)
0.0000	0.25	24.540	19.7063	140270.5	2.16354E+06	118708.3	2.60E+08	0	5.1745E-03	8.3598E-02
0.0079	0.25	23.722	19.4189	135802.0	2.12010E+06	115106.2	2.58E+08	0	4.9940E-03	8.1543E-02
0.0235	0.25	22.266	18.8190	126965.0	2.03144E+06	108399.8	2.54E+08	0	4.6340E-03	7.7843E-02
0.0467	0.25	20.420	17.8130	114195.3	1.89391E+06	97079.3	2.47E+08	0	4.1173E-03	7.0723E-02
0.0770	0.25	18.402	16.5078	98672.9	1.71952E+06	83252.1	2.38E+08	0	3.4639E-03	6.1859E-02
0.1140	0.25	16.328	14.9943	81931.0	1.52134E+06	68865.6	2.27E+08	0	2.7550E-03	5.2658E-02
0.1570	0.25	14.272	13.3849	65695.5	1.31330E+06	54246.2	2.15E+08	0	2.1615E-03	4.2955E-02
0.2055	0.25	12.357	11.7996	50813.7	1.11261E+06	41605.1	2.03E+08	0	1.6117E-03	3.4603E-02
0.2586	0.25	10.563	10.2649	38028.8	9.24024E+05	30757.7	1.89E+08	0	1.1730E-03	2.7214E-02
0.3156	0.25	8.962	8.8088	27619.2	7.56099E+05	21860.2	1.76E+08	0	8.2390E-04	2.0892E-02
0.3754	0.25	7.531	7.4769	19497.0	6.11369E+05	14959.9	1.63E+08	0	5.5620E-04	1.5768E-02
0.4372	0.25	6.262	6.3271	13450.1	4.90361E+05	9926.1	1.51E+08	0	3.7270E-04	1.1817E-02
0.5000	0.25	5.165	5.3383	9111.9	3.93082E+05	6426.7	1.39E+08	0	2.4030E-04	8.8994E-03
0.5628	0.25	4.243	4.6402	6698.3	3.16100E+05	4491.1	1.29E+08	0	1.6960E-04	6.8688E-03
0.6246	0.25	3.429	4.0556	4951.5	2.55790E+05	3131.9	1.20E+08	0	1.2425E-04	5.3540E-03
0.6844	0.25	2.704	3.6078	3704.6	2.09499E+05	2244.9	1.12E+08	0	9.4710E-05	4.2863E-03
0.7414	0.25	2.047	3.2064	2798.8	1.74216E+05	1602.2	1.05E+08	0	6.4870E-05	3.4620E-03
0.7945	0.25	1.443	2.9029	2187.8	1.47865E+05	1193.0	9.95E+07	0	5.3600E-05	2.8864E-03
0.8430	0.25	0.890	2.6618	1742.9	1.28304E+05	924.6	9.47E+07	0	3.8820E-05	2.4673E-03
0.8860	0.25	0.385	2.4662	1441.9	1.13697E+05	760.1	9.09E+07	0	3.3270E-05	2.1599E-03
0.9230	0.25	-0.065	2.3265	1237.9	1.03343E+05	678.5	8.80E+07	0	2.9490E-05	1.9502E-03
0.9533	0.25	-0.448	2.2237	1079.0	9.60274E+04	629.4	8.58E+07	0	1.9990E-05	1.8024E-03
0.9765	0.25	-0.755	2.1696	1015.0	9.11995E+04	595.6	8.43E+07	0	1.8810E-05	1.7075E-03
0.9921	0.25	-0.961	2.1319	974.5	8.80416E+04	570.9	8.33E+07	0	1.8060E-05	1.6426E-03
1.0000	0.25	-1.065	2.1134	954.4	8.64916E+04	562.0	8.28E+07	0	1.7690E-05	1.6146E-03

---------- BLADE MODE SHAPES ----------

0.4239679	BldFl1Sh(2) -	Flap	mode	1,	coeff	of	x^2
-0.4471689	BldFl1Sh(3) -			,	coeff	of	x^3
2.3124564	BldFl1Sh(4) -			,	coeff	of	x^4
-1.0962948	BldFl1Sh(5) -			,	coeff	of	x^5
-0.1929606	BldFl1Sh(6) -			,	coeff	of	x^6
-4.3538818	BldFl2Sh(2) -	Flap	mode	2,	coeff	of	x^2
61.4625506	BldFl2Sh(3) -			,	coeff	of	x^3
-195.778336	BldFl2Sh(4) -			,	coeff	of	x^4
221.2758357	BldFl2Sh(5) -			,	coeff	of	x^5
-81.6061682	BldFl2Sh(6) -			,	coeff	of	x^6
1.0853547	BldEdgSh(2)	-Edge	mode	1,	coeff	of	x^2
-0.4865486	BldEdgSh(3)			,	coeff	of	x^3
-0.0641888	BldEdgSh(4)			,	coeff	of	x^4
1.4426864	BldEdgSh(5)			,	coeff	of	x^5
-0.9773036	BldEdgSh(6)	-		,	coeff	of	x^6

E.3. FAST Output File

These predictions were generated by FAST (v7.02.00d-bjj, 20-Feb-2013) on 07-July-2016 at 03:06:06.
The aerodynamic calculations were made by AeroDyn (v13.00.02a-bjj, 20-Feb-2013).

Composite OCT Blade with fixed yaw error and steady Current.

Time (s)	WindVxi (m/s)	TipDxb1 (m)	RootFxb1 (kN)	RootFyb1 (kN)	RotPwr (kW)
1.000	2.600E+00	2.780E-02	3.644E+00	-1.202E+00	1.417E+01
1.010	2.600E+00	3.467E-02	3.990E+00	-1.698E+00	2.306E+01
1.020	2.600E+00	1.960E-02	2.878E+00	-1.333E+00	1.676E+01
1.030	2.600E+00	3.487E-02	4.002E+00	-1.358E+00	1.706E+01
1.040	2.600E+00	2.559E-02	3.317E+00	-1.579E+00	2.098E+01
1.050	2.600E+00	2.571E-02	3.530E+00	-1.188E+00	1.379E+01
1.060	2.600E+00	3.603E-02	4.138E+00	-1.591E+00	2.115E+01
1.070	2.600E+00	1.973E-02	2.888E+00	-1.441E+00	1.861E+01
1.080	2.600E+00	3.353E-02	3.934E+00	-1.334E+00	1.659E+01
1.090	2.600E+00	2.788E-02	3.506E+00	-1.476E+00	1.922E+01
1.100	2.600E+00	2.350E-02	3.299E+00	-1.206E+00	1.434E+01
1.110	2.600E+00	3.671E-02	4.149E+00	-1.530E+00	2.012E+01
1.120	2.600E+00	2.038E-02	2.963E+00	-1.366E+00	1.738E+01
1.130	2.600E+00	3.197E-02	3.869E+00	-1.349E+00	1.665E+01
1.140	2.600E+00	3.024E-02	3.689E+00	-1.486E+00	1.931E+01
1.150	2.600E+00	2.164E-02	3.106E+00	-1.171E+00	1.363E+01
1.160	2.600E+00	3.672E-02	4.139E+00	-1.531E+00	1.996E+01
1.170	2.600E+00	2.155E-02	3.045E+00	-1.364E+00	1.734E+01
1.180	2.600E+00	3.014E-02	3.769E+00	-1.310E+00	1.598E+01
1.190	2.600E+00	3.246E-02	3.834E+00	-1.648E+00	2.204E+01
1.200	2.600E+00	2.030E-02	2.918E+00	-1.132E+00	1.312E+01
1.210	2.600E+00	3.612E-02	4.063E+00	-1.466E+00	1.879E+01
1.220	2.600E+00	2.320E-02	3.149E+00	-1.526E+00	1.998E+01
1.230	2.600E+00	2.818E-02	3.661E+00	-1.223E+00	1.442E+01
1.240	2.600E+00	3.437E-02	3.963E+00	-1.716E+00	2.323E+01
1.250	2.600E+00	1.965E-02	2.887E+00	-1.305E+00	1.611E+01
1.260	2.600E+00	3.510E-02	4.013E+00	-1.379E+00	1.727E+01
1.270	2.600E+00	2.519E-02	3.286E+00	-1.597E+00	2.114E+01
1.280	2.600E+00	2.611E-02	3.559E+00	-1.193E+00	1.373E+01
1.290	2.600E+00	3.583E-02	4.116E+00	-1.619E+00	2.151E+01
1.300	2.600E+00	1.967E-02	2.887E+00	-1.449E+00	1.856E+01
1.310	2.600E+00	3.380E-02	3.947E+00	-1.343E+00	1.660E+01
1.320	2.600E+00	2.745E-02	3.470E+00	-1.503E+00	1.954E+01
1.330	2.600E+00	2.390E-02	3.346E+00	-1.215E+00	1.429E+01
1.340	2.600E+00	3.664E-02	4.165E+00	-1.546E+00	2.022E+01
1.350	2.600E+00	2.023E-02	2.946E+00	-1.394E+00	1.769E+01
1.360	2.600E+00	3.228E-02	3.882E+00	-1.356E+00	1.666E+01
1.370	2.600E+00	2.981E-02	3.658E+00	-1.477E+00	1.903E+01
1.380	2.600E+00	2.195E-02	3.133E+00	-1.190E+00	1.385E+01
1.390	2.600E+00	3.678E-02	4.170E+00	-1.550E+00	2.012E+01
1.400	2.600E+00	2.130E-02	3.032E+00	-1.357E+00	1.708E+01
1.410	2.600E+00	3.051E-02	3.791E+00	-1.331E+00	1.620E+01
1.420	2.600E+00	3.207E-02	3.808E+00	-1.624E+00	2.151E+01
1.430	2.600E+00	2.051E-02	2.956E+00	-1.138E+00	1.300E+01
1.440	2.600E+00	3.627E-02	4.069E+00	-1.487E+00	1.906E+01
1.450	2.600E+00	2.286E-02	3.130E+00	-1.502E+00	1.947E+01
1.460	2.600E+00	2.856E-02	3.679E+00	-1.244E+00	1.471E+01
1.470	2.600E+00	3.405E-02	3.947E+00	-1.729E+00	2.332E+01
1.480	2.600E+00	1.971E-02	2.875E+00	-1.264E+00	1.535E+01
1.490	2.600E+00	3.532E-02	4.025E+00	-1.400E+00	1.752E+01
1.500	2.600E+00	2.480E-02	3.256E+00	-1.605E+00	2.119E+01

REFERENCES

Akram, M. (2010). *FATIGUE MODELING OF COMPOSITE OCEAN CURRENT TURBINE BLADE by Mohammad Wasim Akram A Thesis Submitted to the Faculty of The College of Engineering and Computer Science in Partial Fulfillment of the Requirements for the Degree of Master of Science Florida A*. Florida Atlantic University.

Asseff, N. S. (2009). *Design and Finite Element Analysis of an Ocean Current Turbine Blade*. Florida Atlantic University.

ASTM. (2011). E1049-85: Standard Practices for Cycle Counting in Fatigue Analysis. *E1049 - 85*, *85*(Reapproved 2011), 1–10. http://doi.org/10.1520/E1049-85R11E01.2

AVAILABLE DATA. (2014). Retrieved from http://coet.fau.edu/resource-measurement-modeling/available-data.html

Bibin John, & Reghunadhan, N. (2010). *Update on Syntactic Foams*.

Bir, G. (2005). *User's Guide to BModes (Software for Computing Rotating Beam Coupled Modes)*. Golden. Retrieved from http://www.nrel.gov/docs/fy06osti/39133.pdf

Bir, G. (2006). *User's Guide to PreComp (Pre-Processor for Computing Composite Blade Properties)*. Golden. Retrieved from http://www.nrel.gov/docs/fy06osti/38929.pdf

Bir, G. (2010). Verification of BModes: Rotary Beam and Tower Modal Analysis Code: Preprint. In *51st AIAA/ASME/ASCE/AHS/ASC Structures, Structural Dynamics, and*

Materials Conference (p. 18). Orlando. Retrieved from http://www.osti.gov/bridge

Borghi, M., Kolawole, F., Gangadharan, S., Engblom, W., Vanzwieten, J., Alsenas, G., & Ravenna, S. (2013). Michael Borghi, Fumbi Kolawole, Sathya Gangadharan, William Engblom, 1–6.

Campbell, F. C. (Flake C. . (2008). *Elements of metallurgy and engineering alloys*. ASM International.

Carolina, M., Machado, P. M., Vanzwieten, J. H., & Pinos, I. (2016). A Measurement-Based Analysis of the Hydrokinetic Energy in the Gulf Stream. *Journal of Ocean and Wind Energy*, *3*(1), 25–30. http://doi.org/10.17736/jowe.2016.asr06

Cenedese, C., & Gordon, A. L. (2011). Ocean current. In *Encyclopædia Britannica*. Retrieved from http://academic.eb.com/levels/collegiate/article/56692#

Cooper, G. R., & Mcgillem, C. D. (1988). *Probabilistic Methods of Signal and System Analysis*. Oxford University Press.

Daniel, I., & Ishai, O. (2005). *Engineering Mechanics of Composite Materials* (2nd ed.). Oxford University Press.

David, L., & Hansen, A. C. (2002). *User's Guide to the Wind Turbine Aerodynamics Computer Software AeroDyn*. Salt Lake City. Retrieved from https://nwtc.nrel.gov/system/files/AeroDyn.pdf

DNV. (2011). Modeling and Analysis OF Marine Operations. *Offshore Standard*.

Endo, T., Mitsunaga, K., & Nakagawa, H. (1967). Fatigue of Metals Subjected to Varying Stress -- Prediction of Fatigue Lives (pp. 41–44). Chugoku-Shikoku Dist.

Fang Zhou. (2013). *Development of an Integrated Computational Tool for Design and Analysis of Composite Turbine Blades Under Ocean Current Loading*. Florida

Atlantic University.

Ferreira, J. A. M., Salviano, K., Costa, J. D., & Capela, C. (2010). Fatigue behaviour in hybrid hollow microspheres/fibre reinforced composites. *Journal of Materials Science*, *45*(13), 3547–3553. http://doi.org/10.1007/s10853-010-4397-4

FGDC. (2010). *12K, 2 x 2 Twill Weave Carbon Fiber*. Brookville. Retrieved from http://cdn.fibreglast.com/downloads/00459.pdf

Freebury, G., & Musial, W. (2000). *Determining Equivalent Damage Loading for Full-Scale Wind Turbine Blade Fatigue Tests*. Reno. Retrieved from http://www.doe.gov/bridge

Goglio, L., & Rossetto, M. (2004). Comparison of fatigue data using the maximum likelihood method. *Engineering Fracture Mechanics*, *71*(4), 725–736. http://doi.org/10.1016/S0013-7944(03)00009-2

Gordon, R. L. (1996). *Principles of Operation A Practical Primer Second Edition for Broadband ADCPs*. San Diego.

Harbor Branch. (2015). *Annual Report*. Retrieved from https://www.fau.edu/hboi/newsroom/HBOI Annual Report SPREAD.pdf

IEC. (2005). *IEC 61400-1 Wind Turbines - Part 1: Design requirements*. *IEC 61400* (Vol. 2005).

James, F. (1994). RANLUX: A Fortran implementation of the high-quality pseudorandom number generator of Lüscher. *Computer Physics Communications*, *79*, 111–114.

Jonkman, B. J., & Kilcher, L. (2012a). *TurbSim User's Guide: Version 1.06.00*.

Jonkman, B. J., & Kilcher, L. (2012b). *TurbSim User's Guide: Version 1.06.00*. Golden.

Jonkman, J. M. (2003). *Modeling of the UAE Wind Turbine for Refinement of FAST_AD*. Golden.

Jonkman, J. M., & Buhl, M. L. (2004). *New Developments for the NWTC's FAST Aeroelastic HAWT Simulator: Preprint*. Golden. Retrieved from http://www.osti.gov/bridge

Jonkman, J. M., & Buhl, M. L. (2005). *FAST User's Guide*. Battelle.

Kong, C., Kim, T., Han, D., & Sugiyama, Y. (2006). Investigation of fatigue life for a medium scale composite wind turbine blade. *International Journal of Fatigue*, *28*(10), 1382–1388. http://doi.org/10.1016/j.ijfatigue.2006.02.034

Krajcinovic, D. (1996). *Damage mechanics*. Elsevier.

Kuroshio. (2016). In *Encyclopædia Britannica*. Retrieved from https://www.britannica.com/place/Kuroshio

LaMonica, M. (2011). Wave and Tidal Power Must Overcome Significant Challenges to Be Useful. *Greenhaven Press*. Detroit. Retrieved from http://ic.galegroup.com/ic/ovic/ViewpointsDetailsPage/DocumentToolsPortletWindow?displayGroupName=Viewpoints&action=2&catId=&documentId=GALE%7CEJ3010723203&zid=d1267daafa613c925d510b46663b7e21&source=Bookmark&u=calyoungmidsch&jsid=1f375432d0a231426f0ef20f

Lemanski, L. (2006). *Center of Excellence in Ocean Energy Technology, Technical Proposal*. Boca Raton.

Lumpkin, R. (2016). NOAA Ocean Currents Map. Retrieved from http://www.adp.noaa.gov/currents_map.html

Lüscher, M. (1994). A portable high-quality random number generator for lattice field

theory simulations. *Computer Physics Communications*, *79*(1), 100–110. http://doi.org/10.1016/0010-4655(94)90232-1

Mahfuz, H., Maniruzzaman, M., Vaidya, U., Brown, T., & Jeelani, S. (1997). Response of SiCf/Si3N4 Composites Under Static and Cyclic Loading—An Experimental and Statistical Analysis. *Journal of Engineering Materials and Technology*, *119*(2), 186. http://doi.org/10.1115/1.2805992

Manwell, J. F., McGowan, J. G., & Rogers, A. L. (2009). *Wind energy explained: theory, design and application*. *John Wiley&Sons Ltd, UK*. http://doi.org/10.1002/9781119994367

Matweb. (2016a). *MatWeb, Your Source for Materials InfPark Electrochemical Nelcote® E-718 Epoxy Prepreg, T-700 24K Uni-Tape Reinforced*.

Matweb. (2016b). *Park Electrochemical Nelcote® E-765 Epoxy Prepreg, 34-700 12K 2x2 Twill Reinforced*.

McCaffrey, K., Fox-Kemper, B., Hamlington, P. E., & Thomson, J. (2015). Characterization of turbulence anisotropy, coherence, and intermittency at a prospective tidal energy site: Observational data analysis. *Renewable Energy*, *76*, 441–453.

Miner, M. A. (1945). Cumulative Damage in Fatigue. *Journal of Applied Mechanics*, *12*, A159–A164.

Moriarty, P. J., & Hansen, A. C. (2005). *AeroDyn Theory Manual*. Golden.

Nelson, W. (2004). *Applied life data analysis*. Wiley-Interscience.

NRC. (2013). *An Evaluation of the U.S. Department of Energy's Marine and Hydrokinetic Resource Assessments*. Washington, D.C.: National Academies Press.

http://doi.org/10.17226/18278

Nystrom, E. A., Rehmann, C. R., & Oberg, K. A. (2007). Evaluation of Mean Velocity and Turbulence Measurements with ADCPs. *http://dx.doi.org/10.1061/(ASCE)0733-9429(2007)133:12(1310)*.

Rahman, M. H. (2013). *DESIGN AND ANALYSIS OF HYBRID TITANIUM-COMPOSITE HULL STRUCTURES UNDER EXTREME WAVE AND SLAMMING LOADS*. Florida Atlantic University.

Raye, R. (2002). *Characterization study of the Florida Current at 26.11 North Latitude, 79.50 West Longitude for ocean current power generation*. Florida Atlantic University.

SNMREC. (2015). *Southeast National Marine Renewable Energy Center (SNMREC)*. Boca Raton. Retrieved from http://coet.fau.edu/sites/default/files/SNMREC Fact Sheet 2015.pdf

Sutherland, H. J. (1999). *A Summary of the Fatigue Properties Wind Turbine Materials*. Albuquerque. Retrieved from http://www.ntis.govlordering.htm

Suzuki, T., Mahfuz, H., & Canino, M. (2015). Fatigue Load and Life Estimation of Composite Turbine Blades under Random Ocean Current. *2015 Oceans - Washington D.C.*

Toshiba. (2014). IHI and Toshiba to Launch Demonstration Research of Ocean Current Power Generation System. Retrieved from https://www.toshiba.co.jp/about/press/2014_12/pr2501.htm

Tsai, S. W. (1988). *Composites design*. Think Composites.

Tsai, S. W., & Wu, E. M. (1971). A General Theory of Strength for Anisotropic

Materials. *Journal of Composite Materials*, *5*, 58–80.

VanZwieten, J. (2003). *MODELING AND CONTROL OF THE "C-PLANE" OCEAN CURRENT TURBINE*. Florida Atlantic University.

VanZwieten, J., Alsenas, G., Smentek-Duerr, A., & Hanson, H. (2013). GLOBAL OCEAN CURRENT ENERGY ASSESSMENT: AN INITIAL LOOK. In *Proceedings of the 1st Marine Energy Technology Symposium*. Washington, D.C.

Vassilopoulos, A. P., Manshadi, B. D., & Keller, T. (2010). Influence of the constant life diagram formulation on the fatigue life prediction of composite materials. *International Journal of Fatigue*, *32*(4), 659–669. http://doi.org/10.1016/j.ijfatigue.2009.09.008

Waloddi Weibull, B. (1951). A Statistical Distribution Function of Wide Applicability. *Journal of Applied Mechanics*, *Vol. 18*, 293–297.

Whitney, J. (1981). Fatigue Characterization of Composite Materials. In *Fatigue of Fibrous Composite Materials* (pp. 133–133–19). 100 Barr Harbor Drive, PO Box C700, West Conshohocken, PA 19428-2959: ASTM International. http://doi.org/10.1520/STP27618S